IEEE TRANSACTIONS ON

GEOSCIENCE AND REMOTE SENSING

MAY 1993 VOLUME 31 NUMBER 3 IGRSD2 (ISSN 0196-2892)

A PUBLICATION OF THE IEEE GEOSCIENCE AND REMOTE SENSING SOCIETY

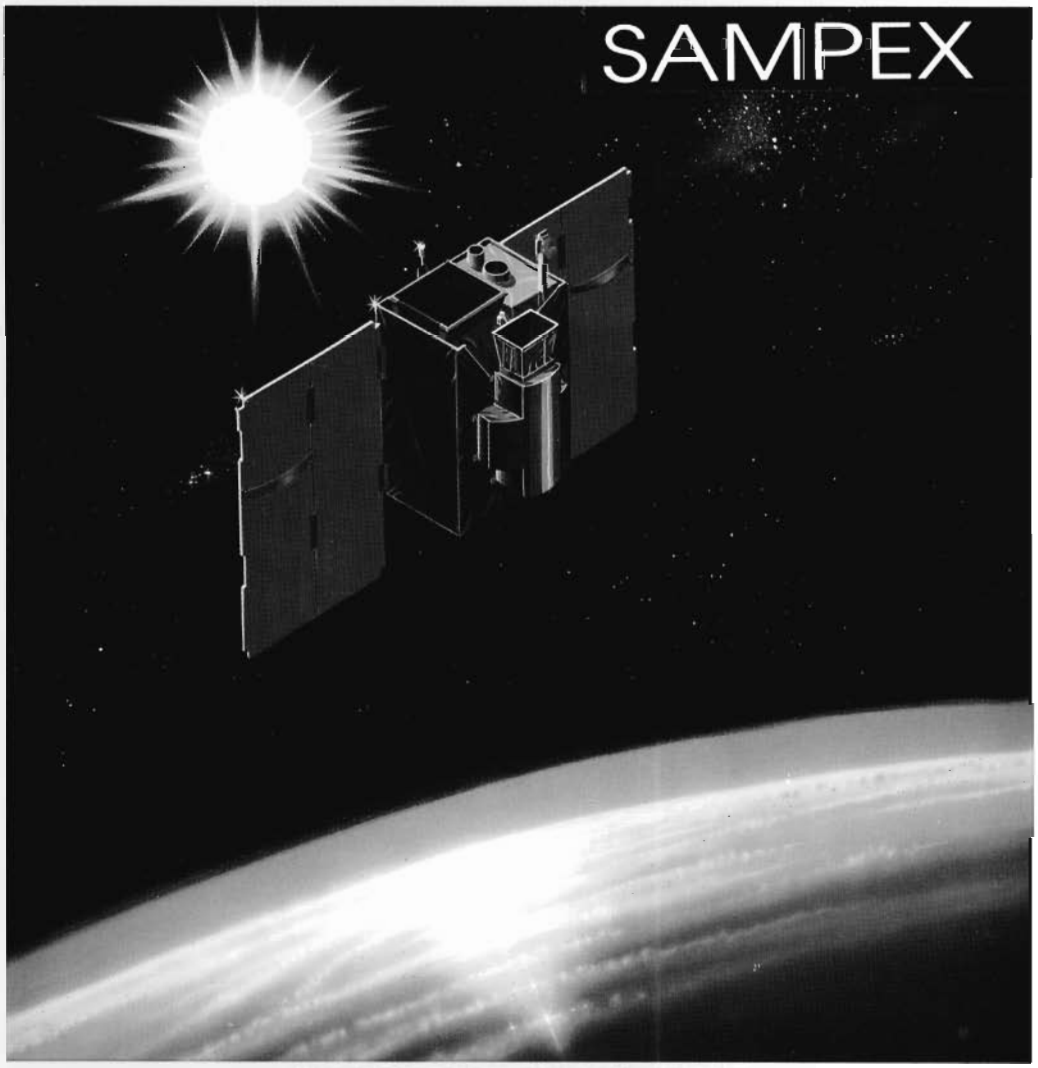

NASA's Solar, Anomalous, and Magnetospheric Particle Explorer (SAMPEX) Satellite

IEEE TRANSACTIONS ON GEOSCIENCE AND REMOTE SENSING is published bimonthly by The Institute of Electrical and Electronics Engineers, Inc. Responsibility for the contents rests upon the authors and not upon the IEEE, the Society/Council, or its members. **IEEE Headquarters:** 345 East 47th Street, New York, NY 10017. **NY Telephone:** 212-705 + extension: Information -7900; General Manager -7910; Public Information -7867; Publishing Services -7560; Spectrum -7556. **Telecopiers:** NY (Headquarters) 212-752-4929; NY (Publications) 212-705-7682. **IEEE Service Center** (for orders, subscriptions, address changes, Educational Activities, Region/Section/Student Services, Standards): 445 Hoes Lane, P.O. Box 1331, Piscataway, NJ 08855-1331. **NJ Telephone:** 201-981-0060; 201-562 + extension: Controller -5365; Technical Activities -3900. **IEEE Washington Office** (for U.S. professional activities): 1828 L Street, NW, Suite 1202, Washington, DC 20036. **Washington Telephone:** 202-785-0017. **Price/Publication Information:** Individual copies: IEEE members $10.00 (first copy only), nonmembers $20.00 per copy. (Note: Add $4.00 postage and handling charge to any order from $1.00 to $50.00, including prepaid orders.) Member and nonmember subscription prices available on request. Available in microfiche and microfilm.

Postmaster: Send address changes to IEEE TRANSACTIONS ON GEOSCIENCE AND REMOTE SENSING, IEEE, 445 Hoes Lane, P.O. Box 1331, Piscataway, NJ 08855-1331. GST Registration No. 125634188. Printed in U.S.A.

An Overview of the Solar, Anomalous, and Magnetospheric Particle Explorer (SAMPEX) Mission

D. N. Baker, G. M. Mason, O. Figueroa, G. Colon, J. G. Watzin, and R. M. Aleman

Abstract—**The scientific objective of the NASA Small-class Explorer Mission SAMPEX are summarized. A brief history of the Small Explorer program is provided along with a description of the SAMPEX project development and structure. The spacecraft and scientific instrument configuration is presented. The orbit of SAMPEX has an altitude of 520 by 670 km and an 82° inclination. Maximum possible power is provided by articulated solar arrays that point continuously toward the sun. Highly sensitive science instruments point generally toward the local zenith, especially over the terrestrial poles, in order to measure optimally the galactic and solar cosmic ray flux. Energetic magnetospheric particle precipitation is monitored at lower geomagnetic latitudes. The spacecraft uses several innovative approaches including an optical fiber bus, powerful onboard computers, and large solid state memories (instead of tape recorders). Spacecraft communication and data acquisition are discussed and the space- and ground-segment data flows are summarized. A mission lifetime of 3 years is sought with the goal of extending data acquisition over an even longer portion of the 11-year solar activity cycle.**

I. Introduction

RECOGNIZING the advantages of small, quick-turnaround projects, NASA's Office of Space Science and Applications recently initiated a program at the NASA Goddard Space Flight Center in Greenbelt, MD, called the Small Explorer Program, or SMEX. SMEX is intended to support disciplines traditionally served by NASA's longstanding Explorer Program, which include astrophysics, space physics and upper atmospheric science. An important aspect of SMEX is that one principal investigator (PI) proposes a complete mission and its experiments. The idea is to have one team responsible for the entire mission and all instruments. The team usually includes scientists at a variety of institutions who have worked together closely in the past. The result is an efficient, highly cohesive research effort [1].

The original SMEX announcement of opportunity was released on May 17, 1988, with proposals due by September 30, 1988. The announcement articulated the following goals:

> "The Small-class Explorer Program seeks to conduct scientific research of modest programmatic scope which can be launched within three years of selection. The program intends to provide a continuing opportunity for quickly implemented flights of small free-flyers to conduct focused investigations which complement major missions, prove new scientific concepts, or make significant contributions to space science in other ways. It is the goal of the program to obtain flight frequency of at least one flight per year."

The cost per mission was to be limited, on average, to $30 million (1988 dollars) which includes both the instruments and the spacecraft but excludes launch services and mission operations costs beyond the first 30 days after launch.

The first SMEX mission is the Solar, Anomalous, and Magnetospheric Particle Explorer, or SAMPEX. SAMPEX measures energetic electrons as well as ion composition of particle populations from ~0.4 MeV/nucleon to hundreds of MeV/nucleon from a zenith-oriented satellite in near-polar orbit. SAMPEX was successfully launched from NASA's Western Test Range (Lompoc, CA) at 1419 UT on July 3, 1992. A photograph of SAMPEX in its final configuration is shown in Fig. 1. This paper summarizes the scientific and technical aspects of the overall SAMPEX mission.

II. Science Overview

The SAMPEX payload combines some of the most sensitive particle sensors ever flown in space. It studies the energy, composition, and charge states of particles from supernova explosions in the distant reaches of the galaxy, from the heart of solar flares, and from the depths of nearby interstellar space. It also monitors closely the magnetospheric particle populations which plunge occasionally into the middle atmosphere of the Earth, thereby ionizing neutral gases and altering the atmospheric chemistry. A key part of SAMPEX is to use the magnetic field of the Earth as an essential component of the measurement strategy. The Earth's field is used as a giant magnetic spectrometer to separate different energies and charge states of particles as SAMPEX executes its near-polar orbit.

In the energy range below ~50 MeV/nucleon, there are at least six elements (He, C, N, O, Ne, and Ar) whose energy spectra show large increases in flux above the quiet-time galactic cosmic ray spectrum during the solar activity

Manuscript received August 3, 1992; revised January 12, 1993.

D. N. Baker is with the Laboratory for Extraterrestrial Physics, NASA/Goddard Space Flight Center, Greenbelt, MD 20771.

G. M. Mason is with the Department of Physics, the University of Maryland, College Park, MD 20742.

O. Figueroa, G. Colon, J. G. Watzin, and R. M. Aleman are with the Engineering Directorate, NASA/Goddard Space Flight Center, Greenbelt, MD 20771.

IEEE Log Number 9208071.

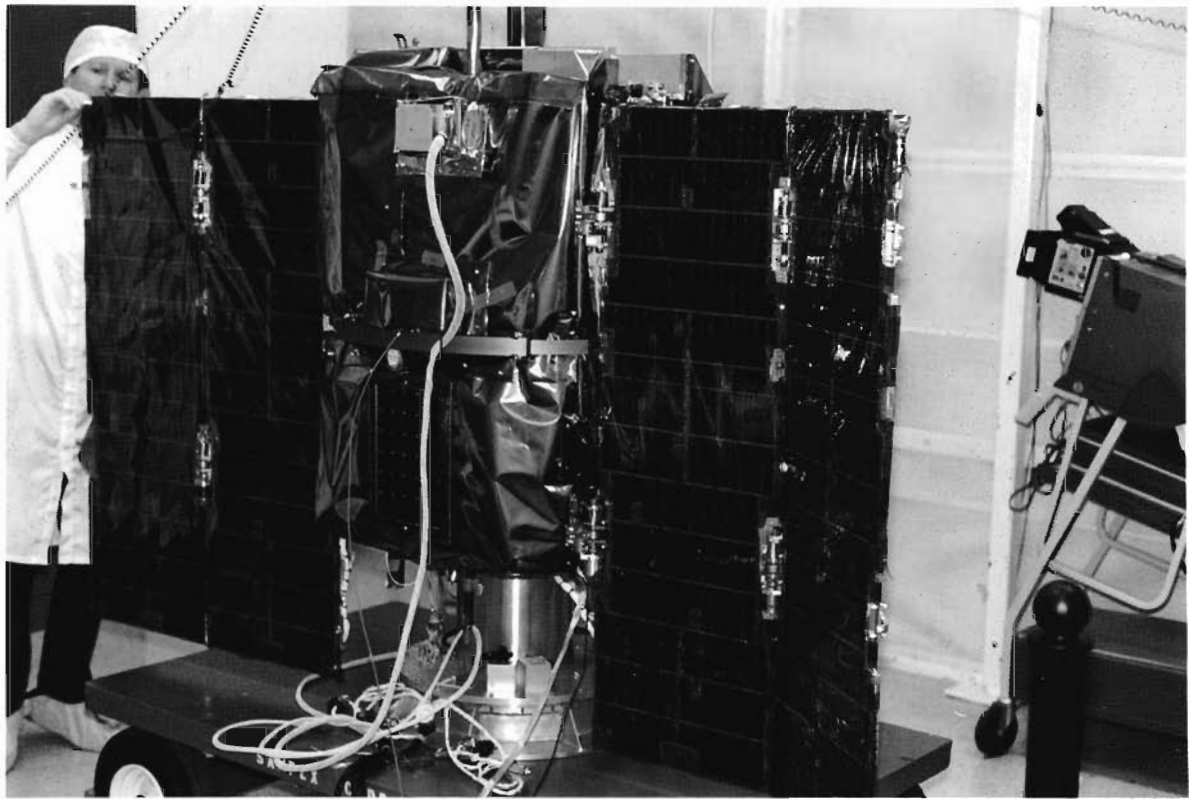

Fig. 1. Photo of SAMPEX spacecraft in final launch configuration.

minimum. This "anomalous" cosmic ray (ACR) component is generally believed to represent neutral interstellar particles that drift into our solar system (i.e., the heliosphere), become ionized by solar wind interactions or solar ultraviolet radiation, and are then accelerated [2]. This model predicts that the ACR particles should be singly ionized, an assertion for which there is now supportive evidence [2]. SAMPEX makes direct measurements of the charge state of He, N, O, and Ne by using the Earth's magnetic field as a charge-state spectrometer. By using sophisticated numerical trajectory calculations for each incident particle, the ACR fluxes are organized according to magnetic cutoff rigidity. This allows SAMPEX to distinguish between a number of possible charge states. If the ACR particles turn out to be singly ionized, then this component represents a direct sample of the local interstellar medium.

Considering more impulsive particle phenomena, solar flares frequently inject large populations of energetic heavy ions into the interplanetary medium. The elemental and isotopic composition of these particles provide crucial information about the history of solar system material and about solar flare acceleration and propagation processes. High sensitivity spectrometers on SAMPEX have 10–100 times more collecting power than previous instruments. The number of electrons stripped from solar energetic particle ions within the sun's atmosphere is determined by plasma conditions at the acceleration site; thus, detailed determinations of the individual ionic species can be derived, in principle, from the charge state distribution measured far from the sun.

Within the Earth's magnetosphere itself, observations at geosynchronous orbit (6.6 Earth radii, R_E) have shown that relativistic ($\gtrsim$1 MeV) electron intensities can increase by orders of magnitude for periods of several days and then return to background levels. These enhancements inside the magnetosphere are related to the presence of recurrent high-speed solar wind streams outside in the interplanetary medium, and show a strong solar cycle (11-year) dependence. Numerical modeling shows that when these electrons precipitate they can cause large energy depositions at 40–60 km altitude in the atmosphere, dominating other ionization sources at these heights. Precipitating relativistic electrons may lead to substantial long-term increases in the levels of odd nitrogen compounds (NOx) in the middle atmosphere with an attendant impact on local ozone levels via the reactions $NO + O_3 \rightarrow NO_2 + O_2$, and $NO_2 + O \rightarrow NO + O_2$. Thus, relativistic electrons may provide a mechanism for coupling the 11-year solar activity cycle into the middle and lower atmosphere [3]. It is therefore a critical problem to determine the actual intensity and spatial extent of relativistic electron precipitation, vital information that SAMPEX will provide.

Galactic cosmic rays are a directly accessible sample of matter from outside the solar system. A spectrometer on SAMPEX carries out measurements of the isotopic composition of this sample of high energy matter, which contains a record of the nuclear history of cosmic rays. Cosmic ray isotope observations have dramatically altered thinking about both cosmic ray origin and propagation. As an example, prior measurements have shown that ^{22}Ne is more than a factor of 3 times more abundant in cosmic ray source material than in the solar system. The abundances of ^{25}Mg, ^{26}Mg, ^{29}Si, and ^{30}Si are all enhanced by a factor of $\sim$1.5. The exposure obtained

on SAMPEX will make it possible to extend the search for isotopic differences between galactic and solar cosmic ray material to many other key elements.

III. Spacecraft Configuration

The broad range of inquiries described briefly above can only be addressed using experimental measurements obtained on a low-altitude, near-polar orbiting spacecraft. The SAMPEX mission uses a spacecraft developed by the SMEX Project at the Goddard Space Flight Center. The spacecraft is required to provide the total support (power, data, thermal, structural, etc.) to four separate scientific instruments and their associated data processing unit. The spacecraft has been designed as a single string system. A system design was selected that uses proven design concepts and flight qualified or readily available hardware wherever possible. A Performance Assurance program with minimum paperwork, best exerimenter judgment, and extensive bench testing has been implemented for the SAMPEX instrument payload. Within this resource-constrained package, there are many innovations including powerful onboard processors, optical fiber busses, solid state memory units, and a highly integrated mechanical design.

The SAMPEX spacecraft was designed to support a minimum mission duration of 1 year, with a mission goal of 3 or more years. Because the four-stage Scout launch vehicle could loft a very limited weight for this mission (<372 pounds), the spacecraft systems were primarily designed in a single-string architecture. The SAMPEX mechanical system basically consists of a primary structure, a deployable solar array system, and a yo-yo despin system. SAMPEX is built up of machined aluminum plates which form a box-like structure that houses all of the spacecraft components (see Fig. 2). An adapter ring on the bottom provides the interface to the Scout 200-E adapter on the fourth stage of the Scout launch vehicle. SAMPEX was designed to fit within the Scout 34-inch diameter heatshield.

The deployable solar arrays are configured in two symmetric wings. The arrays deployed by a damped spring system which prevented the motion from imparting any severe loads on the structure. The arrays consist of four panels, associated deployment mechanisms, position monitors, cabling, gallium arsenide solar cells, and cover glass. The solar array panels are fabricated from aluminum honeycomb and have solar cells bonded to them. Each array has two coarse sun sensors mounted on the upper and lower extreme corners.

The power subsystem is a Direct Energy Transfer system providing an unregulated +28 V direct current bus. Power is generated during the sunlight periods from the solar array paddles and stored in a nickel cadmium battery. Power is drawn solely from the batteries during eclipse periods. A shunt regulator is provided to dissipate excess array power. See Fig. 3 for electrical and power system details.

The power subsystem supplies power to the spacecraft via three busses: the essential bus, the nonessential bus, and the pyrotechnic bus. The essential bus provides continuous power to spacecraft functions including the data system, the telemetry transponder, the heaters, the attitude control system, and the power distribution electronics. The nonessential bus provides power to the spacecraft instruments. The pyrotechnic bus provides unprotected battery power to fire the pyrotechnic devices. All three busses are routed to the power distribu-

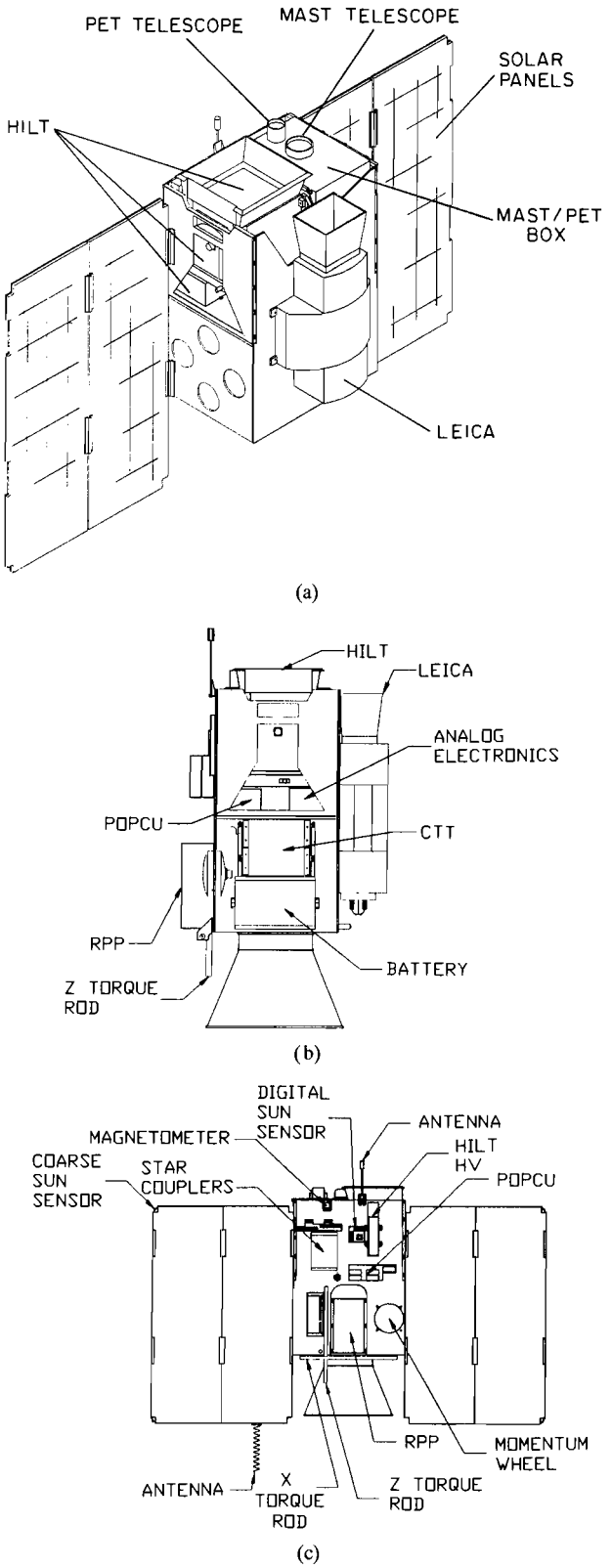

Fig. 2. Mechanical design of the SAMPEX spacecraft and physical layout: (a) Scientific instruments; (b) Side view of subsystems; (c) Back view of subsystem layout.

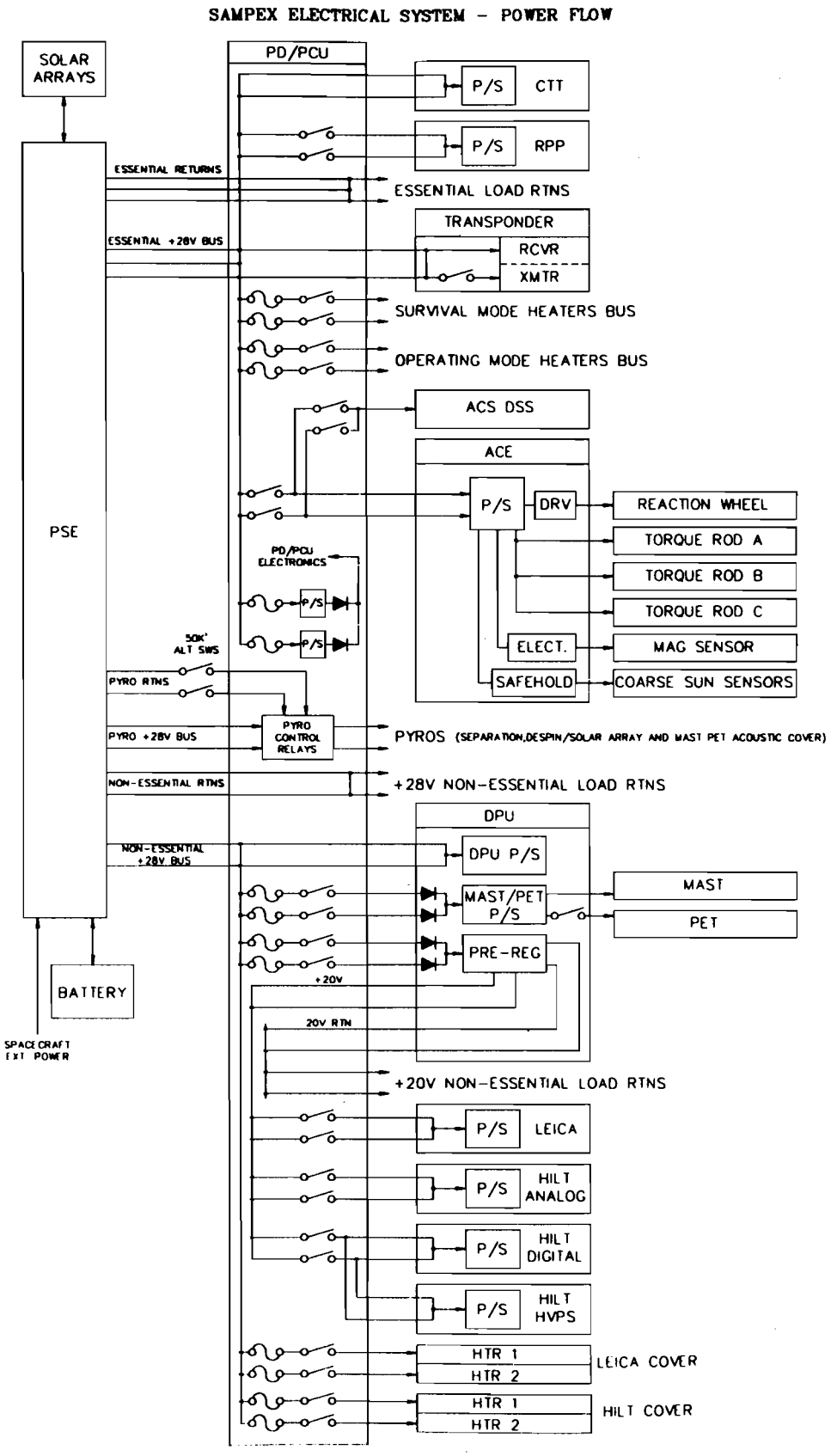

(a)

Fig. 3. Electrical layout and (b) data flow within the SAMPEX spacecraft.

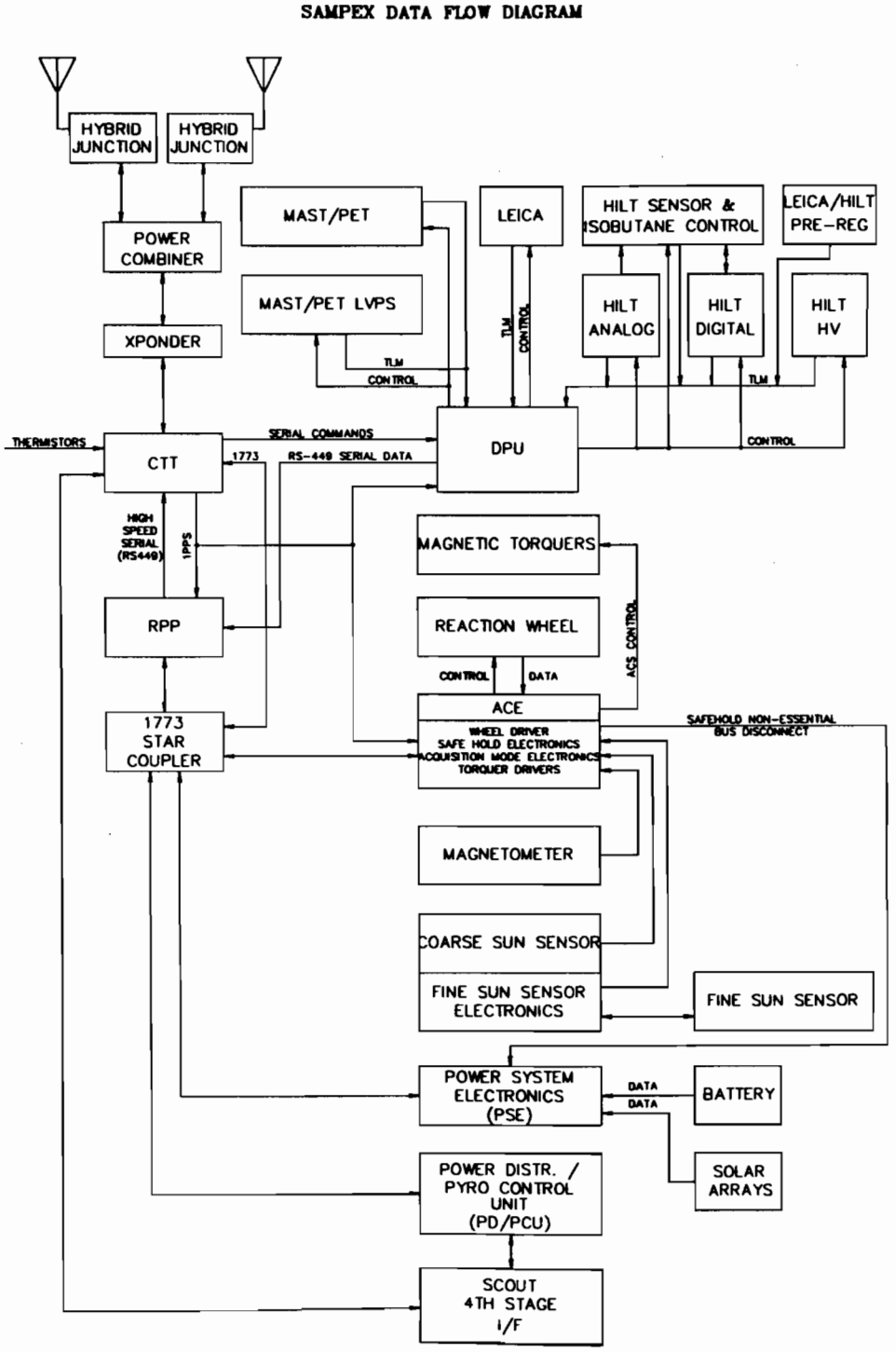

(b)

Fig. 3. *(Continued)*

tion unit for switching and fusing (where appropriate). The power subsystem includes an isolation relay to disconnect the nonessential bus in the event that the spacecraft is drawing excessive current, the battery is in undervoltage, or when the spacecraft goes into safehold. With the exception of the shunt drivers, all power subsystem electronics are designed in a single string, nonredundant configuration. The Power Distribution/Pyro Control Unit (PD/PCU) provide primary power distribution and fusing to other spacecraft subsystems, and control and power to the spacecraft's separation and deployment pyrotechnic devices.

The on-orbit average output power of the system is 102 W with no solar array shadowing and minimum solar intensity at end-of-mission life. During the launch phase, with the spacecraft launched into a full sun orbit, the power system was capable of supplying 200 Wh of energy. This

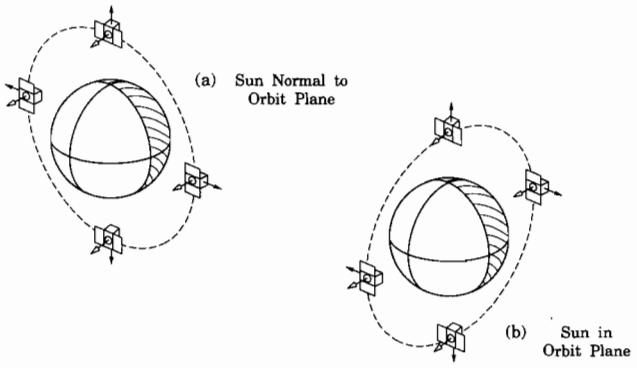

Fig. 4. The pointing strategy for the SAMPEX spacecraft in two illustrative orbit planes.

is based on a 9 Ah battery and an 80% battery depth of discharge.

The Attitude Control Subsystem (ACS) is designed as a solar-pointed/momentum-bias system. The SAMPEX spacecraft points at the sun while it rotates about the sunline once per orbit in order to position the instrument lines-of-sight in the zenith direction when overflying the poles. Pointing requirements for the selected experiments are met by choosing sensor, torquers, and system configurations from a standard set of electronics, sensors, and actuators. The ACS system utilizes one momentum wheel and three electromagnetic torque rods to orient the experiment viewing axis. Pointing ranges within $\pm 15°$ of vertical over the poles. Attitude knowledge accuracy computed onboard the spacecraft is better than 2° (3 sigma). The pointing strategy for SAMPEX is to point the pitch axis (i.e., the normal to the solar panels) directly at the Sun. Then the yaw axis (parallel to the detector bore sights) rotates about the pitch axis once per spacecraft orbit. The spacecraft views north over the north pole, south over the south pole, and parallel to the equator during the equatorial plane crossings (see Fig. 4).

An Attitude Control Electronics (ACE) box which contains signal conditioning electronics and an independent analog safehold mode controls the ACS sensor and hardware discussed previously. The onboard data system performs closed loop real-time attitude determination and control processing. Three-axis attitude determination is provided by comparing the local measured sun vector and magnetic field vector with an on-board ephemeris model. Digital control of the spacecraft attitude is completed by sending appropriate command signals across the spacecraft data bus to the actuators.

The Thermal subsystem maintains internal SAMPEX temperatures between $-10°$ and 50°C. These temperatures are controlled by selected surface-finish application, regulating conduction paths, passive thermal control elements, and thermostatically controlled heaters.

The SAMPEX antenna system is composed of two quadrifilar helices, two 90° hybrid junctions, and a power divider. These omnidirectional antennas are located on the top and on the bottom of the spacecraft. The top antenna is a half-turn quadrifilar with a 150° beamwidth. The bottom antenna is a three-turn quadrifilar with a 210° beamwidth. Each antenna is fed with a 90° hybrid junction to create the proper phasing between elements. A power divider feeds each hybrid junction with a signal of equal amplitude and phase. This system is designed to operate over a 2025–2300 MHz frequency range. The Communications subsystem consists of a near-Earth S-band transponder operating in full duplex mode, providing reception of uplinked commands, transmission of telemetry data, and support of tracking by the designated ground station. The command data rate is 2 kb/s. The telemetry output signal from the transmitter is modulated onto the carrier to produce the downlink signal. The transmitter modulation bandwidth is 10 MHz and its output power is 5 W. The transponder interfaces with the antennas and the Command and Data Handling (C&DH) subsystem.

The SAMPEX C&DH functions are performed by the Small Explorer Data System (SEDS). The SEDS provides on-board computers that can be programmed to perform mission unique functions as required and provides autonomous operations of the spacecraft when it is not in contact with the ground. The SEDS is responsible for the command and data handling functions of the SAMPEX spacecraft (see Fig. 5). The SEDS provides data collection from the different subsystems and instruments, stores the data, processes it, and sends it to the ground. The data system uses solid-state memory instead of conventional tape recorders to record spacecraft telemetry data when the spacecraft is not in contact with the ground. Data transmitted from SEDS to the ground is formatted as a "Packet Telemetry" stream in accordance with the Consultative Committee for Space Data Systems (CCSDS) and Goddard Space Flight Center standards. The SEDS is comprised of three main components:

1) The Recorder/Processor/Packetizer (RPP) provides storage for 26.5 Mbytes of data, packetizes commands and telemetry, and is used as a general purpose processor. The RPP supports overall spacecraft control functions and specific requirements such as attitude control. The RPP generates the telemetry data stream for transmission to the ground.
2) The Command Telemetry Terminal (CTT) connects the SEDS to the transponder, provides uplink command processing, downlink telemetry encoding, time code management, local telemetry acquisition and command distribution, housekeeping, attitude determination, and system monitoring functions. The CTT can control some of the spacecraft functions if the RPP fails.
3) The Military Standard (MIL-STD) 1773 data bus connects SEDS components to the attitude control and power subsystems. The MIL-STD-1773 bus in the implementation of the MIL-STD-1553 military avionics protocol. The 1773 bus uses optical fiber links for a high throughput and low-mass spacecraft harness. It also is a nonconductor so it cannot introduce electronic or radio frequency interference into the system. This fiber optics approach provides spaceflight experience for a new generation of high data rate busses.

These components are used for command reception, telemetry transmission and tracking. The SAMPEX operating radio

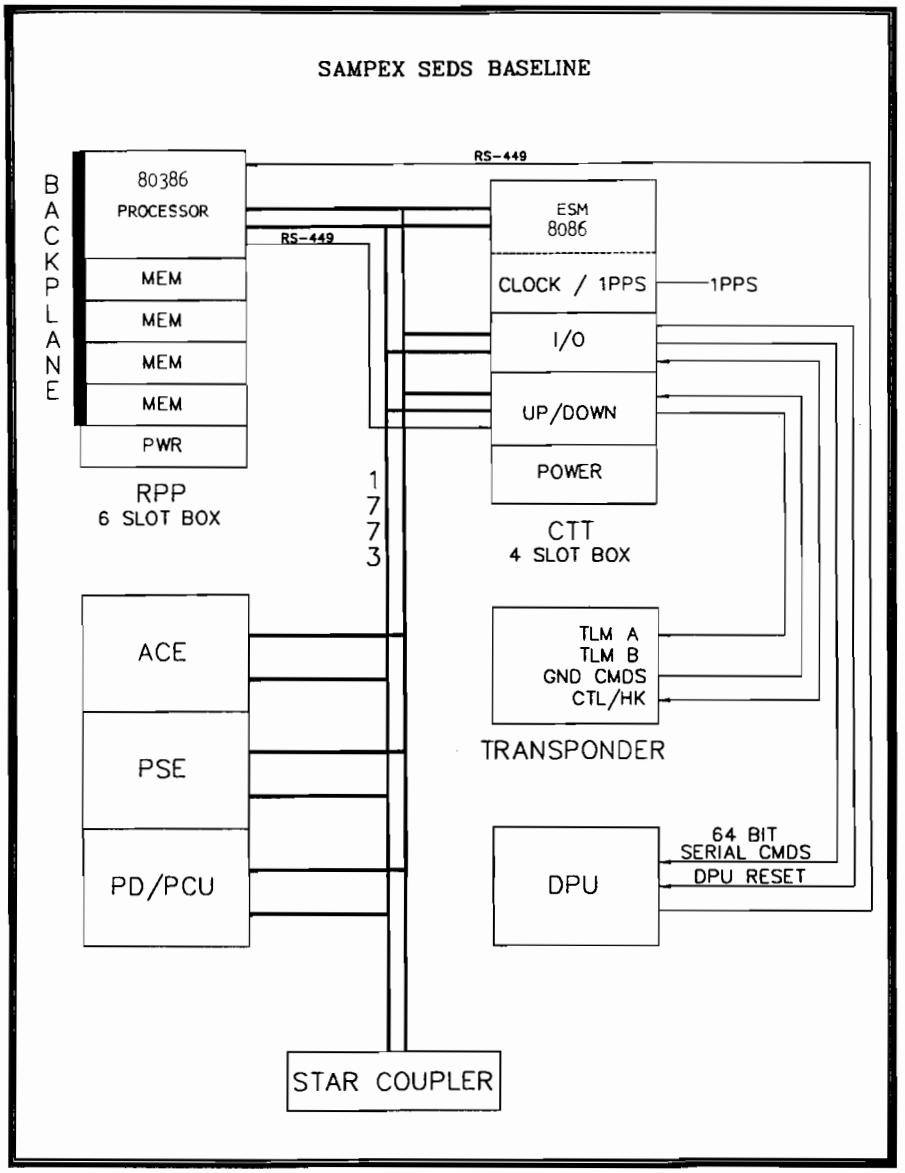

Fig. 5. The Small Explorer Data System (SEDS) functional diagram for the SAMPEX spacecraft.

frequency modes are high- and low-rate modes. Both modes consist of coherent tracking, which provides two-way Doppler and range data, simultaneously with telemetry and command.

The Data Processing Unit (DPU) is responsible for overall control of the science payload [4]. It serves as the interface between the science instruments and the spacecraft. The DPU controls sensor high-voltage power supplies and isobutane regulation based on status feedback from the sensor electronics, and it performs instrument housekeeping functions. It also is responsible for packetizing instrument data and passing these formatted data to the spacecraft.

IV. Instrument Complement

The instruments on the SAMPEX spacecraft are the Low Energy Ion Composition Analyzer (LEICA), the Heavy Ion Large Telescope (HILT), the Mass Spectrometer Telescope (MAST), and the Proton/Electron Telescope (PET).

A. Low Energy Ion Composition Analyzer (LEICA)

The LEICA instrument is a time-of-flight mass spectrometer that identifies incident ion mass and energy by simultaneously measuring the time-of-flight and residual kinetic energy of particles that enter the telescope and stop in an array of four solid state detectors. The time-of-flight is determined by START and STOP pulses from chevron microchannel plate (MCP) assemblies that detect secondary electrons emitted from the entrance foil and a foil in front of the solid state detector, respectively, when the ion passes through them. These secondary electrons are accelerated to approximately 1 KV and deflected onto the MCP's by electrostatic mirrors. The measured energy and velocity are combined to yield the mass of the ion and the energy per nucleon. Details of the LEICA instrument are presented by Mason *et al.* [5].

TABLE I
SAMPEX SCIENTIFIC INSTRUMENTS

Energy Range for:	LEICA	HILT	MAST	PET
Electrons	—	—	—	0.4–30 MeV
H	0.76–6.1	—	—	18–250 MeV
He	0.45–6.1	4.3–38	7–20	18–350 MeV/nuc
C	0.44–11.4	7.2–160	14–210	34–120 MeV/nuc
Si	0.33–5.5	9.6–177	21–330	54–195 MeV/nuc
Fe	0.21–3.1	11.0–90	27–450	70–270 MeV/nuc
Charge range for elements	1–25	2–28	2–28	1–2 1–28*
Charge range for isotopes	2–16	2	2–28	1–2 1–10*
Geometry factor (cm^2sr)	0.8	60	7–14	0.3–1.6
Field of Viw (deg, full angle)	24 × 20	68 × 68	101	58
Mass (kg)	7.4	22.8	8.8	(incl. with MAST)
Power (W)	4.9	5.6	5.3	(incl. with MAST)
Telemetry (kbps)	1.3	0.9	1.4	0.5

*commandable low-gain mode

B. Heavy Ion Large Telescope (HILT)

The HILT sensor is designed to measure heavy ions from He to Fe in the energy range from 8 to 220 MeV/nucleon for oxygen, covering the medium-energy solar energetic ions, the galactic cosmic rays, and the range of maximum intensity of the anomalous cosmic ray component. The sensor consists of a three-element ion drift chamber with two thin multilayer entrance windows followed by an array of 16 solid state detectors and a scintillation counter with photodiodes. The HILT instrument uses a flow-through isobutane system for the drift chamber. The fluid isobutane tank in SAMPEX is located with its longitudinal axis on the spin axis of the payload. The tank is 40.6 cm long by 24.1 cm in diameter with a volume of 1.5×10^4 cm^3. At launch the tank was approximately 90% filled with isobutane fluid. The isobutane storage tank is a major component of the SAMPEX spacecraft as shown in Fig. 2 (see also Klecker *et al.* [6]).

C. Mass Spectrometer Telescope (MAST)

MAST (see Cook *et al.* [7]) is designed to measure the isotopic composition of elements from Li ($Z = 3$) to Ni ($Z = 28$) in the range from approximately 10 MeV/nucleon to several hundred MeV/nucleon. MAST consists of a combination of surface barrier and lithium-drifted solid-state detectors (11 total). Combined matrix detector positions determine the particle trajectories, allowing accurate corrections to be made for the pathlength variation with angle and detector response nonuniformities. Although optimized for isotopic analysis of the elements Li to Ni, MAST also performs measurements of stopping He isotopes from approximately 7 to 20 MeV/nucleon. In addition, MAST analyzes particles that penetrate the entire stack, providing differential energy spectra of the more abundant elements to well beyond the endpoint energy for stopping particles, and integral flux measurements at higher energies. A priority system ensures that the most interesting events are selected for readout, with stopping $Z \geq 3$ events given the highest priority. However, because MAST is assigned a high telemetry data rate, the pulse heights from essentially all stopping $Z \geq 3$ nuclei can be transmitted, even in very large flares.

D. Proton/Electron Telescope (PET)

The PET system is designed to complement MAST by measuring the energy spectra and relative composition of protons (18 to 250 MeV) and helium nuclei (18 to 350 MeV/nuclei) of solar, interplanetary, and galactic origins, and the energy spectra of solar flare and precipitating electrons from approximately 0.4 to ~30 MeV. The instrument measures both trapped and precipitating energetic particles in different parts of the SAMPEX orbit. It also has the capability to look at manmade particle populations such as positrons which are emitted by nuclear reactors that have flown previously in low-Earth orbit. The PET system can also duplicate and extend some measurement capabilities of MAST by providing energy spectra and elemental composition of nuclei from Li through Fe using a commandable high-gain mode. It provides some isotopic information on nuclei from H to Ne. Details of the PET sensor system are provided by Cook *et al.* [8]. Table I summarizes the SAMPEX instrument characteristics and Fig. 6 shows the connectivity of the instruments and subsystems.

V. INFORMATION ACQUISITION AND OPERATIONAL DATA FLOW

The SAMPEX spacecraft is operated through the Project Operations Control Center (POCC) located at Goddard Space Flight Center. The mission operation activity is manned 24 hours a day, 7 days a week. The data are transmitted to the ground twice per day through the Wallops Flight Facility. The data are transmitted as a series of CCSDS transfer frames. Commanding is performed once per day. Command data are also CCSDS compliant. (Notably, SAMPEX is the first NASA mission to fully exercise the CCSDS data system recommendations for packetized command and telemetry.) Spacecraft planning and scheduling determine the spacecraft

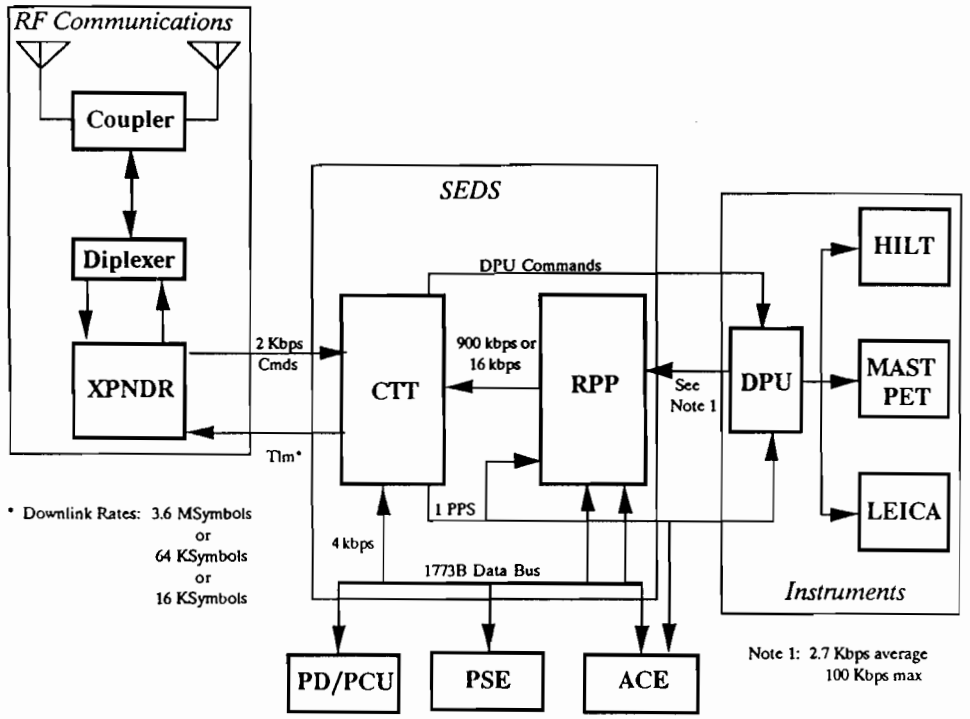

Fig. 6. The science instrument and major subsystem connectivity for the SAMPEX spacecraft.

operations and the coordination of ground system elements to ensure successful science data collection. Science operations for the SAMPEX mission can be described as routine (as opposed to missions which have a campaign or an interactive style of operations). There is no daily interaction between instrument representatives and the spacecraft, and instrument command functions for routine operations are performed by the onboard Data Processing Unit. The DPU is responsible for overall control of the science payload and controls the data acquisition from each instrument and packetizes science data for recording by the Small Explorer Data System. Instrument calibrations are performed on a periodic (~monthly) basis. Requests for special operations originate from instrument representatives and are transmitted to the Flight Operations Team using the University of Maryland Science Operations Center (UMSOC) as intermediary. The UMSOC is the primary point of contact between Flight Operations and the experimenters. Requests for special operations are transmitted to the Operations Team by means of the NASA Science Internet or by means of fax transmission.

Science data are recorded onboard the spacecraft in the SEDS. The details of the data sampling and recording scheme are described by Mabry *et al.* [4]. Science data recording is cycled between two recorder partitions, each recording approximately 12 hours of data. The data are played back twice per day at the Wallops Flight Facility (WFF) Orbital Tracking Station. Playback data quality statistics from ground system elements can be compared to spacecraft telemetry to verify the quality of the downlink. Should the recorder dump quality be unacceptably low, WFF support on the following orbit is then scheduled. Next-orbit playback opportunities are expected to occur approximately 40% of the time. If the second contract does not exist, cannot be scheduled, or if the dump taken at the second Wallops support is still not of acceptable quality, the data partition onboard the spacecraft will be released and the data lost. WFF transfers the data stream to the Goddard Space Flight Center (GSFC). The Packet Processor (PACOR) interfaces with the ground station via the NASA Communications System, and records all incoming data. All data transfers to PACOR occur during real-time contacts with the spacecraft or by playback from the ground station (see Fig. 7).

PACOR performs level zero processing on the incoming telemetry, and extracts the science data. It transmits the science data sets to the UMSOC in 24-hour blocks. The following list outlines the basic functions performed by PACOR:

- Data capture
- Transfer frame extraction from NASCOM blocks
- Checking of cyclical redundancy code
- Separation of virtual channels, packet extraction and reassembly
- Logging of received playback transfer frames to magnetic media
- Grouping and time ordering of data sets
- Deletion of redundant data
- Quality and accounting data generation
- Store and forward prepared data sets to users via electronic transfer

Data are transmitted via electronic links between the ground station and the POCC, the ground station and PACOR, and PACOR and the UMSOC. The data are stored on analog tapes at the ground station and on optical disk (short term) and magnetic tape (long term) by PACOR. UMSOC distributes the science data to all the co-investigators (Langley Research

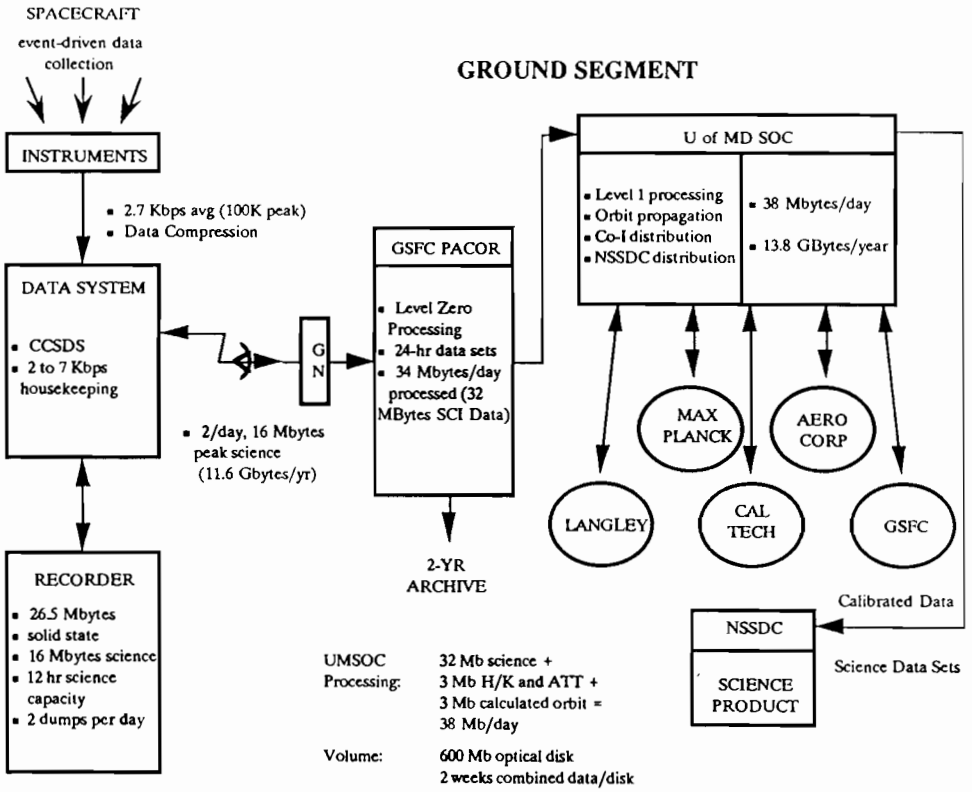

Fig. 7. The overall operational data flow from the SAMPEX spacecraft into the SMEX ground segment.

Center, Max Planck Institute, Caltech, Aerospace Corp, and Goddard Space Flight Center) and to the National Space Science Data Center (NSSDC).

WFF supports science data recorder dumps at 4, 16, and 900 Kbps downlink telemetry rate. The Deep Space Network sites only receive the 4 and 16 Kbps downlink telemetry rate. The Network anticipates station upgrades in 1993 which will allow for the 900 Kbps telemetry rate. The data are transmitted from the ground station to the POCC and PACOR on a 1.544 Mbps link. Level zero processed data are transmitted from PACOR to the UMSOC on a 56 Kbps link.

UMSOC delivers data to the instrument teams using a SAMPEX team standard which is called the tennis standard and is very compatible with the NASA/CCSDS packet standard used for the telemetry downlink and with the NASA/CCSDS Standard Formatted Data Unit. The instrument teams are encouraged to use the tennis standard for internal processing and for data returned to UMSOC for archiving and delivery to the NSSDC. The standard emphasizes self-documenting data structures and minimizes computer and operating system dependences. Monthly summary plots of the instrument performance and particle activity will be published in the U.S. Department of Commerce, National Oceanic and Atmospheric Administration publication, "Preliminary Report and Forecast of Solar Geophysical Data." During the 1-year period of proprietary data ownership, additional publications or data release will generally require the approval of the SAMPEX Science Working Group, with specific written approval provided by the SAMPEX Principal Investigator and the Project Scientist.

ACKNOWLEDGMENT

The authors wish to thank the large team of people who have made the SAMPEX project such a success. They thank the engineering leads on the SAMPEX project at GSFC including: J. Kellogg, P. Salerno, C. Clagett, D. Nguyen, A. Ahmad, G. Rakow, H. Maldonado, G. Cooper, J. Stephens, K. Hersey, B. Patschke, Q. Nguyen, and P. Mule. The authors also thank the Mission Operations team, especially J. Catena, D. Bradley, and D. Welch. The mission software manager is R. Hollenhorst and the flight assurance manager is R. Kolecki. We thank S. Kanekal (GSFC) and R. Boughner (LARC) for general scientific software development. The entire GSFC team has done an outstanding job.

The management of GSFC is acknowledged for its strong, continuing support of the SAMPEX program. Special thanks are extended to Dr. Frank McDonald, former Associate Director of GSFC, for his insightful and effective guidance of the initial SMEX approach. At NASA HQ, we thank Dr. Len Fisk for developing and successfully promoting the SMEX concept to top NASA management and to Congress. We thank Drs. Charlie Pellerin, George Newton, and David Gilman of the Astrophysics Division for their highly effective and supportive management of the SMEX program. We also thank Drs. George Withbroe and Vernon Jones of the Space Physics Division for their continuing help and attention to SAMPEX. Finally, we would like to acknowledge the debt of gratitude owed to the late Dr. Stan Shawhan who played such a key role in the promotion of SMEX and in the early success of the SAMPEX concept.

REFERENCES

[1] D. N. Baker, G. Chin, and R. F. Pfaff, Jr., "NASA's Small Explorer program," *Phys. Today,* vol. 44, p. 44, 1991.

[2] L. A. Fisk, B. Kozlvsky, and R. Ramaty, "An interpretation of observed oxygen and nitrogen enhancements in low-energy cosmic rays," *Astrophys. J. Lett., 190,* L35, 1974; J. H. Adams *et al.,* "The charge state of the anomalous component of cosmic rays", *Astrophys. J. Lett., 375,* L45, 1991.

[3] L. B. Callis, D. N. Baker, J. B. Blake, J. D. Lambeth, R. E. Boughner, M. Natarajan, R. W. Klebesadel, and D. J. Gorney, "Precipitating relativistic electrons: Their long-term effect on stratospheric odd nitrogen levels," *J. Geophys. Res.,* vol. 96, 2939, 1991.

[4] D. J. Mabry, S. J. Hansel, and J. B. Blake, "The SAMPEX Data Processing Unit (DPU)," *IEEE Trans. Geosci. Remote Sensing,* vol. 31, pp. 572–574, May 1993.

[5] G. M. Mason *et al.,* "LEICA: A low energy ion composition spectrometer for the study of solar and magnetospheric heavy ions," *IEEE Trans. Geosci. Remote Sensing,* vol. 31, pp. 549–556, May 1993.

[6] B. Klecker *et al.,* "HILT: A heavy ion large proportional counter telescope for solar and anomalous cosmic rays," *IEEE Trans. Geosci. Remote Sensing,* vol. 31, pp. 542–548, 1993.

[7] W. R. Cook *et al.,* "MAST: A mass spectrometer telescope for studies of the isotopic composition of solar, anomalous, and galactic cosmic ray nuclei," *IEEE Trans. Geosci. Remote Sensing,* vol. 31, pp. 557–564, 1993.

[8] W. R. Cook *et al.,* "PET: A proton/electron telescope for studies of magnetospheric, solar, and galactic particles, *IEEE Trans. Geosci. Remote Sensing,* vol. 31, pp. 565–571, 1993.

Daniel N. Baker received the Ph.D. degree in 1974 from the University of Iowa.

He is the Chief of the Laboratory for Extraterrestrial Physics at NASA's Goddard Space Flight Center. He has done research in spacecraft instrumental design and calibration, space physics data analysis, and magnetospheric modeling. He has studied plasma physical and energetic particle phenomena in magnetospheres of Jupiter and Mercury, and he has studied extensively the plasma sheet and magnetopause boundary regions of the Earth's magnetosphere. His recent experience has been in the analysis of large data sets from spacecraft at geostationary orbit, in the analysis of data from the deep magnetotail and comets, in the study of solar wind-magnetospheric energy coupling, and theoretical modeling of the possible role of heavy ions in the development of magnetotail instabilities. His present interests concentrate on the problem of substorms and magnetosphere-atmosphere coupling. He is the author or co-author of more than 250 scientific papers in refereed journals in the area of space research.

Dr. Baker has served on numerous NASA and NSF committees, and held many other positions such as Magnetospheric Section Secretary for AGU, Associate Editor of Geophysical Research Letters, and U.S. SCOSTEP representative. He is the NASA Small-Class Explorer Project Scientist, the POLAR spacecraft Project Scientist, and is the U.S. Coordinating Scientist for STEP (Solar-Terrestrial Energy Program).

Glenn M. Mason received the B.A. degree in physics from Harvard College, and the Ph.D. degree in physics from the University of Chicago.

He came to the University of Maryland in 1977, and is now Professor jointly in the Department of Physics and the Institute for Physical Science and Technology. His recent research work has concentrated on the composition of solar energetic particles, and the acceleration and transport of particles both in the solar atmosphere and in the interplanetary medium. He is Principal Investigator on the NASA Solar, Anomalous, and Magnetospheric Explorer.

Orlando Figueroa was born in San Juan, Puerto Rico on September 9, 1955. He received the B.S. degree in mechanical engineering from the University of Puerto Rico, Mayaguez campus in 1978 and has completed several graduate studies in mechanical engineering at the University of Maryland.

In his 15 years career at the Goddard Space Flight Center, he has served as a member of the mechanical integration and test team for the Heat Capacity Mapping Mission (HCMM); Cryogenics engineer for the Cosmic Background Explorer (COBE) Diffuse Infrared Background Experiment (DIRBE); head of the Cryogenics Technology Section in the Space Technology Division; manager for the Superfluid Helium on Orbit Transfer (SHOOT) Experiment; and is presently the Project Manager for the SMall EXplorers (SMEX) missions.

Throughout his career, Mr. Figueroa has received several awards for group achievements, outstanding performance and was awarded the NASA Outstanding Leadership medal in March 1993 for the management of the SMEX program during the successful development and launch of the Solar Anomalous and Magnetospheric particle EXplorer. He is a member of the International Academy of Astronautics.

G. Colon, photograph and biography not available at the time of publication.

J. G. Watzin, photograph and biography not available at the time of publication.

Roberto M. Aleman received the B.S. degree in biology in 1982 and the B. S. degree in electrical engineering in 1985, both from the University of Puerto Rico, Mayaguez campus.

He worked for the Department of the Navy until he joined the Antenna Technology Branch at NASA/GSFC as an antenna engineer in July 1987. In May 1990, he joined the Small Explorers (SMEX) Project as the SAMPEX Instruments Manager. He is currently the Instruments Manager for FAST, the second SMEX mission scheduled for launch in August 1994.

HILT: A Heavy Ion Large Area Proportional Counter Telescope for Solar and Anomalous Cosmic Rays

B. Klecker, D. Hovestadt, M. Scholer, H. Arbinger, M. Ertl, H. Kästle, E. Künneth, P. Laeverenz, E. Seidenschwang, J. B. Blake, N. Katz, and D. Mabry

Abstract— **The HILT sensor has been designed to measure heavy ion elemental abundances, energy spectra, and direction of incidence in the mass range from helium to iron and in the energy range 4 to 250 MeV/nucleon. With its large geometric factor of 60 cm^{2}sr the sensor is optimized to provide compositional and spectral measurements for low intensity cosmic rays, i.e. for small solar energetic particle events and for the anomalous component of cosmic rays. The instrument combines a large area ion drift chamber–proportional counter system with two arrays of 16 Li-drift solid state detectors and 16 CsI crystals. The multi dE/dx-E technique provides a low background mass and energy determination. The sensor also measures particle direction. Combining these measurements with the information on the spacecraft position and attitude in the low altitude polar orbit, it will be possible to infer the ionic charge of the ions from the local cutoff of the Earth's magnetic field. The ionic charge in this energy range is of particular interest because it provides unique clues to the origin of these particles and has not been investigated systematically so far. Together with the other instruments on board SAMPEX (LEICA, MAST, and PET), a comprehensive measurement of the entire solar and anomalous particle population will be achieved.**

I. Introduction

THE HILT (Heavy Ion Large Telescope) sensor, together with the LEICA sensor, was originally developed for a Get-Away-Special Payload (G-0335) to measure solar and anomalous cosmic rays in a high inclination shuttle orbit at solar minimum conditions [1]. The payload was scheduled for a series of STS flights starting in 1986. However, because of the Challenger accident, it was delayed and finally flown only once on the space shuttle mission STS-28 in August 1989. In a collaborative effort of the Max-Planck-Institut für Extraterrestrische Physik and the Aerospace Corporation, the HILT sensor has been modified to extend the range of elements and energies covered. The measurements now include heavy ions from helium to iron in the energy range from 4 to 250 MeV/nucleon. The sensor thus covers the maximum intensity of the anomalous component of cosmic rays and the medium energy range of solar energetic ions. The sensor utilizes a large area ion drift chamber, two position sensitive proportional counters, an array of 16 silicon solid state detectors and a CsI crystal unit to determine the nuclear charge, the energy, and the direction of ions entering the telescope. In the low altitude ($\approx$600 km) polar orbit of SAMPEX, this information will be used to infer the ions' ionic charge from the local cutoff of the magnetic field of the Earth.

Manuscript received August 3, 1992; revised January 25, 1993. This work was supported in part by DARA with Contract 50 OC 90021 and at The Aerospace Corporation by the NASA Cooperative Agreement 26979B.

B. Klecker, D. Hovestadt, M. Scholer, H. Arbinger, M. Ertl, H. Kastle, E. Kunneth, P. Laeverenz, and E. Seidenschwang are with the Max-Planck-Institut für Extraterrestrische Physik, W-8046 Garching bei München, Germany.

J. B. Blake, N. Katz, and D. Mabry are with The Aerospace Corporation.

IEEE Log Number 9208070.

II. Scientific Objectives

A. Solar Energetic Particles

During the last few years it has been recognized that solar energetic particle events (SEP) can be divided into two classes, based on the time scale of the electromagnetic emissions of their associated flares. SEP events associated with impulsive flares have mostly low particle intensities, high ^{3}He/^{4}He flux ratios, enhanced abundances of heavy elements, charge states indicative of heated flare plasma ($\approx 10^7$ K), high electron to proton flux ratios and high ratios of solar (interacting or trapped) to interplanetary (escaping) protons. The SEP events associated with gradual flares are characterized by large particle intensities in interplanetary space, low ^{3}He/^{4}He ratios, low electron to proton flux ratios, low ratios of solar to interplanetary proton intensities and charge states indicative of typical (2×10^6 K) coronal temperatures (e.g., [2] and references therein). Due to the limited collecting power of the instrumentation previously flown, composition and energy spectra for impulsive events have been studied only over a small energy range (e.g., [3], [4]). HILT, with its large geometric factor of 60 cm^{2}sr, will provide spectral and compositional information in particular for the low intensity events associated with impulsive flares. At high flux levels (>5 protons/cm^{2}s sr MeV/n at 5 MeV) pulse pile-up and accidental coincidences will degrade the performance of the instrument. However, flux levels exceeding this value are observed in interplanetary space only during very large, shock associated energetic particle events. However, with the four instruments of the SAMPEX payload a comprehensive measurement of the entire SEP population will be achieved (see also [5], [6]).

The large temperature differences as derived from heavy ion charge states observed in impulsive and gradual flares [7] show that the charge state measurements provide crucial

information. So far charge state measurements have been obtained only at energies <3 MeV/nucleon during a limited time period on ISEE-3 [8]. In the low altitude polar orbit of SAMPEX, it will be possible to extend these studies using the geomagnetic cutoff as described below.

B. Anomalous Component of Cosmic Rays

The anomalous component of cosmic rays (ACR) has been studied extensively since its discovery in the 1972–1977 solar minimum. In the energy range below ≈ 50 MeV/nucleon, at least six elements have been found (He, C, N, O, Ne, Ar) whose energy spectra show anomalous increases in flux above the quiet time galactic cosmic ray spectrum and whose composition is different from the solar or galactic cosmic ray composition [9]. There have been a number of models proposed to explain the ACR component. The most plausible theory for the origin of the ACR identifies neutral interstellar gas as the source material (Fisk *et al.* [10]). The neutral particles, after penetrating into the inner heliosphere, are ionized by solar UV radiation or by charge exchange reactions with solar wind protons. After ionization, the now singly charged ions are picked up by the interplanetary magnetic field and carried with the solar wind to the outer heliosphere. There the ions are accelerated to high energies, possibly at the solar wind termination shock [11]. A unique prediction of the model of Fisk *et al.* is that the anomalous cosmic rays should be singly ionized. Although indirect evidence for low charge states of the ACR has been found in many investigations (e.g., [12], [13]), results from a more direct measurement using the transmission of the Earth's magnetic field are sparse [14], [15]. It was only recently that a more systematic study of ACR oxygen charge states was started in a collaborative effort of many institutions [16]. The large collecting power of HILT and MAST [17] combined with an accurate measurement of time, position, and particle direction should overcome many of the difficulties encountered previously and provide definitive measurements of the charge state of oxygen and the less abundant ions of anomalous cosmic rays.

Recently, the discovery of anomalous cosmic ray oxygen trapped in the Earth's magnetosphere after charge exchange at low altitudes has been reported [18]. The low altitude polar orbit of SAMPEX will provide an excellent opportunity to study this newly discovered trapped component in great detail and to extend the present measurement of trapped oxygen to the less abundant ions.

C. Determination of Ionic Charge States

The geomagnetic cutoff can be used to infer the ionic charge of heavy ions. The cutoff rigidity, R_c, depends in general on the location in the magnetic field of the Earth and on the direction of the particle. The local cutoff R_c can be computed by using a model of the magnetic field of the Earth and trajectory tracing techniques. The particle rigidity, R, depends on kinetic energy per nucleon (T), mass (A), total energy per nucleon ($T + E_0$), and ionic charge (Q) as

$$R = T^{0.5*}(T + 2^*E_0)^{0.5*}A/Q\,.$$

Thus, after determining T and A from the measurement, an upper limit for the ionic charge Q can be obtained from the requirement $R > R_c$:

$$Q < T^{0.5}(T + 2^*E_0)^{0.5*}A/R_c\,.$$

For solar energetic particle events, the particle tracing technique can be complimented by the direct determination of the local cutoff rigidity from the cutoff in the proton spectrum, since the ionic charge is known in this case.

III. Instrument Description

The HILT sensor determines the mass, kinetic energy, and direction of particles entering the aperture by measuring the energy loss in a proportional counter–ionization chamber system and the residual energy in an array of 16 solid state detectors and a CsI crystal unit. A view of the sensor and analog and digital electronic in flight configuration is shown in Fig. 1. The instrument characteristics are summarized in Table I. The schematic diagram of HILT in Fig. 2 shows the main sensor components: a three-element ion drift chamber with thin aluminum entrance window (40 μg/cm^2), followed by an array of 16 solid state detectors (SSD) and 16 CsI scintillation counters which are embedded in a plate of PERSPEX material and viewed by four light sensitive silicon diodes. The entrance foil serves as part of the gas enclosure and, in combination with two additional aluminum foils ($2 \times 20\,\mu$g/cm^2), as a shield against micrometeoroid impacts. The entrance foils are protected by an acoustic cover (see Fig. 1) that can be opened and closed after launch.

A. Principle of Operation

The element or mass analysis is based on the combination of a multi dE/dx measurement in the position-sensitive proportional counter and ionization chamber system with the measurement of residual energy in the SSD detector array and the CsI crystal unit. The direction of incidence is derived from two position measurements as described below. With the information of particle energy, mass, and direction, in combination with the spacecraft position and attitude in the low altitude polar orbit, it will be possible to infer the ionic charge of the ions from the local cutoff of the Earth's magnetic field.

B. The Ion Drift Chamber—Proportional Counter System

The drift chamber–proportional counter system consists of three sections (Fig. 2). Electrons generated along the path of incoming ions drift in the electric field (85 V/cm) of the chamber to the front proportional counter (section I, PCF), to a charge collecting plate (section II, IC), and to the rear proportional counter (section III, PCR). The drift field is generated by a set of parallel wires (Mo, diameter 100 μ, spacing 5 mm) enclosing the drift chamber. In order to improve the homogeneity of the drift field near the wires, the inner layer of wires is enclosed by a second layer at a distance of 2 cm (see Fig. 2, note: only the top and bottom layers of wires are shown). In the first and third section of the drift chamber

TABLE I
HILT INSTRUMENT CHARACTERISTICS

Energy Range	Helium I	4.3–9.0	MeV/nuc (^{4}He)	PC-SSD coincid.
	Helium II	9.0–38	MeV/nuc (^{4}He)	PC-SSD-CsI coincid.
	Heavy Ion I	8.2–42	MeV/nuc (^{16}O)	PC-SSD coincid.
	Heavy Ion II	42.–220	MeV/nuc (^{16}O)	PC-SSD-CsI coincid.
Elemental Resolution (ΔZ)				
PC-SSD coincidence		0.3 FWHM	He < 9 MeV/n	
		0.3 FWHM	C, N, O < 42 MeV/n	
		0.6 FWHM	Fe < 75 MeV/n	
PC-SSD-CsI coincidence		0.5 FWHM	C, N, O > 42 MeV/n	
SSD-CsI coincidence		0.8 FWHM	C, N, O > 42 MeV/n (High Energy Mode)	
Mass Resolution (ΔA)		0.6 FWHM	He < 9 MeV/n	
View Angle		68 × 68	degree full angle	
Sensitive SSD area		159	cm^2	
Geometrical Factor		60	cm^2 sr	
Total Mass		22.8	kg including Isobutane supply	
Isobutane Counter Gas		7.2	kg	
Power		5.7	W at 40000 counts/s	
Telemetry		800	bps nominal allocation	

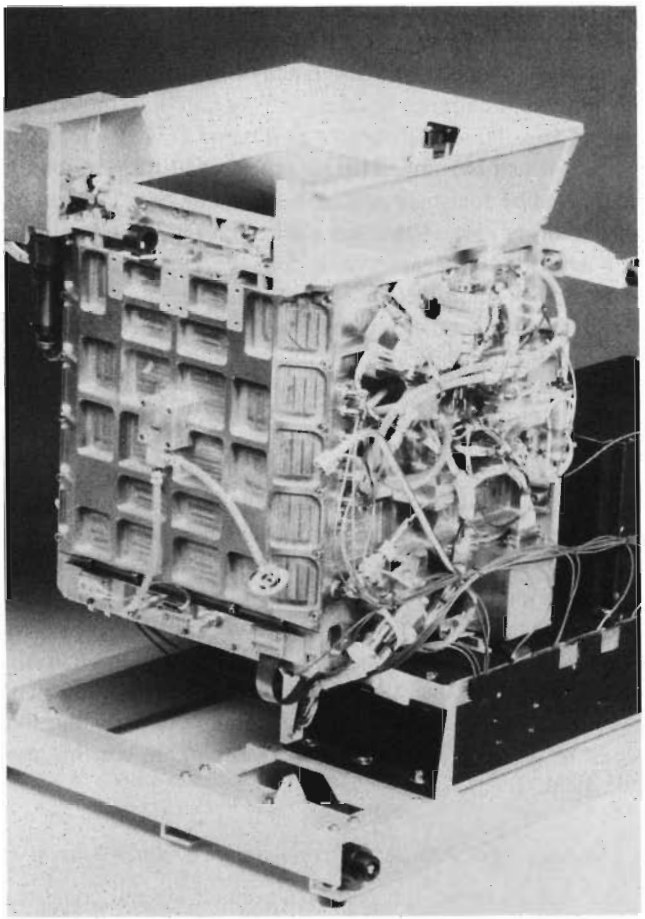

Fig. 1. HILT sensor with protective cover (closed), Isobutane system (right), and electronic box in flight configuration.

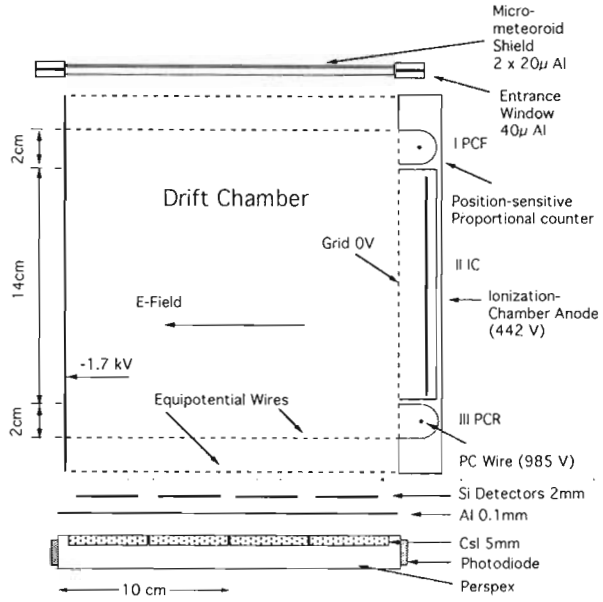

Fig. 2. Schematic cross section of HILT sensor.

energy loss and position of the ions are determined by two position-sensitive proportional counters with triangular shaped cathodes, the center element is operated as an ionization chamber and provides a third energy loss measurement. The energy loss of ions in all three sections is pulse height analyzed. The triple dE/dx measurement, in combination with the determination of the residual energy of the ions, provides a low background identification of ion type and energy in the mass range from helium to iron. In addition to the nuclear charge (element) resolution, the sensor also provides mass identification capability for helium (see also Table I).

The signals of the triangular shaped cathodes of the proportional counters are also pulse height analyzed. The ratios of the position and energy signal are a direct measure of the position along the proportional counter axis. In section I also the time elapsed between the response of the SSD's and the anode of PCF, i.e. the drift time of electrons generated along the track of incoming ions, is determined. Thus, drift time and position response of PCF provide two coordinates for the incoming ions at the top plane of the sensor. At the bottom plane the position response of PCR and the information on the detector row triggered by the incoming particles provide the other two coordinates. The trajectory of the incoming ions can be determined from these four coordinates The accuracy of the determination of the incident angle is limited by the diameter of the detectors and the energy and position response of the

TABLE II
HILT RATE DATA CHARACTERISTICS

Rate Acronym	Time Resolution (s)	Rate Type	Ion	Energy Range (MeV/Nucleon)	Geometry Factor (cm^2sr)
HE1	6	Coincidence	He	4.3–9	60
HE2	6	Coincidence	He	9.0–38	60
HZ1	6	Coincidence	$Z \geq 6$	8.2–42 (for ^{16}O)	60
HZ2	6	Coincidence	$Z \geq 6$	42.–220 (for ^{16}O)	60
HZ1*	6	Coincidence	$Z \geq 1$	5.–22 (for ^{1}H)	60
HZ2*	6	Coincidence	$Z \geq 1$	22.–60 (for ^{1}H)	60
SSD1	24	Single	$Z \geq 1$	> 5 (for ^{1}H)	15
SSD2	24	Single	$Z \geq 1$	> 5 (for ^{1}H)	15
SSD3	24	Single	$Z \geq 1$	> 5 (for ^{1}H)	15
SSD4	24	Single	$Z \geq 1$	> 5 (for ^{1}H)	15
PCFE	48	Single	$Z \geq 1$***	2.5–8 (for ^{1}H)	630
PCRE	48	Single	$Z \geq 1$***	2.5–8 (for ^{1}H)	190
IK	48	Single	$Z \geq 2$	3.0–9 (for ^{4}He)	300**
CsI	48	Single	$Z \geq 1$	22–60 (for ^{1}H)	105
HSSD1	0.1	Single	$Z \geq 1$	> 4 (for ^{1}H)	15
HSSD2	0.1	Single	$Z \geq 1$	> 4 (for ^{1}H)	15
HSSD3	0.1	Single	$Z \geq 1$	> 4 (for ^{1}H)	15
HSSD4	0.1	Single	$Z \geq 1$	> 4 (for ^{1}H)	15
HPCRE	0.1	Single	$Z \geq 1$***	2.5–21 (for ^{1}H)	190
HIK	0.1	Single	$Z \geq 1$	2.5–7 (for ^{1}H)	300**

* High Energy Mode
** energy dependent
*** efficiency for electrons at 0.6 MeV: $2*10^{-4}$

proportional counters and is typically 5° for $Z \geq 6$ ions at ≤ 40 MeV/nucleon. The trajectory information will be used for a path length correction of the energy loss measurement in the proportional counter–ionization chamber system to improve the elemental resolution of the sensor.

C. The Isobutane Regulation System

The drift chamber–proportional counter system operates with Isobutane at a pressure of 100 mbar (at 20°C). The density of the Isobutane is actively controlled by a gas regulation system consisting of a thermally controlled valve, a small ionization chamber with built-in ^{241}Am radioactive source (Alphatron), and regulation electronics. The volume of the Alphatron is directly connected to the sensor volume and the current from the ^{241}Am source is used in the regulation electronics for the control of the Isobutane in- flow by opening or closing the thermal valve. The Isobutane outflow can be controlled by a motor driven vent valve and flow regulation valve. The gas supply consists of 7.2 kg of liquid Isobutane, stored in one cylindrical aluminum–kevlar composite tank in the center of the spacecraft, and is sufficient for a continuous operation of 3 years. Similar regulation systems have been successfully flown on several MPE experiments for the IMP-7/8, S3-2, and ISSE-1/3 missions.

D. The Solid State Detector Array

Low energy ions are stopped in one of 16 circular Li-drift silicon solid state detectors. The thickness of the detectors is 2 mm and the sensitive area is 995 mm^2. The detectors are arranged in an 4×4 array with one row of four detectors connected to one amplifier chain. In addition to the pulse height analyzed energy signal the information on the particular row triggered by an ion is transmitted with the pulse height information. The total sensitive area and the sensor geometry result in a geometric factor of 60 cm^2sr for the coincidence measurement (see also Table II).

E. The CsI Crystal Array

High energy ions penetrating the solid state detectors are stopped in a set of 16 circular CsI crystals of 5 mm thickness and 46 mm diameter which are arranged behind the SSD array. The CsI signal is used to define low energy rates (CsI in anticoincidence) and high energy rates (PC-SSD-CsI coincidences, see also Tables I and II) for helium and $Z \geq 6$ ions. The CsI coincidence measurement extends the energy range of the sensor to 250 MeV/nucleon (for neon), however, without an anticoincidence measurement in the high energy section. The crystals are embedded in a rectangular plate (PERSPEX) of 2 cm thickness and are viewed by four light-sensitive silicon detectors. Due to limitations in the energy resolution of the CsI unit and the smaller signals in the IC-PC system for high energy ions the directional and elemental resolution is reduced, compared to low energies, and not sufficient to provide isotopic resolution for helium. However, elemental resolution for the more abundant elements can still be achieved (see Table I).

F. Electronics and Data Handling

Fast analog electronics provide the basic counting rate information needed for the computation of absolute fluxes,

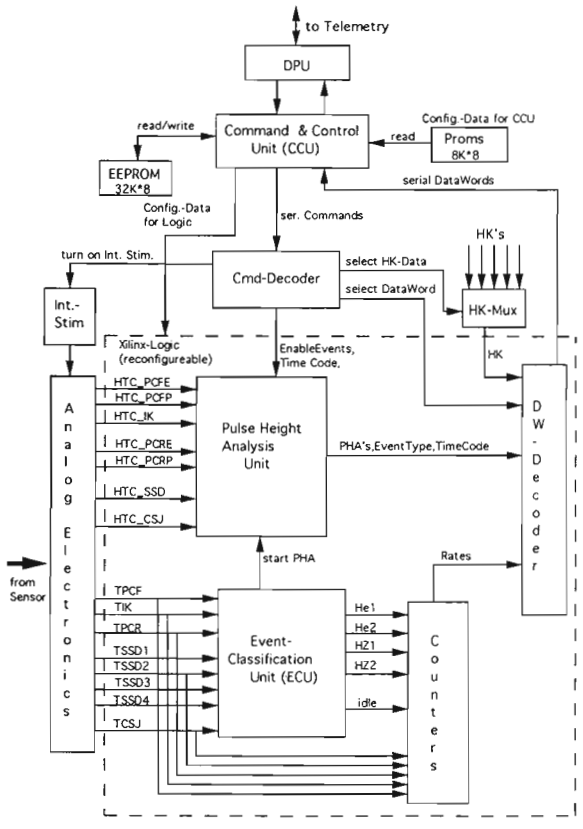

Fig. 3. Schematic block diagram of the HILT electronics.

while pulse height analysis contains the detailed energy, mass, position, and time information. All the information is read out and accumulated in the SAMPEX digital processing unit (DPU) and transmitted from there to the mass memory of the spacecraft data system [19].

The instrument analog electronics are designed to cover the energy range from a few MeV/nucleon to 5000 MeV total energy loss in the detector arrays for the elements in the mass range from helium to iron. A simplified block diagram is shown in Fig. 3. The signals from the analog electronic are processed in the Event Classification Unit (ECU) and Pulse Height Analysis Unit (PHAU). Both units are implemented in two XILINX 3090 programmable gate arrays. The configuration program for these units is stored in an EEPROM and loaded after every startup by the third XILINX, the Command and Control Unit (CCU). The CCU provides also the interface to the digital processing unit (see also [19]).

1) Rate Data: The rate data are derived from fast thresholds at the output of ten charge-sensitive amplifier chains. These thresholds are used in the Event Classification Unit (ECU) to define four rate channels, two for helium and two for $Z \geq 6$ ions (Basic Rates). These rates are accumulated and readout by the Digital Processing Unit (DPU) every 6 seconds. In addition to the Basic Rates, the lowest thresholds of all detector elements used in the ECU, three diagnostic rates on coincidence conditions, and the idle time of the system (to be used for dead time corrections), are monitored with reduced time resolution. These monitor rates provide integral measurements of the particle distribution and information on the health and safety of the experiment. Furthermore, low thresholds on the IC, PCR, and SSD1-4 channels are directly fed into the DPU and read out every 0.1 s providing information on particle intensity variations on a much shorter time scale. The monitor and high time resolution rates from the front and rear proportional counter are also sensitive to electrons which are scattered in the front foil or in the solid state detector array and then penetrate the ionization chamber at oblique angles. However, because of the low efficiency of the electron response (2×10^{-4}, see also Table II), these rates will be dominated by electrons only during passes of the electron radiation belts of the Earth.

The coincidence logic in the ECU can be switched by command into a mode where signals from the PC-IC system are not included in the coincidence conditions (High Energy Mode). This mode will be used after the Isobutane counter gas is all used up and thus will recover the SSD-CsI coincidence measurement. However, because no path-length correction is possible without the proportional counter system, the elemental resolution will be degraded and only allow the resolution of element groups (e.g., He, CNO, see also Table I). With the Isobutane system in operation, this mode can also be used to obtain measurements of proton spectra. A summary of the response of all the rate channels is provided in Table II.

2) Pulse Height Event Data: The signals of all channels are pulse height analyzed. The information on the signal amplitudes, the event type, the SSD row triggered and the time of observation is transmitted as one pulse height event. The DPU has complete control of the HILT event readout and a priority algorithm ensures that for high rates all four event types, corresponding to the four Basic Rates, would be analyzed at about the same rate. The total number of PHA events read out per sensor is limited by the memory allocation in the solid state recorder of the spacecraft (see also [19]), the maximum event rate can be selected by ground command and will be $\approx$10 events per second for each event type.

3) Instrument Performance: The position (and directional) resolution depends on the resolution of the drift time measurement and on the energy loss in the front and rear proportional counters. The resolution therefore depends on particle type and energy and is increasing with particle mass and decreasing with particle energy. Table III provides typical values of the position resolution as derived from calibration measurements. Table III shows that for helium and $Z \geq 6$ ions the position resolution is limited by the resolution of the proportional counter and the size of the solid state detectors, respectively. The resulting resolution of the zenith angle for $Z \geq 6$ ions at energies < 40 MeV/nucleon is typically $< 5°$ FWHM.

The elemental resolution of the sensor depends on the resolution of the energy loss measurement in the proportional counter–ionization chamber system and on the accuracy of the trajectory determination for path length correction. Thus, the elemental resolution depends on particle type and energy (see also Table I). In Fig. 4 the energy loss in the front proportional counter (PCF) and the residual energy in the solid state detector array for carbon and oxygen in a calibration measurement have been converted into a nuclear charge scale. The data show that the nuclear charge resolution in the energy range

TABLE III
HILT POSITION RESOLUTION

Measurementz	^{4}He	^{16}O	^{40}Ar
Energy (MeV/n)	25	30	12.6
Position Resolution in Top Plane (FWHM)	(cm)	(cm)	(cm)
PCF	7.0	0.80	0.40
Drift	1.1	0.85	0.55
Position Resolution in Bottom Plane (FWHM)			
PCR	8.0	1.2	0.6
SSD	3.5	3.5	3.5

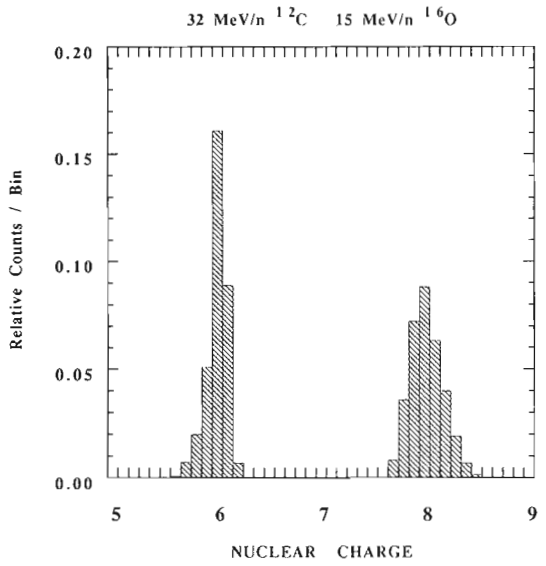

Fig. 4. Nuclear charge histogram derived from the measurement of energy loss in PCF and residual energy in SSD.

10 to 32 MeV/nucleon is $\approx$0.3 (FWHM), i.e. all elements between helium and oxygen can easily be resolved. The elemental resolution of the rear proportional counter and of the ionization chamber is similar to the one shown. This provides some redundancy because all three sections of the proportional counter–ionization chamber system can be used independently for the identification of elements.

4) Data Products: Routine data products from HILT will include time versus counting rate plots of the four Basic Rates and of selected monitor rates. These rate plots will be the basis for the selection of time periods for further detailed analysis of HILT data and for the collaborative investigation of particular events with all sensors on board SAMPEX and other spacecraft. Basic rate data and pulse height data obtained at high geomagnetic latitudes, where cutoff effects are negligible, will be used to compute absolute fluxes and energy spectra for different ions during solar particle events. Pulse height data at lower latitudes will be used to compute the trajectories of the ions in the magnetic field of the Earth to infer the ionic charge of the ions.

ACKNOWLEDGMENT

The authors would like to thank the many individuals and institutions who contributed to the design, fabrication, and test of the instrument. We are also grateful for the devoted work of the technical staff and the workshops at the Max-Planck-Institut für Extraterrestrische Physik and at The Aerospace Corporation.

REFERENCES

[1] D. Hovestadt, B. Klecker, P. Laeverenz, E. Seidenschwang, G.M. Mason, P.D. Bedini, G. Gloeckler, D.C. Hamilton, J.B. Blake, and D. Chenette, "Experiment for charge determination of cosmic rays of interplanetary and solar origin on the space shuttle," *Proc. 20th Internat. Cosmic Ray Conf. (Moscow),* vol. 4, p. 406, 1987.
[2] D.V. Reames, "Energetic particles from impulsive solar flares," *Ap. J. Supp.,* vol. 73, p. 235, 1990.
[3] G.M. Mason, D.V. Reames, B. Klecker, D. Hovestadt, and T.T. von Rosenvinge, "The heavy ion compositional signature in ^{3}He solar particle events," *Ap. J.,* vol. 303, p. 849, 1986.
[4] E. Möbius, M. Scholer, D. Hovestadt, B. Klecker, and G. Gloeckler, "Comparison of helium and heavy ion spectra in ^{3}He-rich solar flares with model calculations based on stochastic Fermi acceleration in Alfvén turbulence," *Ap. J.,* vol. 259, p. 397, 1982.
[5] D.N. Baker, G.M. Mason, O. Figueroa, G. Colon, J.G. Watzin, and R.M. Aleman, "An overview of the Solar, Anomalous, and Magnetospheric Particle Explorer (SAMPEX) Mission," *IEEE Trans. Geosci. Remote Sensing.,* vol. 31, p. 531–541, May 1992.
[6] G.M. Mason, D.C. Hamilton, P.H. Walpole, K.F. Heuermann, T.L. James, M.H. Lennard, and J.E. Mazur, "LEICA: A low energy ion composition analyzer for the study of solar and magnetospheric heavy ions," *IEEE Trans. Geosci. Remote Sensing.,* vol. 31, p. 549–556, May 1992.
[7] A. Luhn, B. Klecker, D. Hovestadt, and E. Möbius, "The mean ionic charge of silicon ^{3}He-rich solar flares," *Ap. J.,* vol. 317, p. 951, 1987.
[8] D. Hovestadt, *et al.,* "The nuclear and ionic charge distribution particle experiments on the ISEE-1 and ISEE-C spacecraft," *IEEE Trans. Geosci. Electr.,* vol. GE-16, p. 166, 1978.
[9] G. Gloeckler, "Compositions of energetic particle populations in interplanetary space," *Rev. Geophys. Space Phys.,* vol. 17, p. 569, 1979.
[10] L.A. Fisk, B. Kozlovsky, and R. Ramaty, "An interpretation of the observed oxygen and nitrogen enhancements in low-energy cosmic rays," *Ap. J. (Letters),* vol. 190, p. L39, 1974.
[11] J.R. Jokipii, "Particle acceleration at a termination shock 1. Application to the solar wind and the anomalous component," *J. Geophys. Res.,* vol. 91, p. 2929, 1986.
[12] R.B. McKibben, "An experimental test for the charge state of the "anomalous" helium component," *Ap. J. (Letters),* vol. 217, p. L113, 1977.
[13] B. Klecker, D. Hovestadt, G. Gloeckler, and C.Y. Fan, "On the charge state of the anomalous oxygen component," *Geoph. Res. Lett.,* vol. 7, p. 1033, 1980.
[14] K. Oschlies, R. Beaujean, and W. Enge, "On the charge state of anomalous oxygen," *Ap. J.,* vol. 345, p. 776, 1989.
[15] R.K. Singh, *et al.,* "Ionization states of the anomalous cosmic rays," *Ap. J.,* vol. 374, p. 753, 1991.
[16] J.H. Adams, Jr., *et al.,* "The charge state of the anomalous component of cosmic rays," *Ap. J. (Letters),* vol. 375, p. L45–L48, 1991.
[17] W.R. Cook *et al.,* "MAST: A mass spectrometer telescope for studies of the isotopic composition of solar, anomalous, and galactic cosmic ray nuclei," *IEEE Trans. Geosci. Remote Sensing.,* vol. 31, p. 557–564, 1992.
[18] N.L. Grigorov, *et al.,* "Evidence for trapped anamolous cosmic ray oxygen ions in the inner magnetosphere," *Geophys. Res. Letters,* vol. 18, p. 1959, 1991.
[19] D.J. Mabry, S.J. Hansel, and J.B. Blake, "The SAMPEX data processing unit (DPU)," *IEEE Trans. Geosci. Remote Sensing.,* vol. 31, p. 572–574, 1992.

Berndt Klecker received the Ph.D. degree in Physics from the Technical University of Munich, Germany, in 1978.

He worked at the Max-Planck-Institut für Extraterrestrische Physik at Garching, Germany, since 1976 specializing on experimental and theoretical cosmic ray physics. He was collaborator and coinvestigator on many energetic particle experiments on several magnetospheric and interplanetary spacecraft (e.g., GRS-A AZUR, ESRO-IV, IMP-7 and -8, ISEE-1, ISEE-3/ICE, AMPTE, SAMPEX, SOHO, CLUSTER).

Dietrich Hovestadt received the Diploma in Physics at the University of Hamburg, in 1960 and the Ph.D. degree in nuclear physics at the Technical University Munich, in 1964.

In 1964 he joined the Max-Planck-Institut for Physik and Astrophysik in Munich, working as the head of the energetic particle group. Since 1966 he has worked experimentally in the field of magnetospheric particle, solar, and interplanetary cosmic ray physics. He participated in many satellite-borne experiments and was principal investigator on several of them.

Manfred Scholer received the Ph.D. degree in physics from the Technical University Munich in 1969.

During 1969–1970 he held a ESA/NASA fellowship at the California Institute of Technology. He joined the Max-Planck-Institut für Extraterrestrische Physik in 1971 as a staff member and became group leader in 1985. He was Collaborator on the spacecraft missions AZUR GRS-1, ESRO IV, IMP-7, IMP-8, and Co-Investigator on ISEE-1, ISEE-3, and AMPTE-IRM. His current interests are numerical simulations of processes in space plasmas.

Dr. Scholer is a member of AGU and the German Physics Society.

H. Arbinger, photograph and biography not available at the time of publication.

M. Ertl, photograph and biography not available at the time of publication.

H. Kästle, photograph and biography not available at the time of publication.

E. Künneth, photograph and biography not available at the time of publication.

P. Laeverenz, photograph and biography not available at the time of publication.

E. Seidenschwang, photograph and biography not available at the time of publication.

J. B. Blake, photograph and biography not available at the time of publication.

N. Katz, photograph and biography not available at the time of publication.

D. Mabry, photograph and biography not available at the time of publication.

LEICA: A Low Energy Ion Composition Analyzer for the Study of Solar and Magnetospheric Heavy Ions

Glenn M. Mason, Douglas C. Hamilton, Peter H. Walpole, Karl F. Heuerman, Tommy L. James, Michael H. Lennard, and Joseph E. Mazur

Abstract— **The SAMPEX LEICA instrument is designed to measure ~0.5–5 MeV/nucleon solar and magnetospheric ions over the range from He–Ni. The instrument is a time-of-flight mass spectrometer which measures particle time-of-flight over a ~0.5 m path, and the residual energy deposited in an array of Si solid state detectors. Large area microchannel plates are used, resulting in a large geometrical factor for the instrument (0.6 cm^2 sr) which is essential for accurate compositional measurements in small solar flares, and in studies of precipitating magnetospheric heavy ions.**

I. Introduction

THE composition of energetic particles accelerated in solar flares, interplanetary shocks, and magnetospheric storm and precipitation events carries information about the source region of the particles and the physical processes involved in their acceleration at the source site and subsequent transport to the observer. Since particle spectra from these events fall steeply with increasing energy, the composition can be most accurately studied at relatively low energies. The Low Energy Ion Composition Analyzer (LEICA) on the Solar, Anomalous, and Magnetospheric Particle Explorer (SAMPEX) mission is designed to investigate these low energy particles. LEICA is a time-of-flight mass spectrometer covering the energy range ~ 0.5-5 MeV/nucleon. The instrument measures ion mass, energy, and arrival direction for the range He–Ni (3–60 AMU).

The LEICA sensor is an evolution of a compact time-of-flight mass spectrometer developed for an interplanetary spacecraft [1], [2]. A full-sized version of the instrument was constructed for flight in a NASA "Get-Away-Special" canister, and, together with the Heavy Ion Large Telescope (HILT) sensor [3], flew on the space shuttle mission STS-28 in August 1989 [4], [5].

II. Scientific Objectives

A. Solar Energetic Particles

Solar flare events typically accelerate particles to energies of tens of MeV/nucleon, with occasional flares producing relativistic particles which are detectable by ground-based neutron monitors. In recent years, two broad classes of energetic particle events have been identified: large events which are characterized by high flux levels and acceleration time scales at the sun of tens of hours (e.g., [6], [7]), and small, impulsive events which are generally enriched in ^{3}He, heavy elements such as Fe, and electrons e.g., [8], [9]. Particle acceleration in large flares seems to be associated with large shocks near the sun, and their average abundances appear to be close to those in the solar corona (reviews by Mason [10], Lin [11]). In contrast, impulsive, small flares appear to accelerate particles at the much hotter flare site itself (e.g., review by Reames [12]).

Additional measurements of solar flare composition, energy spectra, and ionization state can therefore give new information on both the large and impulsive solar flare processes. When SAMPEX is at high geomagnetic latitudes, LEICA will sample solar energetic particles at the low energies where abundances are high enough to make accurate statistical measurements even in relatively small solar flares. At lower magnetic latitudes, the solar particles are excluded by the earth's magnetic field. By measuring the rigidities for which solar flare fluxes are cut off by the geomagnetic field, LEICA will yield information on the mean charge state of the solar flare ions, thus giving insights into, e.g., the temperatures of the originally accelerated material.

In addition to the elemental composition and energy spectra of solar energetic particles, LEICA will measure the isotopic composition over a limited range near 1 MeV/nucleon, thus supplementing the measurements to be performed by the Mass Spectrometer Telescope (MAST) sensor. The significance of the solar isotopic studies is described in the accompanying paper on the MAST instrument [13].

B. Magnetospheric Precipitating Heavy Ions and Energetic Neutrals

Magnetospheric heavy ions of energies near 0.5 MeV/nucleon were first reported by Van Allen *et al.* [14]; in particular, a number of observers discovered low altitude equatorial particles with origin in the ring current [15]–[18]. Scholer *et al.* [19] detected large fluxes of CNO during a geomagnetic storm using instruments on a low earth orbiting satellite (perigee ~ 230 km, apogee ~ 1500 km); more recently, Rassoul

Manuscript received August 3, 1992; revised January 19, 1993.

G. M. Mason, D. C. Hamilton, P. H. Walpole, K. F. Heuerman, T. L. James, M. H. Lennard, and J. E. Mazur are with the Department of Physics, University of Maryland, College Park, MD 20742.

G. M. Mason is also with the Institute of Physical Science and Technology, University of Maryland, College Park, MD 20742.

IEEE Log Number 9208074.

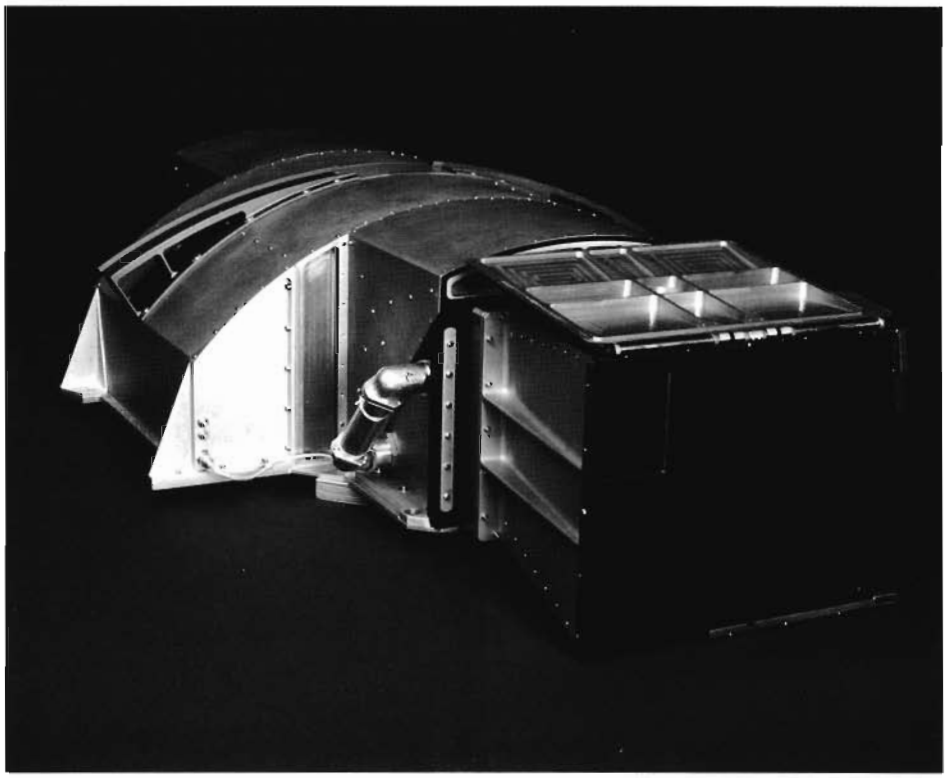

Fig. 1. The LEICA instrument shown with acoustic cover opened and thermal blankets removed. The arc-shaped raised fitting on the electronics box is a cable channel for the spacecraft despin yo-yos.

et al. [20] discussed the optical emissions associated with precipitation of heavy ions and energetic neutrals from the ring current. The CNO/He ratio of $\sim 5.5 \times 10^{-2}$ at 0.25 MeV/nucleon observed by Scholer *et al.* was consistent with either a solar wind or ionospheric origin, but they pointed out that a measurement of the C to O ratio could give a decisive test. The LEICA instrument on SAMPEX will measure many such events with detailed compositional information, making it possible to gain new insights into the dynamics of these magnetospheric particles.

III. Instrument Description

A. Sensor

The LEICA sensor identifies ion type and energy by simultaneously measuring the time-of-flight t and residual kinetic energy E of particles which enter the telescope and stop in one of an array of four Si solid state detectors. An overview of the flight instrument is shown in Fig. 1, and the instrument resource requirements are listed in Table I. Fig. 2 shows a simplified cross sectional view of the basic elements of the telescope sensor. The time-of-flight is determined from START and STOP pulses from chevron microchannel plate (MCP) assemblies which detect secondary electrons that are emitted from the entrance foil and from a foil in front of the solid state detectors when an ion passes through them. The measured energy $E = 1/2\ mv^2$ and the velocity $v = L/t$ (where L is the path length) are combined to yield the mass of the ion

$$m = 2E(t/L)^2 \tag{1}$$

TABLE I
LEICA Resources

Mass	7.43 kg
Power	4.9 W (average)
Bitrate	1.3 kbps
(orbit average)	
Field of view (FOV)	17° × 21°

and the energy per nucleon E/m inside the telescope. The ion's incident energy is obtained after correcting for the energy loss in the entrance foils. Table II gives the energy ranges for selected species analyzed by LEICA, and Table III lists details of the detector characteristics and geometry factor. Since LEICA measures only the mass of the ion, it cannot distinguish isobars such as ^{3}H vs. ^{3}He, or ^{40}Ar vs. ^{40}Ca. However, for the mass range of LEICA (elements $\leq$ 60 AMU) there are only a few stable isobars, and in each case one element dominates the solar system abundances (e.g., [21]) so that this is not a practical problem for the solar energetic and magnetospheric populations that LEICA detects.

Two 0.75μ Ni entrance foils separated by $\sim$ 9 mm are mounted on etched metallic grids, and give immunity to solar and geocoronal UV and visible radiation. The foils were manufactured by Lebow Co., Goleta, CA. The mounting grid is 0.010″ thick gold-plated Cu-Be, with 0.250″ square cell sizes separated by 0.005″-wide grid elements, thus achieving 96% transparency. The double entrance foils are spaced 1.0 cm apart, which prevents single pinholes from allowing sunlight to enter the telescope. The thin foils are protected by an acoustic

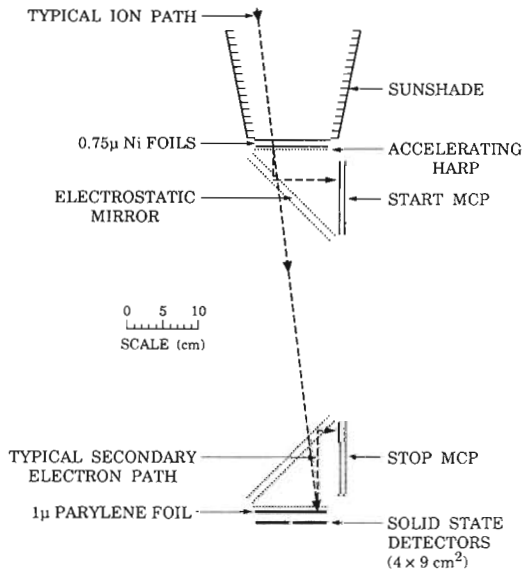

Fig. 2. Cross sectional view of the LEICA sensor. Incident ions enter through the thin foils, and pass through to one of the solid state detectors in the array at the back. The time-of-flight is determined from START and STOP pulses from microchannel plate (MCP) assemblies which are triggered by secondary electrons that are emitted from the thin foil surfaces, then accelerated and deflected by electrostatic mirrors onto the MCP surfaces.

TABLE II
LEICA ENERGY RANGES FOR SELECTED SPECIES

Species	Energy Range (MeV/nuc)	Triggering Efficiency (%)
^{1}H	>0.76	~ 1
^{4}He	0.50-6.57	6
^{12}C	0.49-10.70	64
^{16}O	0.49-8.25	67
^{20}Ne	0.46-6.79	71
^{28}Si	0.39-5.05	78
^{56}Fe	0.21-2.87	79

*measured triggering efficiency near 1 MeV/nucleon for nominal MCP bias settings; proton efficiency is estimated; Ne efficiency interpolated from other species

TABLE III
LEICA DETECTOR CHARACTERISTICS

Element	Description	Thickness (mg cm^{-2})
Outer Front Foil	0.75 μ Ni	0.668
Inner Front Foil	0.75 μ Ni	0.668
Detector foil metallic coating	0.03 μ Al	8.1×10^{-3}
Detector foil base	1 μ parylene	0.11
Detector	Geometrical Factor[1] (cm^2sr.)	Thickness and Material[2]
D1	0.13	300μ Si
D2	0.13	300μ Si
D3	0.16	300μ Si
D4	0.16	300 μ Si
Total:	0.58	

Notes: [1] Geometrical factors in this table are for *triple* coincidence (start-stop-detector) and take account of grid and harp total transmission of 73%, and details of detector and MCP alignments inside telescope

[2] the detector side through which particles enter is coated with 40 μg cm^{-2} of Au

cover (Fig. 1) that is mounted on top of the sunshade, and is opened after launch. The sunshade serves an additional role of limiting solid angle viewed by the front foil, thereby preventing excessive START rates in large solar flare events. Secondary electrons emitted from the inner Ni foil surface (see Fig. 2) are accelerated to ~ 1 kV by an electrostatic potential applied to an accelerating harp ~ 1 cm from the foil. The harp assemblies for acceleration and for the electrostatic mirrors consist of 1-mil tungsten wire strung on 1-mm spacing, thus achieving a transmission of ~ 97.5% for each layer. The use of electrostatic mirrors (e.g., [22], [23]) permits a compact design for secondary electron deflection which has the additional key features that (a) the electron flight paths from foil to MCP for normal incidence are all of the same length and therefore isochronous, and (b) an image of the foils is formed on the front of the MCP's.

The large area (7.5 × 9.3 cm active area, 1.02 mm thickness) Galileo Electro-Optics Corp. MCP's have 25 μ pore size, a channel bias angle of 19°, an open area ratio of 50%, and are mounted in a chevron arrangement. The plates are run at a low nominal bias (800 V and 850 V/plate for START and STOP, respectively) in order to prevent saturation of the position sensing electronics (see below). This low bias on the MCP's results in low overall efficiencies for ^{1}H and ^{4}He (see Table II), but for heavier species the triggering efficiency is large. The MCP bias levels are separately commandable in ~ 4V steps, and can be run at voltages up to 50% higher than nominal, allowing for adjustment post launch if the plate characteristics change. The MCP gains are monitored in flight by noting the background singles count rates of the plates; if count rates decrease noticeably, the bias is adjusted upwards to levels which produce rates comparable to the immediate post-launch values. Because of the highly variable fluxes in low earth orbit, this monitoring and adjustment is good only to a factor of ~ 2 in MCP gain. According to the manufacturer, the MCP's use recently developed glass which results in only small losses of gain vs. the total charge expelled from the plates.

The MCP outputs are directed onto thick-film anodes (manufactured by Detector Systems, Antoich, CA) deposited on alumina substrates. A solid anode on the *back* of the substrate is used to obtain the timing signal, while on the front side facing the MCP there is a wedge-and-strip anode (WSA) which is used to obtain the position of the electron cloud emerging from the MCP. The WSA electrode pattern [24], [25] is such that the analysis of signals from the three segments ("wedge", "strip", and "zigzag") of the anode allows determination of the (x, y) position of the electron cloud from the MCP. The WSA information along with the fact that the electrostatic mirrors produce images on the MCP's allows the location of the points on the Ni and parylene foils where the ion penetrated, thus permitting a determination of the flight path length L inside

the telescope. All pulse-height analyzed events are time tagged to 1-s accuracy, and since the SAMPEX pointing direction changes slowly, each event's arrival direction can be deduced off line.

In biasing of the electron emitting foils and MCP/WSA system, there is the choice of having the emitting foil at ground, and the WSA at positive 3–4 kV, or running the foil at negative 3–4 kV, and the WSA at ground (with the MCP's at appropriate intermediate biases). We obtained better results with the WSA system by running the anode at ground, thus avoiding the use of high voltage capacitors to isolate the electronics from the WSA. Thus, in Fig. 2, the inner Ni foil is biased to a nominal -2.7 kV (the outer foil is kept at ground). Similarly, we preferred keeping the solid state detector front surface at ground, and therefore the electron emitting surface for the STOP pulses is the grid mounted 1μ parylene foil with a 300Å Al coating (electron emitting surface), which was put in front of the detectors and biased at -2.7 kV.

The solid state detector array consists of four standard Ortec circular surface barrier detectors, each with 900 mm^2 active area. The light sensitivity of the solid state detectors required that the LEICA telescope be sealed, yet provision had to be made for venting during the rapid ascent on the Scout launch vehicle where the depressurization reached a maximum rate of ~ 2 lb in^{-2} s^{-1}. For the Get-Away-Special version of the instrument, air outlet vents were installed near the entrance foils; however it was found that during the Shuttle flight, the MCP's were triggered at near saturation levels. Taking account of the day/night and latitude dependencies of the count rates observed on the Shuttle flight, the best explanation for the effect was that ionospheric O^+ was entering the telescope. The O^+ density is quite large (10^5 cm^{-3}) at both Shuttle altitudes and the altitude of the SAMPEX orbit (e.g., [26]), so in the LEICA telescope all venting was through a single "chimney" which included 2 grids based at ± 40 V, which is more than sufficient to stop ions and electrons at SAMPEX altitudes.

B. Electronics

For each ion triggering the instrument, the instrument measures the time-of-flight, the energy signal in the solid state detector, and the pulse sizes from three-collector wedge-and-strip anodes (WSA) in back of both the start and stop MCP's. A triple coincidence requirement (START-STOP-Si detector) with a short ($\sim$ 350 ns) time window gives high background immunity for all analyzed events. The Si solid state detector thresholds are set at 0.5 MeV, and full scale energy deposit is 140 MeV. The primary logic and gating functions are carried out in ACTEL gate-array logic. All events triggering the system have their digitized time-of-flight and Si detector energy deposit measurements converted into pseudo-logarithmic form by fast gate logic. These $ln(t)$ and $ln(E)$ values are then used to determine whether each particle is a proton, He nucleus, or heavier than He. Events triggering LEICA that the pseudo-log lookup system identifies as protons are counted, but no further analysis is performed. Heavier nuclei are then treated as low (He) or high (heavier than He) priority for transmission to the ground. The DPU (see the accompanying article by Mabry *et al.* [27]) ensures that a sample of both priority events will be telemetered, but that low priority events will not crowd out the rarer heavy species.

Because of the very high event rates observed by LEICA in large flares, it is not possible to transmit all particle information within available telemetry allocations. Two types of information are therefore returned: first, detailed pulse-height-analysis (PHA) data at an average rate of 10 events/s, and second, counting rates which make it possible to normalize the PHA data to yield particle fluxes. In order to maximize event collection over the magnetic poles, the PHA events are read out asynchronously as described in the accompanying paper on the Data Processing Unit [28]. Table IV lists the count rates telemetered by LEICA, and Table V lists the contents of each PHA event. Those rates which count events that are analyzed by the ADC's are limited to a few thousand per second. The count rates are stored in 24-bit accumulators in LEICA, and are compressed to 12 bits by the Data Processing Unit (DPU) before telemetering the data.

Because of the low sensitivity to protons (Table II) and helium, the LEICA count rates for triple coincidences are typically very low (few counts/second) and consequently background is also very low. The singles count rates are typically highest when the spacecraft passes through the South Atlantic Anomaly, when the solid state detectors singles rates reach a few thousand per second, and the start microchannel plates count near 20 kHz. These count rates are low enough so that electronic problems such as pulse pile up are not seen with LEICA. LEICA operates in two modes: normal mode, and calibrate mode in which an internal pulser stimulates the solid state detector, time-of-flight, and WSA electronics. The calibrate mode is entered via ground command, and runs for approximately 15 minutes once per month.

C. Performance

High mass resolution analysis is done on the ground using the ion trajectory information telemetered with the PHA data. Mass histograms are formed for selected energy ranges, with the relative abundance of each species determined from the population at the appropriate mass bin in the histogram. Since LEICA has multiparameter analysis it is possible to identify and correct for residual background in the measurement, an essential feature for identifying a broad range of ions with widely differing abundances. The instrument response to heavy ions was measured prelaunch by exposing it to heavy ions beams at the Brookhaven tandem van de Graaff, and the Lawrence Berkeley Laboratory 88-inch cyclotron.

Equation (1) is used to determine the dispersions in mass resolution given the contributing dispersions in the measurement in the time of flight t, the energy deposit E, and the trajectory length L:

$$\left(\frac{\sigma_m}{m}\right)^2 = \left(\frac{\sigma_E}{E}\right)^2 + \left(2\frac{\sigma_t}{t}\right)^2 + \left(2\frac{\sigma_L}{L}\right)^2. \qquad (2)$$

We now consider each of these terms. The solid state detector energy dispersion is relatively small for particle energies above a few hundred keV/nucleon [29], [30]. As a typical value, for monoenergetic 2 MeV/nucleon ^{14}N the energy signal in the solid state detector had a measured standard deviation

TABLE IV
LEICA COUNTING RATES[1]

Name	Logic condition[2]	Type	Response	Energy Range[3]	Geometrical Factor[4] (cm^2 sr.)
D1	D1	singles discr.	All ions & electrons	> 600 keV	0.16
D2	D2	singles discr.	All ions & electrons	> 600 keV	0.16
D3	D3	singles discr.	All ions & electrons	> 600 keV	0.16
D4	D4	singles discr.	All ions & electrons	> 600 keV	0.16
START	START	singles discr.	All ions & electrons	> 250 keV (H); > 25 keV (e)	49.8
STOP	STOP	singles discr.	All ions & electrons	> 250 keV (H); > 25 keV (e)	0.73
Double Coincidence (Valid Stop)	START · STOP	logic rate	All ions	> 250 keV (H); > 25 keV (e)	0.58
Triple Coincidence (TCR)	START · STOP · $D.r$	logic rate	All ions	0.50-6.57 MeV (H)	0.58
Hi Priority	TCR · HP	ADC rate	Z> 5 ions	0.49-10.7 MeV/nuc	0.58
Lo Priority	TCR · $\overline{P}$ · $\overline{HP}$	ADC rate	He	0.50-6.57 MeV/nuc	0.58
Protons	TCR · P	ADC rate	H	>0.76 MeV/nuc	0.58
Cal Event	TCR · Cal	Internal pulser rate	not a particle rate	—	—

Notes:

[1]all counting rates are read out once every 6 seconds.

[2]notation: Dx: detector x discriminator true; HP = high priority test positive; P = proton test positive; Cal = calibrate *on*

[3]energy range shown is for most abundant species

[4]geometry factors are for singles trigger; in Table III the geometry factors are for coincidence triggers

$\sigma_E = 130$ keV. When measured in this manner, this σ_E value includes effects due to system electronics noise, solid state detector FWHM, and straggling in the Ni and parylene foils; however, in (2) the particle straggling does not enter since particles which have, e.g., higher than average losses in the Ni foils, will also have longer times of flight which compensate and therefore don't increase the dispersion. Thus, the value $\sigma_E = 130$ keV is an upper limit. The contributions to this σ_E from system noise is independent of species and energy, and the contribution from the detector FWHM is independent of energy for each species above ~ 100 keV/nucleon.

The dispersion in the time-of-flight in (2) is due primarily to "walk" in the time-to-amplitude converter which occurs when different START and STOP signal sizes trigger the system. The effect is particularly important in systems using MCP's since these plates show a broad FWHM signal size even for heavy ions of the same energy. In the LEICA design, constant fraction discriminators compensate for most of the time-of-flight "walk". In order to estimate the time-of-flight dispersion in the system, we exposed the instrument to a "monoenergetic" ^{28}Si beam at 4.2 MeV/nucleon, and measured a time-of-flight dispersion $\sigma_t = 330$ ps. For particles at this high an energy, energy losses in the thin foils are small, and so energy straggling is also very small; thus, the time-of-flight dispersion for these particles is presumably a measure of dispersions in the electronics, mirror system, etc., and is the same for particles of different energies. Thus, we can use this result to estimate the time dispersion for ~ 1 MeV per nucleon ions; since their the flight time in the telescope is ~ 45 ns, a 330 ps dispersion leads to $\sigma_t/t = 0.007$ in this case.

TABLE V
LEICA PULSE HEIGHT EVENT CONTENTS

Item	Number of Bits
Solid State Detector	12
Time-of-flight	12
START Wedge	12
START Strip	12
START Zigzag	12
STOP Wedge	12
STOP Strip	12
STOP Zigzag	12
Time of day[1]	16
FLAGS:	
Calibrate enable	1
Hi Priority	1
Calibrate event	1
D1 triggered	1
D2 triggered	1
D3 triggered	1
D4 triggered	1
Multiple START pulses	1
Total:	120

Notes: [1]Hour, min, sec

The $\Delta L/L$ term in (2) is derived from the accuracy of the WSA position sensing system, evaluated in terms of the related uncertainty in the particle path length L (~ 50 cm) in the telescope. The MCP/WSA system returns accurate information ($\sigma < 0.2$ mm) information on the location of the secondary

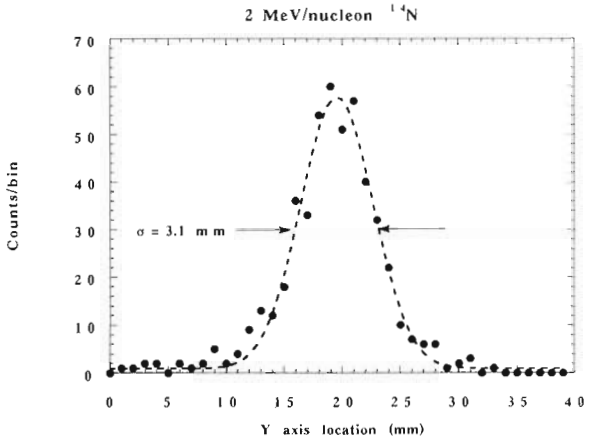

Fig. 3. "Spot" size on the front MCP from a 1-mm diameter beam spot of 2 MeV/nucleon ^{14}N incident on the front foil. The spread of secondary electron emission angles with respect to the foil surface dominates the width of the spot.

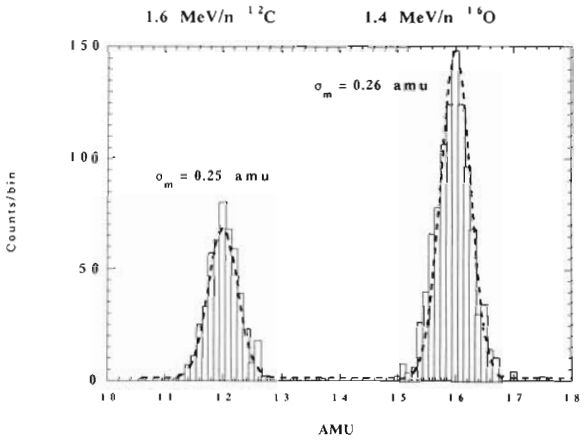

Fig. 4. Mass histograms of ~ 1.5 MeV/nucleon ^{12}C and ^{16}O.

electron impact sites on the front of the MCP. However, the knowledge of where the ions penetrated the foil is less accurate than this because the secondary electron emission angle with respect to the surface normal follows a cosine distribution [31]. Propagated through the LEICA mirror system, the result is that electrons leaving the foil from a single spot may land anywhere within a ~ 1 cm diameter circle on the MCP's. There may be additional effects introduced by the mirrors since their electrostatic fields are not perfectly uniform. For heavy ions, the large numbers (10 s, e.g., [32]) of secondary electrons should compensate for this somewhat since for such events there are multiple electrons hitting the MCP and the spatial dispersions should tend to cancel out. Fig. 3 shows the measured spot size for ~ 2 MeV/nucleon ^{14}N which was collimated to strike the START incident foil through a 1 mm diameter hole. The standard deviation of the distribution is 3.1 mm; combining this uncertainty in both x and y directions for both the START and STOP MCP's, the weighted average uncertainty in the total path length L between the foils is $\Delta L/L = 0.0006$. With these values of the various dispersions, we may estimate the mass resolution for 1.4 MeV/nucleon ^{12}C: after penetrating the foils, this ion deposits 13 MeV in the solid state detector, and has a flight time of 35.5 ns thus:

$$\left(\frac{\sigma_m}{m}\right)^2 = \left(\frac{0.13}{13}\right)^2 + \left(2 \times \frac{.33}{35.5}\right)^2 + (2 \times 0.0006)^2 \quad (3)$$

so

$$\frac{\sigma_m}{m} = 0.021 \quad (4)$$

and

$$\sigma_m = 0.25\, AMU$$

in reasonable agreement with the measured mass resolution shown in Fig. 4.

D. Data Products

Routine data products from LEICA are generated by combining the counting rate and pulse height data to give absolute fluxes and energy spectra of different species. In addition to the calibration and triggering efficiencies mentioned above, it is also necessary to correct for coulomb scattering in the Ni foils in order to recover incident flux levels. This effect is important only below ~ 1 MeV/nucleon.

Time-intensity profile plots are generated on an orbit by orbit basis, and over longer time periods (1 week, 1 month) for studies of longer-lasting events such as large solar flares. Longer time period studies related to solar flare events consist of data taken only at geomagnetic latitudes high enough to be essentially free of distortion from cutoff effects. Short events such as precipitating magnetospheric heavy ions are identified on the orbit plots and then analyzed in detail on high time resolution displays. High mass resolution analyses such as shown in Fig. 4 are done only for periods selected for their interest in solar flare or magnetospheric studies.

ACKNOWLEDGMENT

The construction, testing, and calibration of the LEICA instrument was carried out by the Space Physics group of the Department of Physics. We particularly thank E. Tums, R. Pappalardo, S. Graham, P. Floros, S. Lasley, R. Lundgren, M. Pairel, H. Wats, P. Ipavich, and A. Desrosier for their contributions to the design, construction, and administrative management of the project. The LEICA instrument was constructed under NASA contract NAS5-30704, with key instrument concepts developed under instrumentation grant NAGW-1990.

REFERENCES

[1] G. M. Mason and G. Gloeckler, "A Supra-thermal energetic particle detector (STEP) for composition measurements in the range ~ 20 keV/nucleon to 1 MeV/nucleon," *Proc. 17th Internat. Cosmic Ray Conf., (Paris)*, vol. 8, p. 98, 1981.

[2] D. V. Reames, T. T. von Rosenvinge, R. Ramaty, G. M. Mason, D. C. Hamilton, M. A. Forman, and W. R. Webber, "The energetic particles: acceleration, composition and transport (EPACT) experiment on the ISTP/Wind spacecraft," in *Particle Astrophysics: the NASA cosmic ray program for the 1990s and beyond, A.I.P. Conf. Proc. No. 203*, W. V. Jones, F. J. Kerr, and J. F. Ormes, Eds. New York: A.I.P., p. 32.

[3] B. Klecker, D. Hovestadt, M. Scholer, H. Arbinger, M. Ertl, H. Kästle, E. Künneth, P. Lawverenz, E. Seidenschwang, J. B. Blake, N. Katz, and D.

Mabry, "HILT: a heavy ion large area proportional counter telescope for solar an anomalous cosmic rays," *IEEE Trans. Geosci. Remote Sensing*, vol. 31, pp. 542–548, May 1993.
[4] D. Hovestadt, B. Klecker, P. Laeverenz, E. Seidenschwang, G. M. Mason, P. D. Bedini, G. Gloeckler, D. C. Hamilton, J. B. Blake, and D. Chenette, "Experiment for charge determination of cosmic rays of interplanetary and solar origin on the space shuttle," *Proc. 20th Internat. Cosmic Ray Conf., (Moscow)*, vol. 4, p. 406, 1987.
[5] G. M. Mason, J. E. Mazur, P. H. Walpole, T. L. James, and T. R. Sharp, "Report on the University of Maryland Large Area Telescope (LAT) flight on the Space Shuttle Columbia STS-28, August 1989," Univ. of Maryland, Dept. of Physics, Preprint 91-126, 1990.
[6] G. M. Mason, G. Gloeckler, and D. Hovestadt, "Temporal variations of nucleonic abundances in solar flare events. II. Evidence for large-scale shock acceleration," *Astrophys. J.*, vol. 280, p. 902, 1984.
[7] H. V. Cane, D. V. Reames, and T. T. von Rosenvinge, "The role of interplanetary shocks in the longitude distribution of solar energetic particles," *J. Geophys. Res.*, vol. 93, p. 9555, 1988.
[8] D. V. Reames, T. T. von Rosenvinge, and R. P. Lin, "Solar ^{3}He-rich events and nonrelativistic electrons: a new association," *Astrophys. J.*, vol. 292, p. 716, 1985.
[9] G. M. Mason, D. V. Reames, B. Klecker, D. Hovestadt, and T. T. von Rosenvinge, "The heavy ion compositional signature in ^{3}He-rich solar particle events," *Astrophys. J.*, vol. 303, p. 849, 1986.
[10] G. M. Mason, "The composition of galactic cosmic rays and solar energetic particles," *Rev. Geophys.*, vol. 25, p. 685, 1987.
[11] R. P. Lin, "Solar particle acceleration and propagation," *Rev. Geophys.*, vol. 25, p. 676, 1987.
[12] D. V. Reames, "Energetic particles from impulsive solar flares," *Astrophys. J. Suppl.*, vol. 73, p. 235, 1990.
[13] W. R. Cook *et al.*, "MAST: A mass spectrometer telescope for studies of the isotopic composition of solar, anomalous, and galactic cosmic ray nuclei," *IEEE Trans. Geosci. Remote Sensing*, vol. 31, pp. 557–564, 1993.
[14] J. A. Van Allen, B. A. Randall, and S. M. Krimigis, "Energetic carbon, nitrogen, and oxygen nuclei in the earth's outer radiation zone," *J. Geophys. Res.*, vol. 75, p. 6085, 1970.
[15] J. Moritz, "Energetic protons at low equatorial altitudes: A newly discovered radiation belt phenomenon and its explanation," *Zeit. Geophys.*, vol. 38, p. 701, 1972.
[16] D. Hovestadt, B. Hausler, and M. Scholer, "Observations of energetic particles at very low altitudes near the geomagnetic equator," *Phys. Rev. Lett.*, vol. 28, p. 1340, 1972.
[17] P. F. Mizera, and J. B. Blake, "Observations of ring current protons at low altitudes," *J. Geophys. Res.*, vol. 78, p. 1058, 1973.
[18] J. B. Blake, "On the ionic identity of the ring current particles," *J. Geophys. Res.*, vol. 81, p. 6189, 1976.
[19] M. Scholer, D. Hovestadt, G. Hartmann, J. B. Blake, J. F. Fennell, and G. Gloeckler, "Low-altitude measurements of precipitating protons, alpha particles, and heavy ions during the geomagnetic storm on March 26–27, 1976," *J. Geophys. Res.*, vol. 84, p. 79, 1979.
[20] H. K. Rassoul, R. P. Rohrbaugh, and B. A. Tinsley, "Low-altitude particle precipitation and associated local magnetic disturbances," *J. Geophys. Res.*, vol. 97, p. 4041, 1992.
[21] E. Anders, and M. Ebihara, "Solar-system abundances of the elements," *Geochim. et. Cosmochim. Acta*, vol. 46, p. 2363, 1982.
[22] F. Busch, W. Pfeffer, B. Kohlmeyer, D. Schüll, and F. Pühlhoffer, "A position-sensitive transmission time detector," *Nucl. Instr. and Method.*, vol. 171, p. 71, 1980.
[23] W. Starzecki, A. M. Stefanini, S. Lunardi, and C. Signorini, "A compact time-zero detector for mass identification of heavy ions," *Nucl. Instr. and Method*, vol. 193, p. 499, 1982.
[24] O. H. W. Siegmund, R. F. Malina, K. Coburn, and D. Werthimer, "Microchannel plate EUV detectors for the Extreme Ultraviolet Explorer," *IEEE Trans. Nuc. Sci.*, vol. NS-31, p. 776, 1984.
[25] J. S. Lapington and H. E. Schwarz, "The design and manufacture of wedge and strip anodes," *IEEE Trans. Nuc. Sci.*, vol. 33, p. 288, 1986.
[26] J. Kelley, in *The Earth's Ionosphere*. (International Geophysics Series, vol. 43). New York: Academic Press, 1981, p. 192.
[27] D. J. Mabry, S. J. Hansel, and J. B. Blake, "The SAMPEX data processing unit (DPU)," *IEEE Trans. Geosci. Remote Sensing*, vol. 31, pp. 572–574, May 1993.
[28] ibid.
[29] A. B. Galvin, "Charge states of heavy ions in the energy range ~ 30–130 keV/Q observed in upstream events associated with the earth's bow shock," Ph.D. thesis, University of Maryland, Department of Physics, preprint 82-214, p. 250, 1982
[30] E. D. Klema, F. J. Camelio, and T. K. Saylor, "Energy resolution of silicon surface-barrier detectors for oxygen and sulfur ions," *Nuc. Instr. and Methods.*, vol. 225, p. 72, 1982.
[31] W. Meckbach, "Secondary electron emission from foils traversed by ion beams," in *Beam-Foil Spectroscopy*, (vol. 2), I. A. Sellin and D. J. Pegg, Eds. New York: Plenum Press, 1976, p. 577; see also: H. Stolz, *Ann. Phys.*, vol. 3, p. 196, 1956.
[32] D. Hasselkamp, K. G. Lang, A. Scharmann, and N. Stiller, "Ion induced electron emission from metal surfaces," *Nucl. Instr. and Method.*, vol. 180, p. 349, 1981.

Glenn M. Mason, for a photograph and biography, please see page 541 of this issue.

Douglas C. Hamilton received the B.A. degree in physics and mathematics from the University of Kansas and the Ph.D. degree in physics from the University of Chicago.

He came to the University of Maryland in 1978 and is now Associate Professor in the Department of Physics. His research has concentrated on particle composition, acceleration, and transport in planetary magnetospheres and interplanetary space. He is a Co-investigator on NASA SAMPEX, ISTP, Voyager, and AMPTE missions.

Peter H. Walpole received the B.A. degree in physics from the University of Chicago, where he also took graduate courses in physics.

He came to the University of Maryland in 1978, and was Senior Electronics Engineer for the LEICA instrument. Previously he served an engineer for experiments on Pioneer 10, 11, Mariner 10, ISEE-3, AMPTE, Get-Away-Special and ULYSSES missions.

Karl F. Heuerman received the B.S. and M.S. degrees in physics from Miami University, Ohio.

He joined the University of Maryland Space Physics Group in 1990. He carried out LEICA sensor development, testing, and calibration.

Tommy L. James joined the Space Physics group as Mechanical Designer in 1978, and was responsible for LEICA detailed mechanical design and fabrication. While at Maryland Tom has also worked energetic particle sensor designs on the ULYSSES, AMPTE and Get-Away-Special programs.

Michael H. Lennard received the B.S. degree in electrical engineering from the University of Maryland College Park.

He joined the University of Maryland Space Physics Group in 1990 and designed and tested the LEICA digital electronics; after the instrument was constructed, Mike wrote the basic data capture and processing programs for the SAMPEX Science Operations Center.

Joseph E. Mazur received the B.A. degree in physics from the University of Chicago in 1985 and the Ph.D. degree in physics from the University of Maryland in 1991.

He is now a research associate at the University of Maryland studying flare particle acceleration and composition.

MAST: A Mass Spectrometer Telescope for Studies of the Isotopic Composition of Solar, Anomalous, and Galactic Cosmic Ray Nuclei

W. R. Cook, A. C. Cummings, J. R. Cummings, T. L. Garrard, B. Kecman, R. A. Mewaldt, R. S. Selesnick, E. C. Stone, and T. T. von Rosenvinge

Abstract—**The Mass Spectrometer Telescope (MAST) on SAMPEX is designed to provide high resolution measurements of the isotopic composition of energetic nuclei from He to Ni ($Z = 2$ to 28) over the energy range from $\sim$10 to several hundred MeV/nuc. During large solar flares MAST will measure the isotopic abundances of solar energetic particles to determine directly the composition of the solar corona, while during solar quiet times MAST will study the isotopic composition of galactic cosmic rays. In addition, MAST will measure the isotopic composition of both interplanetary and trapped fluxes of anomalous cosmic rays, believed to be a sample of the nearby interstellar medium.**

I. Introduction

THE Solar, Anomalous, and Magnetospheric Particle Explorer (SAMPEX), NASA's first Small Explorer (SMEX) mission, was launched in July 1992, carrying four instruments to measure the elemental and isotopic composition of energetic particles from solar and galactic sources. Two of these, the Mass Spectrometer Telescope (MAST) and the Proton Electron Telescope (PET; see [1]), were originally part of the Comprehensive Particle Analysis System (COMPAS) selected for flight on the U.S. spacecraft of the International Solar Polar Mission (ISPM). Although that spacecraft was canceled in 1981, midway through the construction of the MAST/PET instruments, MAST and PET were included on SAMPEX, providing the opportunity for MAST to measure the isotopic composition of several diverse energetic particle populations.

MAST is composed of an array of silicon solid state detectors of graduated thicknesses, including four position-sensitive detectors that measure the trajectories of incident nuclei. A mass resolution of $\leq$0.25 amu should be achieved for energetic nuclei from He to Ni. Fig. 1 illustrates the energy range over which isotope resolution of these nuclei is possible. In this paper we describe the operation of MAST and summarize the scientific objectives that it will address. Descriptions of the other SAMPEX instruments (LEICA, HILT, and PET) can be found in accompanying articles by Mason *et al.* [2], Klecker *et al.* [3], and Cook *et al.* [1]; an overview of the SAMPEX spacecraft and mission appears in Baker *et al.* [4].

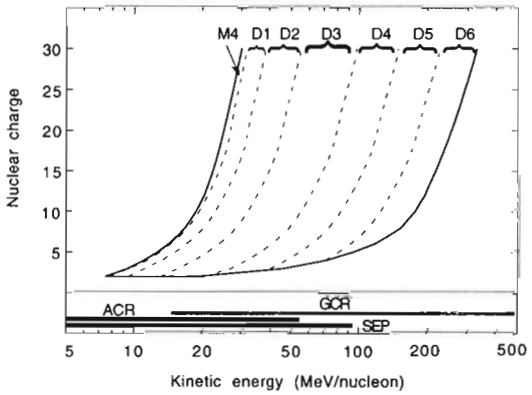

Fig. 1. The range of nuclear charge and energy/nucleon over which MAST is capable of resolving isotopes is shown between the solid curves. The dashed curves indicate the boundaries between energies where a nucleus stops in a given detector, for the case of normal incidence. The bars indicate the energy range for which solar energetic particles (SEP), anomalous cosmic rays (ACR), and galactic cosmic rays (GCR) typically show a significant flux.

II. Science Objectives

A. The Isotopic Composition of Solar Energetic Particles

Although the Sun contains > 99% of solar system material, we have only limited direct knowledge of its elemental composition and almost no *direct* knowledge of its isotopic composition. Spectroscopic observations of solar isotopes are difficult; there are isotope observations for only a few elements and the uncertainties are large. Almost all of the *isotopic* abundances in the Anders and Ebihara table of "solar system" abundances [5] are actually based on terrestrial material, while meteoritic measurements are the standard source of solar system *elemental* abundances.

Solar energetic particles (SEP) represent a sample of solar material that can be used to make direct measurements of the Sun's elemental and isotopic composition. Studies of the elemental composition of large solar flares (see, e.g., [6]) have shown that the relative abundances of elements in the solar corona with first ionization potential $\geq$10 eV (including, e.g., He, N, O, and Ne) are depleted by a factor of $\sim$4 compared to their abundances in the photosphere. Although the first

Manuscript received August 3, 1992; revised January 21, 1993. This work was supported by the National Aeronautics and Space Administration under Contract NAS5-30704 and Grant NAGW-1919.

W. R. Cook, A. C. Cummings, J. R. Cummings, T. L. Garrard, B. Kecman, R. A. Mewaldt, R. S. Selesnick, and E. C. Stone are with the California Institute of Technology, Downs Laboratory 220-47, Pasadena, CA 91125.

T. T. von Rosenvinge is with the NASA/Goddard Space Flight Center, Greenbelt, MD 20771.

IEEE Log Number 9208072.

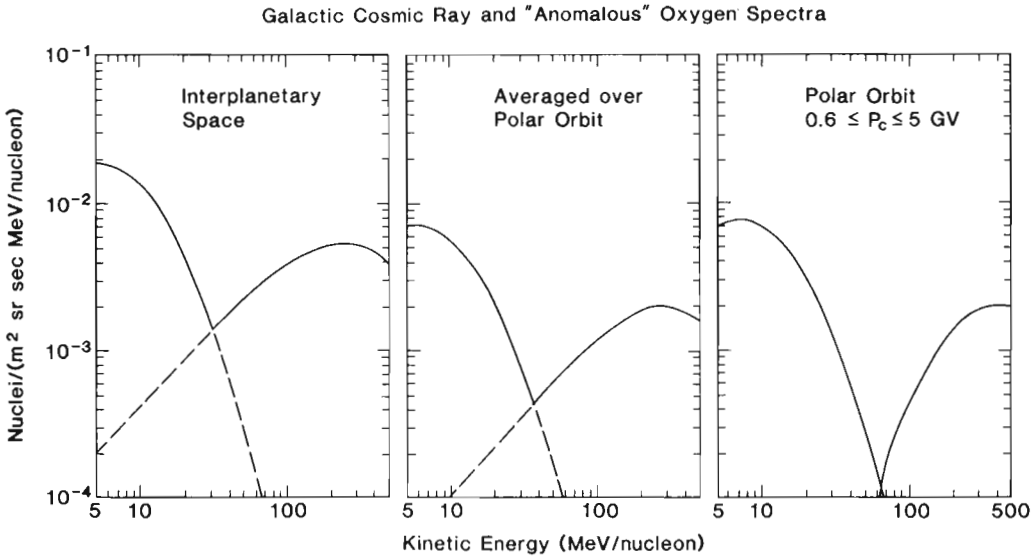

Fig. 2. The flux of oxygen in the anomalous cosmic rays (left, or lower energy, peak in each panel) and galactic cosmic rays at solar minimum. The three cases are for interplanetary space, a polar orbit average, and a polar orbit average limited to regions where the magnetic rigidity cutoff is 5 GV $\geq P_c \geq$ 0.6 GV. This figure illustrates how, by limiting the data set to regions of high magnetic rigidity, MAST can collect a sample of pure ACR, which are singly ionized.

measurements of the SEP isotopic composition were made in the late 1970's, such measurements are available for only a few elements in a limited number of solar events (see, e.g., [7] and references therein), and the uncertainties are large. SAMPEX will extend determinations of coronal composition to isotopes, as well as provide high precision measurements of elemental abundances over a broad range of energies. With its greatly improved collecting power over earlier instruments, MAST can substantially advance our knowledge of the Sun's isotopic composition.

B. The Isotopic Composition of Anomalous Cosmic Rays and the Local Interstellar Medium

Observations of quiet-time cosmic rays below ~40 MeV/nuc offer a unique opportunity to study matter from interstellar space. During solar minimum conditions there are several elements (He, C, N, O, Ne, Ar, and perhaps H) whose energy spectra have shown anomalous increases in flux above the quiet time galactic cosmic ray spectrum (see, e.g., [8], [9]). This so-called "anomalous cosmic ray" (ACR) component is now thought to represent a sample of neutral interstellar particles that have drifted into the heliosphere, become ionized by the solar wind or UV radiation and then are accelerated to energies up to tens of MeV/nuc [10]. The solar wind termination shock is the probable site of this acceleration [11]. An important prediction of this model is that anomalous cosmic rays should be singly ionized, in comparison to galactic cosmic rays which are essentially fully stripped. Strong evidence supporting this prediction was recently provided by Adams *et al.* [12], who reported a charge of +1 for ACR oxygen. On SAMPEX, HILT and MAST will measure more directly the charge states of anomalous He, N, O, and Ne using the geomagnetic field as a rigidity filter (see discussion in [3]).

Because the ACR component apparently represents a direct sample of the local interstellar medium, it carries important information about galactic evolution in the solar neighborhood over the time interval since the formation of the solar nebula—information that can be obtained by comparing the isotopic composition of ACR nuclei with that of solar system nuclei, including those measured by MAST in large solar flares. Radio and optical spectroscopy studies of interstellar matter indicate that interstellar abundances of isotopes such as ^{13}C, ^{15}N, ^{17}O, and ^{18}O may differ by a factor of ~2 from solar system abundances [13], [14], consistent with the predictions of some galactic evolution models.

The polar orbit of SAMPEX offers a significant advantage for studying ACR isotopes because the Earth's magnetic field can be used as a filter to select a pure sample of ACR nuclei, uncontaminated by solar or galactic cosmic ray nuclei, which are highly ionized. Fig. 2 illustrates an example of this "double-spectrometer" approach. Note that over the geomagnetic cutoff range from ~0.6 to ~5 GV (singly ionized) ACR nuclei with ~15–40 MeV/nuc can penetrate the Earth's field, but solar and galactic cosmic rays with < 50 MeV/nuc are completely excluded. Thus a pure sample of ACR oxygen and other ACR ions is obtained, a significant advantage over earlier ACR isotope studies [15], [16]. The isotopic composition of anomalous Ne will be of particular interest, because of the diverse range of $^{22}Ne/^{20}Ne$ ratios observed in various samples of solar system material, and the factor of at least four excess of ^{22}Ne observed in galactic cosmic rays. As solar minimum conditions approach, MAST should observe ~200 ACR Ne nuclei per year.

C. Investigations of Trapped Anomalous Cosmic Rays

Recently, Grigorov *et al.* [17] reported evidence for the existence of a radiation belt that is comprised of trapped ACRs. This trapping, which was predicted by Blake and Friesen [18], apparently occurs when a singly charged anomalous cosmic ray with a rigidity somewhat above the geomagnetic cutoff

penetrates deeply into the magnetosphere and loses some or all of its remaining electrons in the upper atmosphere, such that its resulting rigidity is suddenly below the trapping limit. The existence of this radiation belt, which apparently waxes and wanes over the solar cycle, provides opportunities for a number of exciting new studies by SAMPEX.

Although the study by Grigorov *et al.* [17] identified only trapped anomalous oxygen; it is expected that anomalous ions such as N, Ne, Ar, and possibly even He will also be trapped. The intensity of the trapped oxygen flux can be up to $\sim 10^3$ times that in interplanetary space. These studies will be significantly enhanced by results from SAMPEX, which will provide both temporal and spatial resolution so that the trapped intensities can be mapped for the first time. Measurements of the composition of the trapped ACR's in this new radiation belt will be of particular interest, including searches for rarer anomalous species such as C and Kr. Measurements by MAST may provide a new means of studying the isotopic abundances of the neutral interstellar gas.

D. The Isotopic Composition of Galactic Cosmic Rays

Galactic cosmic rays represent an accessible sample of matter that originates outside the solar system. The isotopic composition of this sample of matter contains a record of the nuclear history of cosmic rays, including their synthesis in stars, and subsequent nuclear interactions with the interstellar gas. Cosmic ray isotope observations have already revolutionized the interpretation of both cosmic ray origin and transport in the Galaxy by demonstrating that the isotopic composition of cosmic ray source material differs from solar system material, implying differences in their nucleosynthetic history, and by revealing that the mean cosmic ray lifetime is $\sim$10 million years (see, e.g., [19])—a factor of $\sim$3 longer than expected. In addition to earlier reported enhancements in the abundance of the neutron-rich isotopes of Ne, Mg, and possibly Si in cosmic ray source material (see, e.g., [20]), there are also recently reported excesses in the abundance of GCR ^{18}O [21] and ^{60}Ni [22]. MAST will extend isotope studies to additional elements with a collecting power several times greater than those of earlier satellite instruments.

III. Instrument Description

A. Approach

Resolution of isotopes in MAST is accomplished by a refinement of the standard technique [23] of measuring the energy loss ΔE of a particle penetrating a detector of thickness L_o and its residual energy loss E' in another detector where the particle stops. To illustrate, the range of a particle of mass M, charge Z, and kinetic energy E can be approximated by

$$R = k\left(\frac{M}{Z^2}\right)\left(\frac{E}{M}\right)^{\alpha}.$$

Combining this with a similar equation for the residual range R–L of the particle after traversing a pathlength $L = L_o \sec \Theta$, we find

$$M = \left\{\frac{k[(\Delta E + E')^{\alpha} - (E')^{\alpha}]}{Z^2 L_o \sec \Theta}\right\}^{1/(\alpha-1)}. \quad (1)$$

Isotope resolution, then, depends on precise measurements of the energy losses ΔE and E', the pathlength L (which depends on L_o and the zenith angle Θ), and an accurate range-energy relationship.

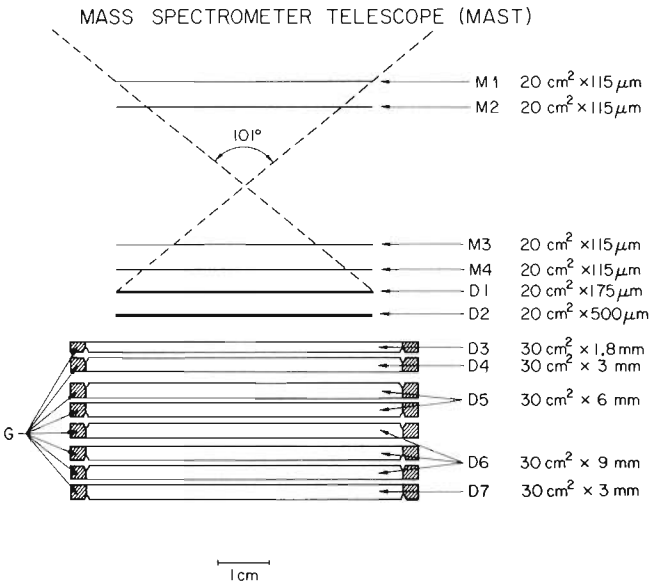

Fig. 3. A schematic representation of the detectors in MAST. The top four detectors (M1–M4) measure the position of the track of an incoming particle, and also its energy loss rate. The other detectors provide a precise measurement of the energy loss down to the detector in which the particle stops. The last detector in the stack (D7) and the guard rings (G) detect particles which exit the telescope. D5 and D6 are composite detectors of more than one wafer connected to a single amplifier. The dashed lines indicate the extreme trajectories intersecting the edge of D1, which defines the usable range for nuclei which stop in M4. See also Table I for more information.

B. The Telescope

The MAST detector stack, shown schematically in Fig. 3, consists of silicon detectors of graduated thickness. The upper section of the telescope is comprised of six surface-barrier devices, labeled M1 through D2, ranging in thickness from 115 μm to 500 μm. Four position-sensitive detectors (PSD's), M1 through M4, determine the trajectories of penetrating particles, as well as measuring their energy loss. The lower section has eight lithium-drifted (LiD) silicon wafers combined electronically into five detectors (D3 to D7). Table I summarizes the dimensions and other characteristics of the detectors.

Each of the LiD's has two circular grooves that divide the signal electrode into three annular regions, creating two independent concentric detectors and an outer dead area, a design used earlier in instruments on Voyager [24] and ISEE-3 [23]. The outer active rings serve as anti-coincidence guards that permit discrimination against events in which a particle exits or enters through the side of the detector stack.

The central regions of all detectors except D7 are connected to charge-sensitive preamplifiers, shaping amplifiers, and 4095-channel ADC's. The center of D7 and the guard

TABLE I
MAST DETECTORS

Detector Name	Type of Measurement	Detector Type	Thickness (mm)	Diameter (cm)
M1	Trajectory, ΔE	PSD SB	0.13	4.95
M2	Trajectory, ΔE	PSD SB	0.12	4.95
M3	Trajectory, ΔE	PSD SB	0.11	4.95
M4	Trajectory, $\Delta E, E'$	PSD SB	0.11	4.95
D1	$\Delta E, E'$	SB	0.16	4.95
D2	$\Delta E, E'$	SB	0.5	4.95
D3	$\Delta E, E'$	LiD	1.8	6.14 (center)
D4	$\Delta E, E'$	LiD	3.1	6.14 (center)
D5	$\Delta E, E'$	LiD (2 wafers)	6.2	6.14 (center)
D6	$\Delta E, E'$	LiD (3 wafers)	9.3	6.14 (center)
D7	Penetration	LiD	3.1	6.14 (center)

PSD: Position Sensitive
SB: Surface Barrier
LiD: Lithium Drifted

regions of D3 to D7 are connected to preamplifiers, shaping amplifiers, and discriminators. The guards have a two-level discriminator set at ~0.4 and 5 MeV. D7 is used to identify those high-energy events in which a particle penetrates entirely through the detector stack.

The MAST telescope has two windows, spaced 1.5 cm apart, which provide electrical shielding and protection from micrometeorites and sunlight. The outer window is 0.025 cm thick, and the inner 0.076 cm thick. Both are made of Kapton, aluminized on the inner surface and coated with indium-tin oxide on the outer surface. A 0.125 cm thick aluminum collimator, with its rim 4.15 cm above M1, shields the front detectors from low energy particles incident at wide angles without blocking the 101° viewing angle of the telescope.

C. The Trajectory System

The pathlength, L, through the ΔE detectors varies due to particles' varying angles of incidence and also due to nonuniformities in the detector thickness. Calibrations with Si and Fe beams at the Lawrence Berkeley Laboratory (LBL) Bevalac heavy ion accelerator have provided maps of these thickness variations. Thus, a trajectory measurement allows an accurate calculation of the pathlength through each of the ΔE detectors.

Detectors M1 to M4 are each a one-dimensional PSD. On one side of these devices the electrode consists of 93 strips, with 0.5 mm pitch, interconnected through 19 ohm resistors to form a 92 resistor chain. A current pulse from the passage of a charged particle is divided into two charge-sensitive preamps on opposite ends of the divider network, with each of the pulse-heights (X1 and X2) approximately inversely proportional to the distance of the impacted strip from its end. The sum $X1+X2$ is then a measure of total energy loss in the detector, and the one-dimensional position coordinate, X, is given by the ratio $X = X1/(X1+X2)$. Because of the signal shaping time constants employed, there is a "ballistic deficit" in the summed charge (easily correctable) which varies with position, reaching a maximum of ~10% for particles passing through the center strip of the detector. The strips on adjacent detectors are perpendicular to each other so that a trajectory can be calculated from the two X, Y coordinate pairs.

D. Electronics

MAST uses the signal processing technology originally developed for the Caltech EIS experiments (flown on IMPs 7 and 8) and further developed in thin-film hybrids for the Caltech HIST experiment on ISEE-3 [23]. The instrumentation consists of independent, parallel signal processing chains for each digitized parameter. Because these signal processors operate in a "normally open" linear gate mode, delay lines in the signal path, along with their attendant nonlinearity, poor temperature coefficient, and extra weight, are eliminated. The 4095-channel ADCs operate over a dynamic range of up to 1000 :: 1 (full scale :: threshold). Double integration, double differentiation, single pole RC shaping is used.

Each of the ADCs also has two digital discriminators whose outputs are used (in combination with those from the other triggered detectors) to classify events. The A discriminator is set for each detector at an energy just above the maximum possible energy deposit by a proton at maximum angle. The B discriminator is set just above the maximum energy deposit by an alpha particle at maximum angle. A He nucleus ($Z = 2$) will trigger at least one A discriminator if it stops in the telescope, and a $Z > 2$ nucleus will trigger both A and B discriminators. The logical OR of all the A discriminators and the OR of all the B discriminators sorts the events into one of three element categories: $Z = 1, Z = 2$, and $Z > 2$. Events with $Z > 2$ are given highest priority for readout, and of these, events with the deepest triggered detector have the highest priority. The next highest priority events, where D7 is triggered, are called penetrating events. Table II summarizes the logic requirements and event priorities.

MAST shares with PET [1] a common instrument housing and structural support. They also share a low voltage power supply assembly (LVPSA) which is contained in an external box. The power to each instrument is switched separately by relays in the LVPSA, controlled by the instrument Data Processing Unit (DPU, see [25]). Power to the LVPSA is controlled by the SAMPEX spacecraft.

E. MAST Data

The scientific data from MAST can be divided into two types, "event data" and "rate data." To generate an "event" in MAST a particle must satisfy the coincidence equation M1·M2·M3·M4. For such events we measure the trajectory in M1 through M4, and the individual energy losses in M1 through D2 and the centers of D3 through D6. Each event

TABLE II
MAST COINCIDENCE LOGIC

Event Type	Readout Priority	Logic Equation
Calibration	1	Calibration flag
$Z \geq 3$, R4-6	2	$M \cdot Z3 \cdot (D4 + D5 + D6) \cdot \overline{D7} \cdot \overline{G2}$
$Z \geq 3$, R3	3	$M \cdot Z3 \cdot D3 \cdot \overline{D4} \cdot \overline{D5} \cdot \overline{D6} \cdot \overline{D7} \cdot \overline{G2}$
$Z \geq 3$, R2	4	$M \cdot Z3 \cdot D2 \cdot \overline{D3} \cdot \overline{D4} \cdot \overline{D5} \cdot \overline{D6} \cdot \overline{D7} \cdot \overline{G2}$
$Z \geq 3$, R1	5	$M \cdot Z3 \cdot D1 \cdot \overline{D2} \cdot \overline{D3} \cdot \overline{D4} \cdot \overline{D5} \cdot \overline{D6} \cdot \overline{D7} \cdot \overline{G2}$
$Z \geq 3$, R0	6	$M \cdot Z3 \cdot \overline{D1} \cdot \overline{D2} \cdot \overline{D3} \cdot \overline{D4} \cdot \overline{D5} \cdot \overline{D6} \cdot \overline{D7} \cdot \overline{G2}$
Penetrating	7	$M \cdot D7 \cdot \overline{G2}$
$Z = 2$	8	$M \cdot Z2 \cdot \overline{D7} \cdot \overline{G1}$
$Z = 1$	9	$M \cdot Z1 \cdot \overline{D7} \cdot \overline{G1}$

"{—}" means logical complement,"+" means logical OR, and "·" means logical AND.

"M" means that each of the matrix detectors is triggered, so that a valid trajectory is obtained.

"Z3" is the OR of the detector B discriminator levels, signifying $Z > 2$.

"Z2" is the OR of the detector A discriminator levels · $\overline{Z3}$, signifying $Z = 2$.

"Z1" is $\overline{Z2} \cdot \overline{Z3}$, signifying $Z = 1$.

"G1" is the OR of the low level guard discriminators (~0.4 MeV).

"G2" is the OR of the high guard discriminators (~5 MeV).

therefore has a trajectory measurement and anywhere from 3 to 9 measurements of the energy loss rate due to ionization. Such redundant measurements permit the identification of the charge, mass, and energy of incident nuclei, as well as identification of events which undergo charge or mass changing nuclear interactions within the material of the telescope.

Events are read out of MAST by the SAMPEX DPU, which formats them for telemetry by the SAMPEX data system [4]. The DPU imposes a "throttle" on the rate of MAST events that are accepted for telemetry, typically allowing 10 or more MAST events per second, with highest priority given to $Z > 2$ events, as shown in Table II. Each instrument has a quota of the spacecraft memory in order to ensure that no instrument will be shut out in a high particle flux situation.

Because the telemetry rate is insufficient to transmit every event in large solar flares, event accumulators are used to count events during six second intervals. The rate data consist of the trigger frequency for individual detectors and discriminators, and the counting rate of various detector combinations that satisfy the criteria for an event (e.g. the event types listed in Table II). For example, the counting rates of both $Z = 2$ and $Z > 2$ nuclei are monitored in seven separate energy intervals every 6 seconds. In addition, the counting rate of a continuous pulser is monitored to measure instrument "livetime." The individual detector counting rates are sampled over a 6-second period every 96 seconds. Such data are used to normalize particle fluxes and monitor instrument health. All of the coincidence equations and some of the discriminator levels can be modified by command to allow for the possibility of noisy or failed detectors, and to optimize the instrument's response to $Z > 2$ isotopes.

TABLE III
MAST RESOURCES

Mass	7.5 kg (including PET)
Power	3.3 W
Bit Rate	1430 bps (orbit average)

MAST has a built-in internal calibrator that can be initiated either periodically (every 6.8 hours) or by command (see also [1]). The calibrator includes an 8-bit DAC that provides a reference voltage to the internal test-pulsers for each of the signal channels. These are stimulated both individually and in combination in order to perform limited tests of the coincidence logic, measure the thresholds of the various discriminators, and check the gain, linearity, and long-term stability of the ADCs. Calibration "events" are flagged and stored in a special buffer for readout along with the regular data.

F. Resources

The MAST and PET instruments on SAMPEX are housed in a common box of dimensions 25 cm × 36 cm × 17 cm, with power provided by a supply housed in a separate box of dimensions 13 cm × 12 cm × 6 cm. Table III summarizes the spacecraft resources required by MAST. Although they share a common power supply, MAST and PET are electrically isolated. The peak power drawn by the instruments during large flares may increase by ~25%. MAST's average data rate of 1430 bits/second corresponds to ~6 transmitted events per second averaged over the orbit, but MAST will achieve significantly higher data rates during limited periods of activity through data management by the SAMPEX DPU. During launch operations both the MAST and PET telescopes were acoustically and thermally protected by a common 0.08 cm-thick Al cover that was opened by command prior to instrument turn-on.

G. Mass Resolution and Calibrations

The design of MAST reflects the evaluation and optimization of all parameters affecting the mass resolution and collecting power, taking into account available resources. Statistical uncertainties due to fluctuations in the ΔE measurements are minimized by making anywhere from 3 to 9 measurements of ΔE. The trajectory measurements provided by the PSDs, along with detector thickness maps obtained at the Bevalac, will allow determination of the pathlength L to an accuracy of ~0.1%. Electronic contributions to the mass resolution are expected to be negligible. Detailed evaluations show that MAST should achieve an rms mass resolution of $\sigma_m \leq 0.25$ amu for nuclei from He to Ni ($Z = 2$ to 28), sufficient, in principle, to separate adjacent isotopes that differ in abundance by a factor of 100 to 1.

Because present knowledge of range energy relations for heavy ions is inadequate, MAST was exposed to beams of ^{28}Si and ^{56}Fe (and their fragments) at the LBL Bevalac to calibrate

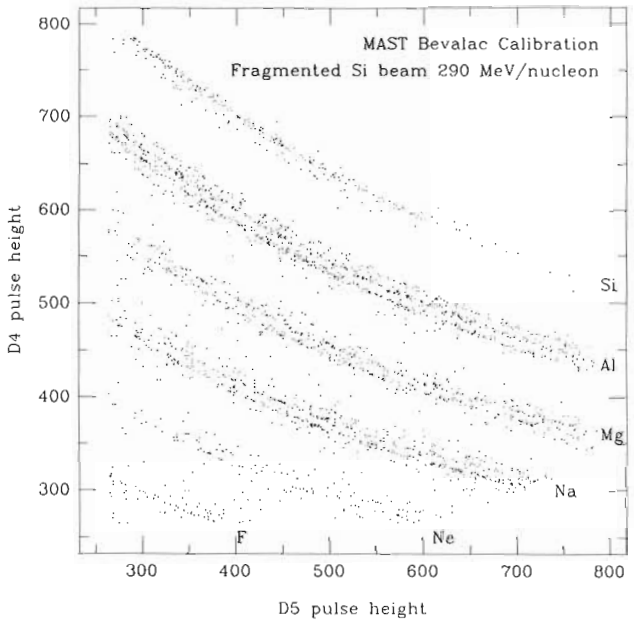

Fig. 4. Raw data from a calibration of MAST at the LBL Bevalac heavy ion accelerator. The plot shows the uncorrected pulse heights from D4 vs. D5, for a fragmented silicon beam at an incidence angle of 7.5°. Isotope tracks are clearly visible for elements from F through Si. Corrections for thickness variations in the detectors obtained from this calibration will further improve the resolution of isotope tracks. The beam energy was about 290 MeV/nucleon, but the target thickness was adjusted to produce particles stopping in D5.

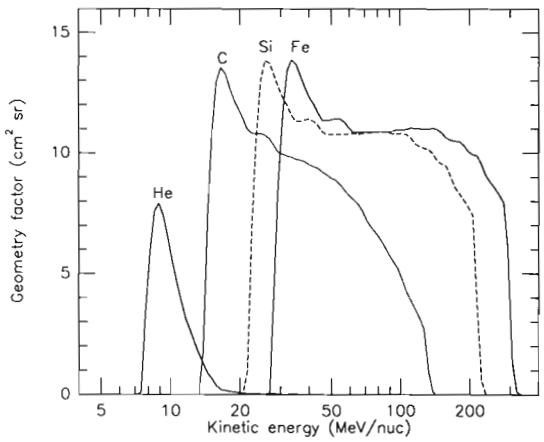

Fig. 5. The geometry factors of MAST for He, C, Si, and Fe vs. energy/nucleon based on Monte Carlo simulations. These geometry factors are for nuclei which stop in the active detector volume and that produce sufficiently large signals in the PSDs to permit isotopic analysis (this requirement reduces the geometry factor for He and C at higher energies). Elemental analysis will have somewhat larger geometry factors than those shown here for the lighter elements, and will extend to somewhat higher energies for all elements. The shape of the curves is due to the varying size of the detectors and to the reduction of available incident angles as particles (with higher energy) stop deeper in the telescope.

directly the individual isotope tracks. Fig. 4 shows an example of such calibration data in a ΔE by E' plot of raw data from D4 and D5. The isotope resolution demonstrated here will be further improved when the measurements from earlier detectors (M1 to M4 and D1 to D3) are included in the mass determination, and when corrections for detector thickness variations are employed. Preliminary analysis of accelerator data shows a mass resolution of less than 0.2 amu for ^{28}Si nuclei.

The accelerator measurements will also permit mapping of the thickness of insensitive layers of material between the active detector volumes. Measurements with alpha particle sources show that "deadlayers" are of the order of 30 μm for the LiD detectors (on the signal, or grooved, side), and less than 1 μm for the surface barrier detectors. In addition, there is 13 μm of aluminized mylar placed between facing signal sides of the LiD detectors in order to prevent crosstalk. Particles stopping in the deadlayers can be identified by their position on ΔE vs. E' plots such as Fig. 4.

H. Collecting Power

Fig. 5 shows the expected geometry factors of MAST for analysis of He, C, Si, and Fe isotopes as functions of energy/nucleon, based on Monte Carlo simulations of the instrument's response. Because of the requirement to trigger the thresholds on the matrix detectors, MAST is less sensitive to low Z nuclei (lighter than about oxygen) than high Z nuclei.

Over the lifetime of SAMPEX, MAST is expected to collect significantly more anomalous cosmic ray events suitable for isotope analysis than all previous instruments combined, to make greatly improved measurements of the isotopic composition of solar energetic particles, and to obtain a large enough sample of galactic cosmic ray isotopes to permit a comparison of these three samples of galactic matter.

ACKNOWLEDGMENT

Significant contributions to the implementation of the MAST experiment were made by H. Marshall and T. Harrington of MDH Ind.; D. Snyder and G. Takahashi of Ball Brothers Western Laboratories; D. Aalami of Space Instruments Inc.; N. Preketes of Perkin-Elmer Corporation, Applied Sciences Division; H. Crawford and the Bevalac staff at LBL; D. Mabry, S. Hansel, and K. Crawford of the Aerospace Corporation; W. Davis, G. Cooper, J. Kellogg, and H. Trexel of Goddard Space Flight Center; and W. Althouse, B. Gauld, K. Hargreaves, R. Vogt, and D. Williams of Caltech.

REFERENCES

[1] W. R. Cook, A. C. Cummings, J. R. Cummings, T. L. Garrard, B. Kecman, R. A. Mewaldt, R. S. Selesnick, E. C. Stone, D. N. Baker, T. T. von Rosenvinge, J. B. Blake, and L. B. Callis, "PET: A proton/electron telescope for studies of magnetospheric, solar, and galactic particles," *IEEE Trans. Geosci. Remote Sensing*, vol. 31, pp. 000–000, May 1993.

[2] G. M. Mason, D. C. Hamilton, P. H. Walpole, K. F. Heuerman, T. L. James, M. H. Lennard, and J. E. Mazur, "LEICA: A low energy ion composition spectrometer for the study of solar and magnetospheric heavy ions," *IEEE Trans. Geosci. Remote Sensing*, vol. 31, pp. 549–556, May 1993.

[3] B. Klecker, D. Hovestadt, M. Sholer, H. Arbinger, M. Ertl, H. Kastle, E. Kunneth, P. Laeverenz, and E. Seidenschwang, "HILT: A heavy ion large proportional counter telescope for solar and anomalous cosmic rays," *IEEE Trans. Geosci. Remote Sensing*, vol. 31, pp. 542–548, May 1993.

[4] D. N. Baker, G. M. Mason, O. Figueroa, G. Colon, J. G. Watzin, and R. M. Aleman, "An overview of the Solar, Anomalous, and Magnetospheric Particle Explorer (SAMPEX) Mission," *IEEE Trans. Geosci. Remote Sensing*, vol. 31, pp. 531–541, May 1993.

[5] E. Anders and M. Ebihara, "Solar system abundances of the elements," *Geochimica et Cosmochimica Acta,* vol. 46, p. 2363, 1982.
[6] E. C. Stone, "Solar abundances as derived from solar energetic particles," *AIP Conference Proceedings,* 183, p. 72, 1989.
[7] R. A. Mewaldt and E. C. Stone, "Isotope abundances of solar coronal material derived from solar energetic particle measurements," *Ap. J.,* 337, p. 959, 1989.
[8] A. C. Cummings and E. C. Stone, "Elemental composition of the very local interstellar medium as deduced from observations of anomalous cosmic rays," *Proceedings of the 21st International Cosmic Ray Conference* (Adelaide), vol. 6, p. 202, 1990.
[9] E. R. Christian, A. C. Cummings, and E. C. Stone, "Evidence for anomalous cosmic ray hydrogen," *Ap. J.* 334, p. L77, 1988.
[10] L. A. Fisk, B. Kozlovsky, and R. Ramaty, "An interpretation of the observed oxygen and nitrogen enhancements in low-energy cosmic rays," *Ap. J. (Ltrs.),* 190, p. L35, 1974.
[11] M. E. Pesses, J. R. Jokipii, and D. Eichler, "Cosmic ray drift, shock wave acceleration, and the anomalous component of cosmic rays," *Ap. J. (Ltrs.),* 246, p. L85, 1981.
[12] J. H. Adams, M. Garcia-Munoz, N. L. Grigorov, M. A. Kondratyeva, M. I. Panasyuk, Ch. A. Tretyakova, D. A. Zhuravlev, B. Klecker, G. M. Mason, R. E. McGuire, R. A. Mewaldt, and A. J. Tylka, "The charge state of the anomalous component of cosmic rays," *Ap. J. (Ltrs.)* 375, p. L45, 1991.
[13] A. A. Penzias, "Nuclear processing and isotopes in the galaxy," *Science,* vol. 208, p. 663, 1983.
[14] P. G. Wannier, "Nuclear abundances and evolution of the interstellar medium," *Ann. Rev. Astron. Astrophys.,* vol. 18, p. 399, 1980.
[15] R. A. Mewaldt, J. D. Spalding, and E. C. Stone, "The isotopic composition of the anomalous low-energy cosmic rays," *Ap. J.,* 283, p. 450, 1984.
[16] A. C. Cummings, E. C. Stone, and W. R. Webber, "Isotopic composition of anomalous cosmic ray neon," *Proceedings of the 22nd International Cosmic Ray Conference, Dublin, Ireland,* vol. 3, p. 362, 1991.
[17] N. L. Grigorov, M. A. Kondratyeva, M. I. Panasyuk, Ch. A. Tretyakova, J. H. Adams, Jr., M. Schulz, R. A. Mewaldt, and A. J. Tylka, "Evidence for trapped anomalous cosmic ray oxygen in the inner magnetosphere," *Geo. Res. (Ltrs.),* vol. 18, p. 1959, 1991.
[18] J. B. Blake and L. M. Freisen, "A technique to determine the charge state of the anomalous low-energy cosmic rays," *Proceedings of the 15th International Cosmic Ray Conference, Plovdiv, Bulgaria,* vol. 2, p. 341, 1977.
[19] J. A. Simpson and M. Garcia-Munoz, "Cosmic ray lifetime in the galaxy: Experimental results and models," *Sp. Sci. Rev.,* vol. 46, p. 205, 1988.
[20] R. A. Mewaldt, "The abundances of isotopes in the cosmic radiation," *AIP Conference Proceedings,* vol. 183, p. 124, 1989.
[21] P. S. Gibner, R. A. Mewaldt, S. M. Schindler, E. C. Stone, and W. R. Webber, "The isotopic composition of cosmic ray B, C, N and O: Evidence for an overabundance of ^{18}O," *Ap. J.,* 391, p. L89, 1992.
[22] R. A. Leske, B. Milliken, and M. E. Wiedenbeck, "The isotopic composition of iron-group cosmic rays," *Ap. J. (Ltrs.),* 390, p. L99, 1992.
[23] W. E. Althouse, A. C. Cummings, T. L. Garrard, R. A. Mewaldt, E. C. Stone, and R. E. Vogt, "A cosmic ray isotope spectrometer," *Geoscience Electronics,* vol. 16, pp. 204–207, 1978.
[24] E. C. Stone, R. E. Vogt, F. B. McDonald, B. J. Teegarden, J. H. Trainor, J. R. Jokipii, and W. R. Webber, "Cosmic ray investigation for the Voyager Missions; Energetic particle studies in the outer heliosphere—and beyond," *Space Science Reviews,* vol. 21, pp. 355-376, 1977.
[25] D. J. Mabry, S. J. Hansel, and J. B. Blake, "The SAMPEX Data Processing Unit (DPU)," *IEEE Trans. Geosci. Remote Sensing,* vol. 31, pp. 572–574, May 1993.

Walter R. Cook received the B.S. degree in physics from Stevens Institute of Technology and the Ph.D. degree in physics from the California Institute of Technology.

He has been employed at Caltech's Space Radiation Laboratory since 1980 and is currently the principal electronics engineer and a Member of the Professional Staff. His research work has included studies of the composition of solar energetic particles on Voyager 1 and 2 and gamma-ray astronomy using the GRIP balloon-borne telescope, for which he serves as project scientist and electronics engineer. He was principal electronic engineer for the MAST/PET instruments on SAMPEX.

Alan C. Cummings received the B.A. degree in physics from Rice University in 1966. After a year at Churchill College, Cambridge University, he entered graduate school at Caltech where he received the Ph.D degree in physics in 1973.

He accepted the position of Research Scientist in Caltech's Space Radiation Laboratory in 1973 and now holds the position of Senior Scientist and Member of the Professional Staff. He has been responsible for hardware on the Voyager and ISEE-3 missions and was Project Manager during the development of the Gamma Ray Imaging Payload balloon instrument, as well as serving as the MAST/PET Project Manager on the SAMPEX mission. His research interests include all aspects of the anomalous cosmic ray component. He is Co-Investigator on the Voyager and ACE missions.

Jay R. Cummings received the Ph.D. degree from the University of Minnesota in 1989.

He is a Senior Research Fellow in Physics at the California Institute of Technology. His recent research includes investigation of the composition of particles trapped in the Earth's magnetosphere and of anomalous cosmic rays using the SAMPEX MAST and PET instruments, and studying fragmentation of relativistic heavy ions with the Ultra-Heavy Ion Cross-section collaboration.

Thomas L. Garrard received the B.A. degree in physics from Rice University and the Ph.D. degree in physics from the California Institute of Technology.

He became a Staff Scientist at Caltech in 1972 and is now a Senior Scientist and Member of the Professional Staff. He is currently involved in SAMPEX, ACE, Galileo, Voyager, and other projects, with emphasis on composition of cosmic rays and solar energetic particles.

Branislav Kecman received the B.S. degree in electrical engineering from the University of Belgrade, Yugoslavia, in 1987, and the M.S.E.E. degree from the California Institute of Technology in 1989.

He worked as an Associate Electronics Engineer with the Space Radiation Laboratory at Caltech since 1989, where he is involved in design and testing of analog and digital electronic systems. For his efforts on the SAMPEX Spacecraft Integration and Test Team he was awarded NASA's Special Act Group Award in 1992.

Richard A. Mewaldt received the Ph.D. degree in physics from Washington University, St. Louis, MO.

He has been a member of the Space Radiation Laboratory at the California Institute of Technology since 1971. He is currently a Senior Research Associate in physics at Caltech. His research interests have centered on the study of energetic nuclei and electrons accelerated in solar flares, in interplanetary space, and in galactic cosmic rays, and on the development of high resolution spaceflight and balloon-borne instrumentation to measure the composition of these particles. He has been a Co-investigator on experiments for the NASA missions IMP-7 & 8, ISEE-3 (ICE), ISPM, and ACE, and is a co-investigator on SAMPEX.

Richard S. Selesnick received the Ph.D. degree in space plasma physics from the Massachusetts Institute of Technology in 1988.

He is a Senior Research Fellow in Physics at the California Institute of Technology. His current research interests include the physics of planetary magnetospheres and cosmic rays.

Edward C. Stone received the Ph.D. degree in physics from the University of Chicago in 1964.

He then joined the faculty of the California Institute of Technology, where he became Professor of Physics in 1976. He is currently the Director of the Jet Propulsion Laboratory and Vice President of Caltech. He has served as Project Scientist for the Voyager Mission to the outer planets since 1972. He has been a principal investigator on nine NASA spacecraft and a co-investigator on four others, including SAMPEX.

Tycho T. von Rosenvinge received the B.A. and Ph.D. degrees in physics from Amherst College and the University of Minnesota, respectively.

In 1969 he came to NASA/Goddard Space Flight Center, where he is currently head of the Low Energy Cosmic Ray Group. He was Project Scientist for the International Sun-Earth Explorer ISEE-3 (1971–1983) and for the International Cometary Explorer, the first spacecraft to intercept a comet (1984–1989). He is currently Principal Investigator of the EPACT instruments on the GGS/WIND spacecraft. His scientific interests include the acceleration, composition, and transport of energetic particles in space, particularly particles from solar flares and the anomalous component.

PET: A Proton/Electron Telescope for Studies of Magnetospheric, Solar, and Galactic Particles

W. R. Cook, A. C. Cummings, J. R. Cummings, T. L. Garrard, B. Kecman, R. A. Mewaldt, R. S. Selesnick, E. C. Stone, D. N. Baker, T. T. von Rosenvinge, J. B. Blake, and L. B. Callis

Abstract—**The Proton/Electron Telescope (PET) on SAMPEX is designed to provide measurements of energetic electrons and light nuclei from solar, galactic, and magnetospheric sources. PET is an all solid-state system that will measure the differential energy spectra of electrons from ~1 to ~30 MeV and H and He nuclei from ~20 to ~300 MeV/nuc, with isotope resolution of H and He extending from ~20 to ~80 MeV/nuc. As SAMPEX scans all local times and geomagnetic cutoffs over the course of its near-polar orbit, PET will characterize precipitating relativistic electron events during periods of declining solar activity, and it will examine whether the production rate of odd nitrogen and hydrogen molecules in the middle atmosphere by precipitating electrons is sufficient to affect O_3 depletion. In addition, PET will complement studies of the elemental and isotopic composition of energetic heavy ($Z > 2$) nuclei on SAMPEX by providing measurements of H, He, and electrons. Finally, PET has limited capability to identify energetic positrons from potential natural and man-made sources.**

I. Introduction

BOTH the MAST and PET sensors on the polar-orbiting Solar, Anomalous, and Magnetospheric Particle Explorer (SAMPEX) were originally part of the Comprehensive Particle Analysis System (COMPAS) selected for flight on the U.S. spacecraft of the International Solar Polar Mission (ISPM), and MAST and PET are housed within a common box. As part of ISPM PET was designed to provide exploratory studies of energetic H, He, and electrons from solar and Galactic sources on ISPM's flight out of the ecliptic plane and over the solar poles. Although that spacecraft was canceled in 1981, midway through the construction of the MAST/PET instruments, MAST and PET were later proposed, and approved, for inclusion on SAMPEX, NASA's first Small Explorer (SMEX) mission. The response of both instruments is well-suited for studying the diverse particle populations that will be encountered over the SAMPEX orbit.

PET is composed of an array of silicon solid state detectors that identify and measure the kinetic energy of electrons from ~1 to ~30 MeV and of H and He isotopes from ~20 to ~80 MeV/nuc. In addition PET includes a counting rate for electrons > 0.4 MeV and protons > 4 MeV that has 0.1 second time resolution for studies of magnetospheric particles, and it has limited capability for identifying energetic positrons. In this paper we describe the operation of PET and summarize the scientific objectives that it will address. The Mass Spectrometer Telescope (MAST) is described in a companion paper in this volume by Cook *et al.* [1]. Also included in the SAMPEX payload are a Low Energy Ion Composition Analyzer (LEICA; see reference [2]) and a Heavy Ion Large Telescope (HILT; see [3]). For an overview of the SAMPEX mission, see Baker *et al.* [4].

Manuscript received August 3, 1992; revised January 21, 1993. This work was supported by NASA under Contract NAS5-30704 and Grant NAGW-1919.

W. R. Cook, A. C. Cummings, J. R. Cummings, T. L. Garrard, B. Kecman, R. A. Mewaldt, R. S. Selesnick, and E. C. Stone are with the California Institute of Technology, Pasadena, CA 91125.

D. N. Baker and T. T. von Rosenvinge are with the Goddard Space Flight Center, Greenbelt, MD 20771.

L. B. Callis is with the Langley Research Center, Hampton, VA 23681.

IEEE Log Number 9208073.

II. Scientific Objectives

A. High Energy Magnetospheric Electron Precipitation

Long-term observations in the outer magnetosphere demonstrate that energetic particle fluxes are strongly modulated by solar wind streams. Lower energy ($\leq$300 keV) particle fluxes track the solar wind variations quite closely and appear to be the direct product of magnetospheric substorm activity that is controlled by the solar wind. Higher energy ($\geq$300 keV) particle fluxes are also modulated by the solar wind streams, but are not directly related to substorm acceleration mechanisms. Since very energetic electrons may play a key role in linking together the magnetospheric-ionospheric-atmospheric system [5]–[9], it is an important element of applied magnetospheric science to understand solar wind influence on energetic electron acceleration and transport.

New results for relativistic magnetospheric electrons suggest interesting coupling possibilities that extend the traditional relativistic electron precipitation (REP) picture [7] in several ways. First, the energies of electrons that have been measured are far greater than those in REP events and thus the energy deposition, ionization, and chemistry modification will extend much deeper into the atmosphere than previously suspected [7], as illustrated in Fig. 1. Secondly, there is strong solar cycle variability in the multi-MeV electron component (see Fig. 2) which will, in turn, impose a strong variability on ionization and chemistry effects upon the middle atmosphere, possibly extending deep into the stratosphere. Thirdly, relatively broad midlatitudinal bands of the Earth's surface are involved, implying a truly global effect.

The PET sensor in the low, polar orbit of SAMPEX is well suited to monitor the precipitation of relativistic electrons into the upper atmosphere. It will make direct observations of electron precipitation over the energy range 0.4–30 MeV,

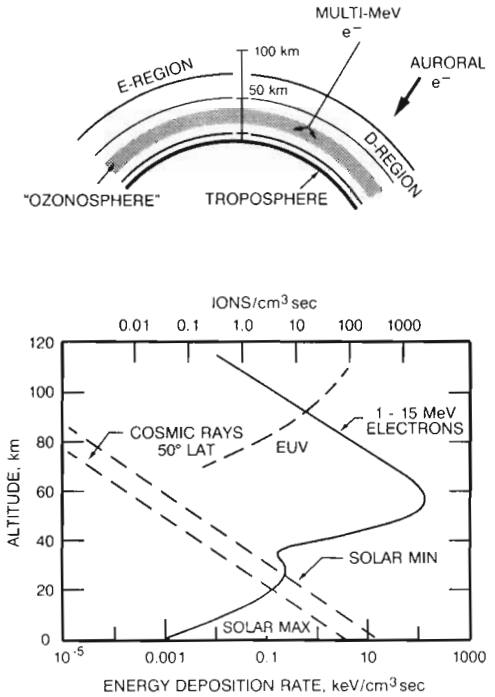

Fig. 1. (Top) A diagram illustrating the much greater depth to which precipitating relativistic electrons can penetrate into the Earth's atmosphere as compared to characteristically lower-energy auroral electrons. (Bottom) Multi-MeV electrons, when present, represent the dominant ionization source in the middle atmosphere (40–80 km altitude). The figure shows the expected energy deposition versus altitude if an energetic (1–15 MeV) electron event observed at geostationary orbit were to precipitate into the atmosphere. This is contrasted with solar extreme ultraviolet (EUV) ionization at high altitude and the effect of galactic cosmic rays at low altitude.

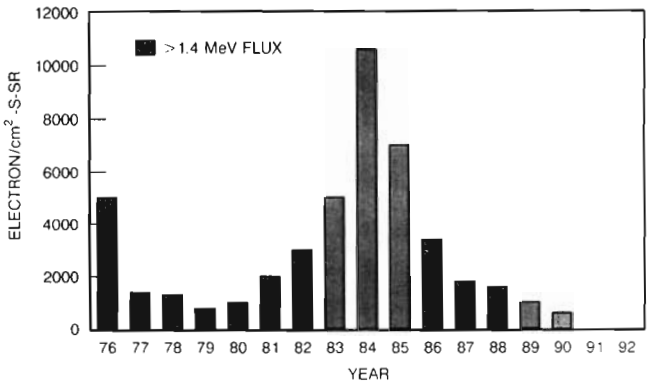

Fig. 2. Annual flux averages of the directional intensity of electrons with energies greater than 1.4 MeV as measured by sensor systems at geostationary orbit alt. = 35,700 km (6.6 Re). A large flux maximum occurred in 1984 with minima in 1979 and 1990. This strong temporal variation is consistent with a significant solar cycle (11-year) dependence of relativistic outer-zone magnetospheric electrons.

measurements that are effectively impossible from a high-altitude spacecraft. The polar orbit will allow coverage at all latitudes, and, over the course of a day, rotation of the Earth under the SAMPEX orbit will allow coverge at all longitudes. Over the course of the mission coverage at all local times will be achieved. As Fig. 3 indicates, the SAMPEX mission should sample the time periods when both major solar flares and intense relativistic electron events reach their maximum frequency.

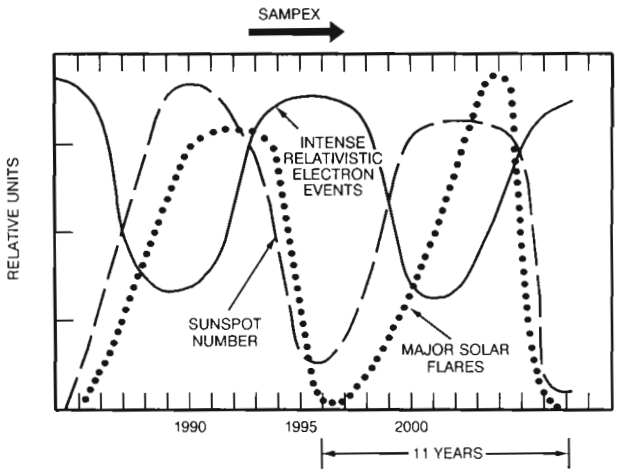

Fig. 3. A schematic illustration of the 11-year solar-cycle effects thought to occur in the solar terrestrial system. The long dash curve shows the relative sunspot number, or solar activity cycle. Major solar flares tend to track the sunspot number, often showing more events slightly after sunspot maximum. Intense relativistic electron events are in antiphase with sunspot number.

B. Effects of Precipitating Electrons on the Middle Atmosphere

Multi-MeV electrons can penetrate deeply into the atmosphere and model calculations show that they can dominate other sources of ionization in the middle altitude regions [7], as shown in Fig. 1. Solar energetic particle events and relativistic electron precipitation events can lead to significant atmospheric production of odd nitrogen (NO, NO_2, NO_3, HNO_4, N_2O_5, and $ClONO_2$) and odd hydrogen (H, OH, HO_2, H_2O_2). This occurs through ion chemistry initiated by the atmospheric ion pair production associated with these events. Both of these chemical families are important to the global O_3 balance [10], and hence to the thermal structure of the middle atmosphere. Thorne [5], [6] suggested that precipitating relativistic electrons, through the production of odd hydrogen and odd nitrogen, could lead to local O_3 depletions in the 40–80 km region of the middle atmosphere. Callis *et al.* [8], [9] have carried out simulations which suggest that the production of odd nitrogen species in this altitude region and in the fall, winter and early spring, may be carried by the normally descending advective motions to the lower stratosphere. During these seasons, the photodissociation rates of NO are small, and due to the long lifetime of NO_y in the mid-to-lower stratosphere, accumulation may occur with attendant O_3 destruction. Events occurring in these seasons and in the polar night would certainly lead to accumulations of NO_y and HO_x.

Large, recurrent solar wind streams emanating from persistent coronal holes are a prominent aspect of the Sun's 11-year and 22-year activity cycle. These coronal holes extend down to the solar equator and give rise to high speed solar wind streams at ≥ 1 AU only during the approach to solar (sunspot) minimum. The high speed streams, in turn, strongly control the presence or absence of multi-MeV electrons in the Earth's outer magnetosphere. If relativistic electrons, when precipitated into the middle atmosphere, significantly modify O_3 and NO_y concentrations [6], [7], they could leverage and modify a much larger energy supply, viz., solar UV radiation.

Thorne [5] suggested that modulation of stratospheric O_3 might affect the thermal structure and radiative processes of the atmosphere. If such changes ocur in the 22–35 km region, zonal winds and planetary wave structure could be altered which may then affect tropospheric patterns. This could be a mechanism for producing an 11-year cycle in the Earth's middle and lower atmosphere. The radiative budget of the troposphere could also be affected.

It is conceivable that these chemical perturbations could also lead to substantial temperature changes in the mesosphere, with consequent changes in the phase and amplitude of the upwardly propagating long planetary waves, and changes in the energy deposition by these waves and by the breaking gravity waves. The NO_x increases may also lead to changes in the D-region electron density.

C. Man-Made Sources of Magnetospheric Particles

The former Soviet Union has flown low-altitude, near-polar satellites powered by nuclear reactors, the so-called RORSATS. When in operation the reactors emit intense fluxes of both neutrons and gamma rays. Pair production by the gamma flux in the skin of the vehicle creates electrons and positrons which are injected into the magnetosphere [11]. The energies of these particles range up to several MeV and are determined by the gamma-ray leakage spectrum. Although never reported, protons from the decay of reactor leakage neutrons must be injected as well, and might be detectable by the HILT sensor. The reactor serves as a point source for the pair-produced particles, whereas the neutron decay particles are not localized at the spacecraft. The neutrons decay in flight as they move away from the reactor, and thus the injection site will be the point of the decay, not the location of the reactor. The energy spectrum of the protons reflects the energy spectrum of the leakage neutrons.

If a satellite powered by a nuclear reactor is in operation in low Earth orbit during the SAMPEX mission, the pair-produced electrons and positrons will be readily detectable by the PET sensor. These particles are unlike particles injected by natural processes in that their origin is a true point source, albeit a moving one. In addition, positrons are well suited to serve as field-line tracers, providing the opportunity for detailed studies of the type pioneered by Hones *et al.* [11] of the near-Earth magnetic field-line geometry and atmospheric loss processes.

D. Secondary Magnetospheric Particles

Eastern European space scientists have repeatedly reported on observations of very energetic electrons and positrons ($E \geq$ tens of MeV) at SAMPEX altitudes (cf, [12], [13] and references therein). It has been suggested that these electrons are, at least in part, secondary particles from the interactions of inner-zone protons and galactic cosmic rays with the residual atmosphere. These interactions can lead to the creation of pions with the residual π-μ-e decays yielding highly relativistic electrons. If these electrons are injected into the magnetosphere at near 90° pitch angle in the region of the South Atlantic Anomaly, the drift averaged atmospheric density can be sufficiently low to permit a relatively long particle lifetime. Thus they will be able to drift around the Earth many times before being removed by energy loss in the residual atmosphere due to ionization and bremstrahlung

The PET sensor, with its large geometry factor, and high time resolution, will permit a detailed study of this secondary magnetospheric particle population. These particles, which are able to penetrate deeply into the space vehicle because of their very high energy, are also of interest in completely defining the space station radiation environment.

E. Solar Energetic Particles

Recent comprehensive surveys of energetic particles accelerated in solar flares have shown that there are two general classes of such particle events: large events that are characterized by extended risetimes and relatively long durations, and somewhat smaller "impulsive" events that are typically marked by enhanced fluxes of heavy nuclei, the rare isotope ^{3}He, and energetic electrons (see, e.g., [14]). Indeed, energetic electron fluxes are one of the most useful means of identifying impulsive solar flare events (e.g., [15]). PET will complement the composition studies of solar events to be carried out on SAMPEX by LEICA, HILT, and MAST [2], [3], [1] with measurements of 1 to 30 MeV electrons, and by extending spectral studies of ^{1}H, ^{3}He, and ^{4}He nuclei to the energy range from ~20 to ~100 MeV/nuc.

F. Anomalous and Galactic Cosmic Ray Studies

Among the primary objectives of SAMPEX are studies of the charge states and isotopic composition of the so-called "anomalous cosmic ray component." These low energy nuclei apparently originate from neutral interstellar atoms (including H, He, C, N, O, Ne, and Ar) that have been swept into the heliosphere, singly ionized, and then accelerated at the solar wind termination shock to energies of ~10 to 10^2 MeV/nuc.

On SAMPEX the HILT and MAST instruments will use the geomagnetic field as a rigidity filter to measure the charge states of anomalous He, N, and O, while MAST will measure the isotopic composition of He, N, O, Ne, and Ar. PET will complement these instruments by extending studies of anomalous He to higher energies(100 MeV/nuc) than before using the Earth's magnetic field to separate for the first time the relative contribution of ACR and galactic cosmic ray (GCR) He beyond 50 MeV/nuc. PET measurements of the ^{3}He/^{4}He ratio will aid in this effort by using ^{3}He as a tracer of the GCR component, since there is negligible anomalous ^{3}He. PET will also search for evidence of predicted fluxes of anomalous H at ~100 MeV/nuc that may penetrate into the inner solar system at times of minimum solar modulation [16], [17].

III. Instrument Description

A. The Telescope

The PET telescope, shown schematically in Fig. 4, consists of a series of eight Li-drifted silicon detectors (P1 to P8) with thicknesses ranging from 2 to 15 m. The telescope opening aperture is defined by a passive collimator, followed by two

TABLE I
PET DETECTOR, ADC, AND DISCRIMINATOR CHARACTERISTICS

Detector Name	Nominal Thickness (mm)	Central Active Area (cm^2)	Guard Active Area (cm^2)	Nominal ADC Threshold (MeV)	Nominal ADC Full Scale (MeV)	Nominal Discriminator Thresholds (MeV)	Guard Discriminator Thresholds (MeV)
P1	2	8.0	–	0.35	157	P1A = 3.1	–
P2	2	8.0	–	0.35	157	–	–
P3	15 (5 × 3 mm)	9.2	4.5	0.7	317	P3A = 2.8 P3B=12	0.3, 5
P4–P7	3	4.5	8.0	0.36	337	0.23	0.3, 1.2
P8	3	4.5	8.0	–	–	0.3	0.3, 1.2

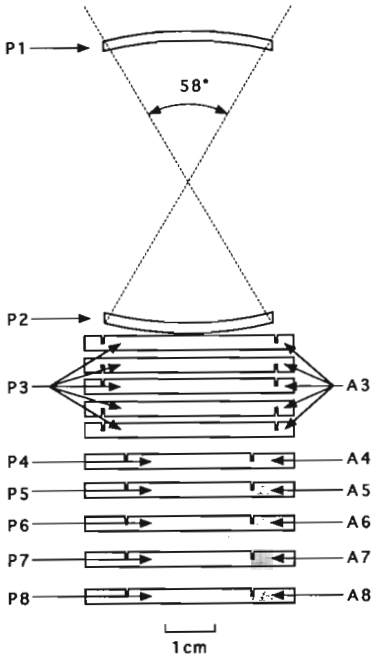

Fig. 4. Schematic of the PET Telescope. The primary analysis mode requires P1 and P2 (58° field of view); a "wide-angle" 90° FOV that requires P2 and P4 but not P1 is also available for electrons. Detector parameters are summarized in Table I. The regions labeled A4 through A8 are annular "guard" regions used to detect particles that enter or leave through the side of the stack.

curved (spherical) aperture detectors (P1 and P2) designed to minimize pathlength variations over the telescope's 58° opening angle. They are followed by eight flat detectors (P3 through P8), where the P3 detector is comprised of five identical devices with a combined thickness of 15 mm. Detectors P3 through P8 are double-grooved devices with a central area for measuring energy loss and an annular guard region (labeled A) used to detect particles that enter or leave through the side of the telescope, a design used previously on Voyager 1&2 [18] and ISEE-3 [19].

Particles satisfying the P1·P2 coincidence enter through a 1.5 cm long collimator (not shown in Fig. 4) that is nominally 0.75 mm thick at its thinnest point, and that preserves the 58° opening angle. The collimator also supports two windows (each 12.5 μm thick aluminized Kapton) that provide electrical shielding and protection from sunlight.

Detectors P1, P2, and the center of P3 are each direct coupled to separate charge-sensitive preamplifiers, shaping amplifiers, and 10-bit ADC's. The summed output of the centers of P4 through P7 is fed into a fourth 10-bit ADC. The center of D8, and the guard regions of D3 to D8 are each connected to preamplifiers, shaping amplifiers and discriminators. Each guard signal channel has two discriminators: A1 is sensitive to minimum ionizing particles while the A2 levels are ~1.2 MeV for A4–A8 and ~5 MeV for A3. Table I summarizes the characteristics of the PET detectors and their analysis chains.

Packaging PET within the available size and mass constraints was accomplished by using custom hybrid circuitry on planar multilayer printed circuit boards. PET includes a total of 79 hybrids, including 12 pre–post amplifiers, 15 test pulsers, 13 discriminators, and 4 ADCs that are each comprised of two hybrid circuits.

B. Analysis Modes

PET uses the conventional dE/dx—total energy technique to identify electrons, protons, and heavier nuclei, an approach which is based on the range–energy relations of energetic particles. With this approach a comparison of the rate of energy loss of energetic particles with their total energy loss can be used to identify both the charge and mass of energetic nuclei, as well as measure their kinetic energy. In practice, the rate of energy loss is determined by measuring the energy loss (ΔE) in a detector of known thickness, such as P1 or P2 on PET. In order to minimize the variations in the pathlength over the telescope's 58° opening angle, P1 and P2 have been constructed from spherical segments of silicon. As a result PET should be capable of identifying elements from H to Ni (Z = 1 to 28), with isotope identification extending through Ne (Z = 10). Although the range–energy characteristics of electrons are not nearly so precise as those of nuclei, electrons are easily separable from protons because of their much lower rate of energy loss.

PET includes a number of separate analysis modes that are designed to identify electrons and nuclei over selected energy intervals. We describe here the primary "Lo-Z" mode planned for nominal operations, in which PET provides the differential energy spectra of electrons and of H and He nuclei. A commandable "Hi-Z" mode, in which the gain of P1, P2, and P3 is reduced by a factor of ten, also allows PET to measure the energy spectra of the elements from Li to Ni (Z = 3 to 28). Although it is not presently planned to use this mode during normal operations, it provides a possible backup for the MAST and HILT sensors on SAMPEX.

TABLE II
PET RESPONSE

Particle	Nominal Energy Interal (MeV or MeV/nuc)	Typical Geometry Factor (1) (cm^2 sr)	Detector (2, 3) Combination	Associated Counting Rates: Name	Resolution (sec)	Duty Cycle
Electrons	> 0.4	10	P1	P1	0.1	0.5
	~1–4	1.8	$P1 \cdot \overline{P1A} \cdot P2 \cdot \overline{P3} \cdot \overline{A}$	ELO	6	1
	~4–20	1.7–1.1	$P1 \cdot \overline{P1A} \cdot P2 \cdot P3 \cdot \overline{P4} \cdot \overline{A}$	EHI	6	1
	~12–30	0.5–0.3	$P1 \cdot P2 \cdot P4 \cdot \overline{P8} \cdot \overline{A}$	RNG	6	1
	~12–30	2.8–0.9	$\overline{P1} \cdot P2 \cdot \overline{P3B} \cdot P4 \cdot \overline{P8} \cdot \overline{A}$	EWG	6	1
H, He	> 4	10	P1	P1	0.1	0.5
	19–28	1.8	$P1A \cdot P2 \cdot \overline{P3} \cdot \overline{A}$	PLO	6	1
	28–64	1.7–1.1	$P1A \cdot P2 \cdot P3 \cdot \overline{P4} \cdot \overline{A}$	PHI	6	1
	64–85	0.5–0.3	$P1 \cdot P2 \cdot P4 \cdot \overline{P8} \cdot \overline{A}$	RNG	6	1
	> 85	0.3	$P1 \cdot P2 \cdot P8 \cdot \overline{A}$	PEN	6	1
$Z \geq 3$ Nuclei (4)	60–200	1.7–1.1	$P1 \cdot P2 \cdot \overline{P4} \cdot \overline{A}$	PLO, PHI	6	1

(1) Based on calculation with straight tracks; accelerator calibration data will modify values for electrons.

(2) "A" represents the logical "or" of the guard rings on P3 to P8.

(3) P1A, P3A, and P3B are digital discriminators on the P1 and P3 outputs set at 3.1, 2.8, and 12 MeV, resp.

(4) Commandable mode for $Z \geq 3$ nuclei; energy range indicated is for Si-28.

The pulse height analysis of an "Event" is triggered whenever one of the coincidence equations in Table II is satisfied. The results, along with other information such as the state of various discriminators, are stored in one of five separate event buffers. These event buffers are read out into the telemetry stream by a rotating priority system that ensures that all event types are represented under conditions that range from periods dominated by intense fluxes of solar flare nuclei to periods domniated by trapped protons and electrons.

Because the telemetry rate is insufficient to transmit every event, rate accumulators are used to count events during 6-s intervals. A total of 32 such "counting rates" record instrument live time, the frequency of electrons and nuclei in several energy intervals defined by the coincidence logic, and the triggering frequency of a variety of discriminator levels. Table II summarizes some of the counting rates of physical interest. In addition, the "singles" counting rate of the front detector (P1) is sampled for 0.05 s out of every 0.10 s to measure the flux of magnetospheric electrons > 0.4 MeV and protons > 4 MeV on a fast time scale. This "high-resolution rate" is recorded whenever the count rate exceeds a (commandable) level of ~50 counts/s. All of the coincidence equations and some of the discriminator levels can be modified by command to allow for the possibility of noisy or failed detectors, and to optimize the instrument's response to the various particles of interest.

C. Calibrations

The response of PET to electrons has been calibrated over the energy range from ~0.3 to ~27 MeV with electron beams incident at a variety of energies and zenith angles. At higher energies the linear electron accelerator at the EG&G Santa Barbara facility was operated in a low-intensity mode to provide monoenergetic beams at fourteen separate energies from 1.5 to 27 MeV. Calibrations at somewhat lower energies (0.3 to 3 MeV) were carried out with a beta spectrometer. PET was also calibrated with radioactive sources to determine its positron detection efficiency and its response to gamma rays that Compton scatter in the telescope producing a possible background for electron and positron measurements. For accelerator calibrations, where beam time is often limited and expensive, PET has a special port that allows events to be read out at rates of several thousand per second.

PET has a built-in internal calibrator that can be initiated either periodically (every 6.8 hours) or by command (see also [1]). The calibrator includes an 8-bit DAC that supplies reference voltages to the test-pulsers of each of the signal channels. The test pulsers can be stimulated either individually, or in groups, to perform limited tests of the coincidence logic, measure the thresholds of the various discriminators, and check the gain, linearity, and long-term stability of the ADCs. Calibration "events" are flagged and stored in a special buffer for read out and telemetry along with the regular data.

D. Positron Detection with PET

Although designed primarily for measurements of electrons, H, and He, PET also has limited efficiency for identifying ~1 to ~20 MeV positrons. When a low energy positron stops and annihilates in the telescope, one of the two 0.511 MeV annihilation gamma rays may Compton-scatter and be detected in a later detector, a technique used successfully in similar telescopes flown on IMP-7&8 [20], [21]. An example of a positron-like event signature for positrons stopping in

TABLE III
PET RESOURCES

Mass	7.5 kg (including MAST)
Power	1.2 W
Bit Rate	500 bps (orbit average)

P2 is P1·P2·$\overline{P3}$·(P4+P5+P6+P7)·$\overline{P}$8, where the energy loss in the earlier detectors (P1 and P2) must be consistent with that of an electron, where P3 must not trigger, and where the pulse height in the later detector (P4, P5, P6, or P7) must be $\leq$0.34 MeV, the maximum-energy Compton-recoil from a 0.511 MeV gamma ray. The estimated efficiency for identifying P1·P2 positrons with this signature is ~0.003. For somewhat higher energy positrons that stop in P3 the corresponding efficiency is estimated to be ~0.005.

The capability of PET to detect positrons was verified by calibrations with a Ge-68 β^+-decay source prior to launch. Further analysis of these data, combined with Monte Carlo simulations, will establish the positron detection efficiency. The principal source of background for positron measurements is expected to be gamma rays that Compton-scatter in two separate detectors (see [20] and [21]).

E. Resources

The MAST and PET instruments on SAMPEX are housed in a common box of dimensions 25 cm ×36 cm ×17 cm, with the two cylindrical telescopes extending ~6 cm above the box. Power is provided by a supply housed in a separate box of dimensions 13 cm ×12 cm ×6 cm. Table III summarizes the spacecraft resources required by PET. Although they share a common power supply, MAST and PET are electrically isolated. The peak power drawn by the instruments during large flares may increase by ~25%. PET's average data rate of 0.5 kbps corresponds to ~9 transmitted events per second. However, PET may achieve significantly higher data rates during limited periods of activity through the novel data management approach of the SAMPEX Data Processing Unit (see [22]). During launch operations both the MAST and PET telescopes were acoustically and thermally protected by a common 0.08 cm-thick Al cover that pwas opened by command prior to instrument turn-on.

ACKNOWLEDGMENT

Essential contributions to the implementation of the PET experiment were made by J. H. Marshall and T. Harrington of MDH, Ind.; Ball Brothers Western Laboratories under the direction of D. Snyder and G. Takahashi; D. Aalami of Space Instruments, Inc.; the Applied Science Division of Perkin-Elmer, under the direction of N. Preketes; F. Shaffer of Goddard Space Flight Center; and W. Althouse, B. Gauld, K. Hargreaves, and R. Vogt of Caltech.

REFERENCES

[1] W. R. Cook, A. C. Cummings, J. R. Cummings, T. L. Garrard, B. Kecman, R. A. Mewaldt, R. S. Selesnick, E. C. Stone, and T. T. von Rosenvinge, "MAST: A Mass Spectrometer Telescope for isotope studies of solar, anomalous, and galactic cosmic rays," *IEEE Trans. Geosci. Remote Sensing,* vol. 31, pp. 557–564, May 1993.

[2] G. M. Mason, D. C. Hamilton, P. H. Walpole, K. F. Heuerman, T. L. James, M. H. Lennard, and J. E. Mazur, "LEICA: A Low Energy Ion Composition Spectrometer for the study of solar and magnetospheric heavy ions," *IEEE Trans. Geosci. Remote Sensing,* vol. 31, pp. 549–556, May 1993.

[3] B. Klecker, D. Hovestadt, M. Sholer, H. Arbinger, M. Ertl, H. Kastle, E. Kunneth, P. Laeverenz, and E. Seidenschwang, "HILT: A Heavy Ion Large Proportional Counter Telescope for solar and anomalous cosmic rays," *IEEE Trans. Geosci. Remote Sensing,* vol. 31, pp. 542–548, May 1993.

[4] D. N. Baker, G. M. Mason, O. Figueroa, G. Colon, J. G. Watzin, and R. M. Aleman, "An overview of the Solar Anomalous and Magnetospheric Particle Explorer (SAMPEX) Mission," *IEEE Trans. Geosci. Remote Sensing,* vol. 31, pp. 531–541, May 1993.

[5] R. M. Thorne, "Energetic radiation belt precipitation: A natural depletion mechanism for stratospheric ozone," *Science,* vol. 21, pp. 287–289, 1977.

[6] R. M. Thorne, "The importance of energetic particle precipitation on the chemical composition of the middle atmosphere," *Pure Appl. Geophys.,* vol. 118, p. 128, 1980.

[7] D. N. Baker, J. B. Blake, D. J. Gorney, P. R. Higbie, R. W. Klebesadel, and J. H. King, "Highly relativistic electrons: A role in coupling to the middle atmosphere," *Geophys. Res. Lett.,* vol. 14, pp. 1027–1030, 1987.

[8] L. B. Callis, D. N. Baker, J. B. Blake, J. D. Lambeth, R. E. Boughner, M. Natarajan, R. W. Klebesadel, and D. J. Gorney, "Precipitating relativistic electrons: Their long-term effect on stratospheric odd nitrogen levels," *J. Geophys. Res.,* vol. 96, pp. 2939–2976, 1991.

[9] L. B. Callis, R. E. Boughner, M. Natarajan, J. D. Lambeth, D. N. Baker, and J. B. Blake, "Ozone depletion in the high latitude lower stratosphere: 1979–1990," *J. Geophys. Res.,* vol. 96, pp. 2921–2937, 1991.

[10] G. Brasseur and S. Solomon, *Aeronomy of the Middle Atmosphere.* Dordrecht/Boston/Lancaster: D. Reidel Publishing Company, 1984.

[11] E. W. Hones and P. R. Higbie, "Distribution and detection of positrons from an orbiting nuclear reactor," *Science,* 244, p. 448, 1989.

[12] S. A. Averin, A. M. Galper, V. M. Grachev, V. V. Dmitrenko, V. D. Maslov, and S. E. Ulin, "High-energy electrons in the earth's external radiation belt," *Cosmic Research,* vol. 26, p. 274, 1988.

[13] L. V. Kurnosova, L. A. Razorenov, and M. I. Fradkin, "Flux of electrons with energies above 100 MeV in the earth's inner radiation belts," *Cosmic Research,* vol. 29, p. 609, 1992.

[14] R. P. Lin, "Solar particle acceleration and propagation," *Reviews of Geophysics,* vol. 25, pp. 676–684, 1987.

[15] D. V. Reames, H. V. Cane, and T. T. von Rosenvinge, "Energetic-particle abundances in solar electron events," *Ap. J.,* vol. 257, pp. 259–270, 1990.

[16] E. R. Christian, A. C. Cummings, and E. C. Stone, "Evidence for anomalous cosmic ray hydrogen," *Ap. J. Letters,* vol. 334, pp. L77–L80, 1989.

[17] R. A. Mewaldt, "Temporal variations of anomalous cosmic rays and further evidence for anomalous cosmic ray hydrogen," *Proc. 21st International Cosmic Ray Conference (Adelaide),* vol. 6, pp. 160–163, 1990.

[18] E. C. Stone, R. E. Vogt, F. B. McDonald, B. J. Teegarden, J. H. Trainor, J. R. Jokipii, and W. R. Webber, "Cosmic ray investigation for the Voyager missions; Energetic particle studies in the outer heliosphere—and beyond," *Space Science Reviews,* vol. 21, pp. 355–376, 1977.

[19] W. E. Althouse, A. C. Cummings, T. L. Garrard, R. A. Mewaldt, E. C. Stone, and R. E. Vogt, "A cosmic ray isotope spectrometer," *Geoscience Electronics,* vol. 16, pp. 204–207, 1978.

[20] G. J. Hurford, R. A. Mewaldt, E. C. Stone, and R. E. Vogt, "Observations of the ratio of low-energy cosmic-ray positrons and electrons during solar quiet times," *Proceedings 13th International Cosmic Ray Conference (Denver),* vol. 1, pp. 330–335, 1973.

[21] R. A. Mewaldt, E. C. Stone, and R. E. Vogt, "The quiet time flux of 0.16 to 1.6 MeV positrons," *Proceedings 14th International Cosmic Ray Conference (Munich),* vol. 1, p. 401, 1975.

[22] D. J. Mabry, S. J. Hansel, and J. B. Blake, "The SAMPEX Data Processing Unit (DPU)," *IEEE Trans. Geosci. Remote Sensing,* vol. 31, pp. 572–574, May 1993.

Walter R. Cook, for a biography, please see page 563 of this issue.

Alan C. Cummings, for a photograph and biography, please see page 563 of this issue.

Jay R. Cummings, for a photograph and biography, please see page 563 of this issue.

Thomas L. Garrard, for a photograph and biography, please see page 563 of this issue.

Branislav Kecman, for a photograph and biography, please see page 563 of this issue.

Richard A. Mewaldt, for a photograph and biography, please see page 563 of this issue.

Richard S. Selesnick, for a photograph and biography, please see page 564 of this issue.

Edward C. Stone, for a photograph and biography, please see page 564 of this issue.

Daniel N. Baker, for a photograph and biography, please see page 541 of this issue.

Tycho von Rosenvinge, for a biography, please see page 564 of this issue.

J. B. Blake received the B.S. degree in engineering physics and the M.S. and Ph.D. degrees in physics from the University of Illinois.

He joined the Aerospace Corporation in 1962, where he is presently Department Director of the Space Particles and Fields Department in the Space and Environment Technology Center. His recent work has concentrated on particles and fields in planetary magnetospheres, cosmic-ray physics, and nuclear astrophysics. He is Co-Investigator on the NASA Solar, Anomalous, and Magnetospheric Explorer (SAMPEX) mission, and Principal Investigator for the Comprehensive Energetic Particle Pitch Angle Distribution (CEPPAD) experiment on the NASA POLAR mission.

Len B. Callis received the B.S. degree in aerospace engineering from Virginia Polytechnic Institute and the M.S. degree in aerospace engineering from Cornell University.

He has been at the NASA Langley Research Center since 1962 and is currently a Senior Research Scientist in the Atmospheric Sciences Division. Recently, his research work has concentrated on magnetospheric–atmospheric coupling via precipitating relativistic electrons. He is currently a Co-investigator on the Solar, Anomalous, and Magnetospheric Particle Explorer (SAMPEX).

Communication

The SAMPEX Data Processing Unit

D. J. Mabry, S. J. Hansel, and J. B. Blake

Abstract—**The SAMPEX Data Processing Unit provides overall control of the scientific payload while acquiring, combining, and compressing science data to produce the science telemetry for the mission. Section I of this paper describes data manipulation techniques employed to intelligently use the on-board recorder storage. Some key features of the Data Processor design are given in Section II.**

I. Introduction

The SAMPEX Data Processing Unit (DPU) provides timing and control signals to the four sensors to manage data acquisition and mode switching while simultaneously combining sensor and DPU data to form telemetry packets which are transmitted to the Small Explorer Data System (SEDS) for recorder storage. DPU algorithms are designed to maximize the science output for the SAMPEX mission by controlling the data storage rate over the ~ 12-hour storage period. Fig. 1 shows a system connection block diagram for the sensors, DPU, and the SEDS.

The DPU is based on the Harris 80C85RH microprocessor and includes 24 Kbytes of PROM and 56 Kbytes RAM. Actel Field Programmable Gate Arrays (FPGA's) are utilized to gain a high degree of parallel hardware processing, redundancy, and fault tolerance without the penalty of greatly increased power or weight. Actel FPGA's are especially attractive for satellite instrumentation since each chip provides approximately 2000 logic gates in a quad flatpack package of 2.2 cm^2. The DPU box, including power preregulators for the HILT and LEICA sensors, measures 7″(L)×7″(W)×9.7″ (H) and weighs 7 lbs.

II. Data Manipulation

A. Recorder System Overview

The primary function of the DPU is to collect sensor data to create telemetry packets for transmission to the solid-state recorder located within the Small Explorer Data System (SEDS). The 22 Mbyte recorder is dumped only twice per day, therefore a key task of the DPU is to throttle packet outputs so that the recorder is not filled too soon following a ground pass, yet is almost full at the time of each acquisition. The DPU guarantees each sensor a minimum allocation of recorder memory for data storage in each orbit; unused memory allocation for the recently completed orbit is redistributed to future orbits so that highly active sensors are allocated greater data storage.

B. Pulse Height Analyzed (PHA) Event Data Handling

PHA events are output from the scientific sensors asynchronously at a rate dependent on the particle flux incident on detectors within the sensor. The DPU's sensor interfaces are capable of receiving up to 150 events per second from the combined payload, but outputting to the recorder at that rate would exhaust the recorder capacity within 2 hours. The DPU more slowly fills the recorder over the 12-hour "inter-pass" period by using a two-tiered quota system. The two types of quotas maintained by the DPU are one second quotas and orbit quotas. One second quotas limit the instantaneous burst rate of events from each sensor, thus providing a method of prioritizing event data items.

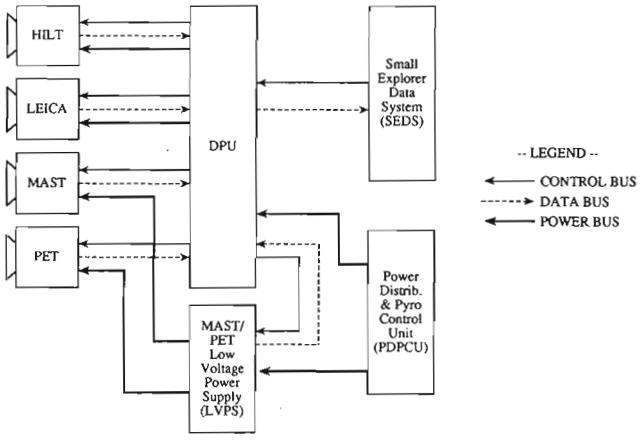

Fig. 1. System overview.

Orbit quotas limit the amount of recorder memory available to each sensor for event packet storage. When an event packet (four distinct types, one per sensor) is output to the telemetry stream, the appropriate orbit quota is decremented by the length (in bytes) of the packet transmitted. If the packet's orbit quota becomes zero as a result of the decrement operation, then further packets of that type are blocked from output to the recorder for the remainder of the current orbit. At the end of each orbit (~ 90 min), the DPU performs a memory reallocation algorithm which provides additional memory to each of the orbit constrained packet types.

C. Rate Scaler Data Handling

1) Low Resolution Rates: Low resolution rate data is accumulated in the DPU for all four sensors and output unconditionally every 6 s to the SEDS for storage.

2) High Resolution Rates & Triggering: The DPU supports high resolution rate (HRR) data processing for 6 HILT rates and 1 PET rate. For these items, data is read once every 100 ms to produce high time resolution packets. To limit the amount of recorder memory expended for storage of uninteresting data, the DPU supports a ground-programmable "trigger level" which, when compared against data in the accumulation array (6-s coverage for HILT, 48 s for PET), determines if data should be recorded. High resolution rate data packets are subjected to orbit quotas similar to those given for PHA event packets, therefore limited space is made in the recorder for their output.

3) History Data Buffers: A large fraction of the low resolution rate data items are accumulated longer term to produce quick-look scalers. When combined with some subset of analog housekeeping data, these items make up an orbital history which, when requested

Manuscript received Aug. 3, 1992; revised Jan. 21, 1993. This work was supported under NASA Cooperative Agreement 26 979B.

The authors are with the Space and Environment Technology Center, The Aerospace Corporation, El Segundo, CA 90245.

IEEE Log Number 9208069.

at the time of initial transponder acquisition from the ground station, give a summary for data which existed in the orbit immediately preceding the ground pass. The DPU supports the orbital history with a circular buffer which is written with a new data point every 96 s for HILT and LEICA, and every 192 s for MAST and PET.

D. Memory Reallocation

Following boot-up of the DPU system or reception of a "Reset Quota" command, the DPU initializes the running orbit quotas with the ground-programmable baseline allocations. Upon output of a PHA event or high resolution rate data packet, the associated running quota is decremented by the packet length. As the orbit proceeds, the orbit quotas are decremented. Further packet outputs are blocked when the associated orbit quota reaches zero, at least until the next reallocation period is reached. For the first orbit, this assures that at least the minimum recorder memory is made available for each of the quota-controlled data packets.

At the end of the orbit, the DPU collects unused recorder memory quota for redistribution in the next orbit. As in the first orbit, each data type is given the baseline allocation, but each is also given additional quota based on the excess from the previous orbit as determined by ground-programmable redistribution percentages. This system redistributes unused memory from previous orbits so that highly active sensors can utilize unused memory from less active sensors, but only after those less active sensors have first forfeited the opportunity to use it.

III. System Description

A. Sensor Interface Electronics

Due to the high density of the Actel Gate array, each sensor interface is implemented in a single, dedicated sensor interface gate array. Each of these sensor gate arrays can be individually enabled or disabled, allowing the DPU to continue functioning in the event of a catastrophic failure in a gate array or sensor. Each sensor interface includes an instrument clock generator, command interface, data interface, and Direct Memory Access (DMA) circuitry. The DMA capability allows the sensor interface to transfer data directly from the sensor to processor memory with minimal processor intervention, freeing the processor for other tasks such as data compression.

B. Spacecraft Command Interface

Commands are transferred from the spacecraft to the DPU serially through a differential three signal interface consisting of a clock, gate, and data running at a rate of 2 kilobits per second (KB/S). Commands consist of 64 bits with the last 8 bits defined as the command checksum. Using this checksum, the DPU verifies the integrity of each received command and all included parameters prior to execution. A total of 59 commands are recognized; one of which allows for modifying DPU code and data, therefore making modification of the DPU program after launch possible.

C. Spacecraft Telemetry Interface

Telemetry data is transferred from the DPU to the spacecraft over a four signal interface at a rate of 100 kb/s. The signals are all differential and consist of a "Request to Send" from the DPU, a "Clear to Send" from the spacecraft, a clock and a data signal. The telemetry interface directly accesses the processor memory so that entire packets of data can be sent with a single processor operation.

The basic unit of data transferred from the DPU to the SEDS is a packet consisting of a primary header (6 bytes), a secondary header (10 bytes), and a variable length data block. The DPU hardware interface transmits fixed length packets, each of length 512 bytes to the SEDS, however packets are truncated to the length specified in the secondary header by the SEDS before storage. Each packet contains and application ID (APID) which specifies the type of data enclosed and a 16-bit checksum which certifies the integrity of the complete packet.

D. Spacecraft Interface Redundancy & Selection

The DPU's spacecraft interface (including command, telemetry, and time distribution interfaces) is implemented within the DPU using a single Actel FPGA. Spacecraft interface redundancy is achieved by collocating two copies of the Spacecraft Interface chip on the interface board. The best of the two spacecraft interfaces is chosen during the DPU's power on diagnostics where the SEDS provides an echo feature to help with the selection process.

E. Memory Mapper

The Memory Mapper is included in the DPU design to protect against system failure caused by RAM chip or cell failure. The RAM array consists of seven 8K $\times$ 8 bit RAM chips of which only six are needed to perform all DPU functions. As the DPU powers on, an exhaustive memory test is performed which tests not only the RAM cells, but also address and data input lines as well. As the memory verification process proceeds, the Memory Mapper maps good chips to lower memory locations and bad or suspect chips to higher locations. Data in the DPU is organized so that critical data, such as the flight program, are placed in lowest memory locations, therefore if several RAM chips do fail, less important data will be stored in the faulty locations. With this scheme, one RAM chip can fail with no impact on DPU operations; up to three RAM's can fail with only the loss of nonessential operations.

F. Task Scheduling Concept

Each sensor contains multiple hardware ports which support a different data type (e.g., digital status, counting rates, or PHA data), but organized so that only one type of data can be output at a time. The DPU software must coordinate read-outs from the sensors so that all data items are read as needed for the creation of low and high-resolution rates and digital status packets while simultaneously using any available interface dead time to readout asynchronously occurring PHA event data. In addition, the software system must schedule the creation of telemetry packets, the use of the spacecraft interfaces, and processing time for data compression or packet checksum calculation.

To organize time and resources available to the DPU, task scheduling algorithms were implemented to fully control the use of all DPU resources. The task scheduling scheme allows separate subroutines, each with a finite function (read counting rates, process spacecraft command, check HILT high voltage, reset watchdog timer, etc.), to be coded and tested independently. The task scheduling algorithms then allows operations, whether sensor interface related or processing related, to be combined to form the final software product. Incompatible operations can be separated in time, and processor and interface hardware may be load balanced for most efficient use of system resources.

G. System Reconfiguring

The DPU hardware system contains no nonvolatile RAM, therefore changing the DPU's executable code or parameter set would usually require ground intervention. To overcome this situation, the DPU provides a special set of boot-up operations which, with support from the spacecraft, allow for modifying the default power-on DPU state even in the absence of ground contact. A set of relative time sequences (RTS's) are maintained in the spacecraft nonvolatile

RAM which contain DPU commands capable of modifying the DPU program, data structures, or default parameter states. As the DPU boots, while still in a partially dormant state, the DPU requests the RTS's, then processes the incoming modification commands. The complete program begins execution immediately following reception of the last modification command.

ACKNOWLEDGMENT

Successful testing of the DPU system relied heavily on the use of robust Ground Support Equipment (GSE) for which we thank Kirk Crawford and David Lau of the Aerospace Corporation. The GSE was originally designed for testing of the DPU system, but during launch and early orbit operations of the SAMPEX mission the GSE has provided scientific data displays as well. The quick-look capabilities of the GSE system, particularly those related to the early orbit operations, were crucial for early health monitoring of the scientific payload.

We are especially grateful to Dave Welch of Bendix Corporation for his dedication to understanding the operations of the sensors and DPU so that he could design the necessary procedures for testing and operating the SAMPEX science payload while on orbit.

INFORMATION FOR AUTHORS

Subject Matter: The IEEE TRANSACTIONS ON GEOSCIENCE AND REMOTE SENSING (hereafter referred to as TGARS) is a bimonthly Publication for theoretical and applied papers on geoscience and remote sensing. Papers should relate to the theory, concepts, and techniques of science and engineering as applied to sensing the earth, oceans, atmosphere, and space, and the processing, interpretation, and dissemination of this information. The technical content of papers must be both new and significant. Experimental data must be complete and include sufficient description of experimental apparatus, methods, and relevant experimental conditions.

Submitting Papers: Membership in the IEEE is not required of authors. Five copies (original plus four copies) of each manuscript must be submitted to the Editor as well as an abstract of not more than 200 words. Manuscripts should be limited to 35 double-spaced typewritten pages, typed on one side of the page only, with a maximum of 15 figures. A pamphlet, "Information for IEEE Authors," is available upon request from the IEEE Publishing Department, 345 East 47th St., New York, NY 10017. Authors are urged to organize their papers following the recommendations presented in this pamphlet.

Style: TGARS is addressed to readers with a wide variety of interests. The author should refrain from using terminology that may not be familiar to readers and carefully explain terminology that is used. In addition, the author should provide brief introductory remarks and references that will permit the reader to relate the paper to other work in the author's field of specialty. Clarity of both writing and illustrations is required. TGARS is published only in English and the use of correct English is required of all authors. Thus, contributors for whom English is not a native language should have their papers edited for style, form, grammar, and spelling suitable for publication *prior* to submittal to TGARS. Papers should be accompanied by brief biographies and clear glossy photographs of the authors.

Submission of a manuscript is assurance that it has not been copyrighted, published, or accepted for publication elsewhere; that it is not currently being considered for publication elsewhere; and that it will not be submitted elsewhere while under consideration by TGARS, unless the author states otherwise. The original copy only will be returned for manuscripts not accepted.

References and Figure Captions; Begin references on a separate sheet of paper. They must be double-spaced. Follow the same guideline for figure captions. Do not include captions on the illustrations. Captions are set in type separately. Figure captions should be sufficiently clear so that the figures can be understood without detailed reference to the accompanying text. Axes of graphs should have self-explanatory labels, not just symbols (e.g., Electric Field rather than E).

Illustrations: Submit original illustrations as well as four sets of copies for the reviewers. All line drawings (graphs, charts, diagrams, etc.) should be prepared in black on a white background. Photostatic copies of originals are acceptable only when they are exceptionally clear, with high contrast, preferably on glossy paper. Lettering should be large enough to be readily legible when the drawing is reduced from the original by as much as 4:1, to a two- or one-column width. All materials, including drawings and photographs, should be no larger than 22 × 28 cm (8½ × 11 in.). Tables are not typeset and should be treated as illustrations. All photographs must be glossy prints.

Page Numbers: Number *all* pages, including illustrations (which should be grouped at the end), in a single series with no omitted numbers. Identify figures by number and author's name. Use a soft pencil when identifying photographs and keep the information in the margin of the figures.

Review Process: Papers are usually reviewed by at least three qualified referees. A decision is made on the disposition of a manuscript and the author is notified of the decision.

Communications and Letters to the Editor: Communications are technical contributions which are narrower in scope than regular papers. Communications should be prepared and submitted according to the instructions given above for regular papers but for the following changes: limit the abstract to 50 words; limit the paper to three (3) printed pages (i.e., 13 double-spaced manuscript pages), including illustrations. Very brief contributions, letters to the Editor, and comments on, or corrections to, a published paper may be reviewed only by an Editor.

Page Charges: A mandatory *Excessive Paper Length* charge of $150.00 per page (beginning with page 6 and beyond) is required for papers in excess of five (5) printed pages. The author will be notified of the estimated paper length upon receipt of the original manuscript. The author will be requested, conditional upon favorable technical review, to pay an optional sustaining page charge of $110 per printed page to cover the cost of publication of the first five pages and will receive 100 reprints of the paper or communication if this charge is honored. Authors are encouraged to seek institutional support for all page costs. Authors who cannot pay mandatory charges will be required to reduce their manuscripts to five printed pages or less prior to final acceptance and scheduling for publication. This reduction will occur after technical review of the manuscript. The above policy has no relationship to requests by the Editor to reduce very long manuscripts prior to technical review.

Copyright: It is the policy of the IEEE to own the copyright to the technical contributions it publishes on behalf of the interests of the IEEE, its authors, and their employers, and to facilitate the appropriate reuse of this material by others. To comply with the U.S. Copyright Law, authors are required to sign an IEEE copyright transfer form before publication. This form, a copy of which appears in the January 1993 issue of TGARS, returns to the authors and their employers full rights to reuse their material for their own purposes. Authors must submit a signed copy of this form with their manuscripts.

Manuscript Submittal Checklist: Original and four copies of typewritten, double-spaced manuscript; original and four copies of figures and tables; number *all* pages of a manuscript in a single series with no omitted numbers; edit manuscript for correct English usage; provide complete mailing address, telephone and FAX numbers of corresponding author (include country and city codes); signed IEEE Copyright Form; brief biography and photo for each author.

TGARS papers accepted for publication may be submitted on the following recording media: IBM PC 3½″ or 5¼″ disks; Macintosh disks; 0.25″ magnetic tape cartridges (Unix: tar, dump); 3.5″ floppy disk (UNIX workstations). Any of the following word processing formats may be used: Microsoft Word; Multimate; Wordstar 2000; DCA/RFT; Wang IWP; Volkswriter 3; Sprint; DIF; Officewriter 6.0; ASCII; First Choice; XyWrite; Writing Assistant; RTF; Chiwriter; TEXtures; WordPerfect; Wordstar; Displaywrite; DCA/FFT; Samna; WordMarc; CEOwrite; DX; ProWrite 1.0/2.0; Mass-11; PFS: Write A,B,C; SmartWare II; Nota Bene; TROFF/NROFF; Exp. 2.0. A manuscript of the final version of the accepted paper must accompany the electronically formatted version.

Please submit papers and communications manuscripts to:

Dr. James A. Smith
Editor, TGARS
Code 920
Laboratory for Terrestrial Physics
NASA Goddard Space Flight Center
Greenbelt, MD 20771

INSTITUTIONAL LISTINGS

The IEEE Geoscience and Remote Sensing Society invites applications for Institutional Listings from firms interested in geoscience and remote sensing.

An Institutional Listing recognizes contributions to support the publication of the IEEE TRANSACTIONS ON GEOSCIENCE AND REMOTE SENSING. Minimum rates are $50.00 for listing in one issue; $200.00 for six consecutive issues. Larger contributions will be most welcome. No agency fee is granted for soliciting such contributions. Inquiries, or contributions made payable to the IEEE, plus instructions on how you wish your Institutional Listing to appear, should be sent to Marilyn Prusan, Finance Administrator, IEEE Technical Activities, 445 Hoes Lane, P.O. Box 1331, Piscataway, NJ 08855-1331.